

Martine Irene Østlie

Development of a liquid chromatography tandem mass spectrometry method for the determination of organophosphate flame retardants in baby food

Master's thesis in Natural Science with Teacher Education

Supervisor: Alexandros Asimakopoulos

June 2020

Martine Irene Østlie

Development of a liquid chromatography tandem mass spectrometry method for the determination of organophosphate flame retardants in baby food

Master's thesis in Natural Science with Teacher Education
Supervisor: Alexandros Asimakopoulos
June 2020

Norwegian University of Science and Technology
Faculty of Natural Sciences
Department of Chemistry



Kunnskap for en bedre verden

Preface

This thesis marks the completion of my Master's degree in Analytical Chemistry at the Department of Chemistry at Norwegian University of Science and Technology. This thesis is a part of the Natural Science with Teacher Education program. I am grateful that I have been able to dig deep into analytical chemistry as the scientific and structural knowledge from working with this project will be beneficial for my future as a teacher.

I would like to send my thanks to the people who have made this project possible. Firstly I would send a special thanks to my supervisor Alexandros Asimakopoulos. Without your guidance and enthusiasm this project would not have been possible to complete. With the university closing as a result of SARS-CoV-2, forcing the project to change, it has been a blessing to have a supervisor with a "no worries, we fix"-mindset. Thank you for always, without a doubt, answering questions and explaining things, and thank you for always being super positive making it feel like anything is possible and everything is solvable.

Thanks also to Shannen Thora Lea Sait and Susana Villa Gonzáles for help with the LC-MS/MS analysis. Also thank you to Kristine Vike-Jonas for always being available for questions and for guidance in the MS-processing lab.

I would also like to thank my lab buddies for always making it fun to work in the lab. Thank you to Eirik for great discussions on OPFRs and collaboration in the lab, and to Hanne and Ragnhild for encouragement, support and fun times as the "Analytical Chemistry Team" in the teaching education program. Also thank you to the rest of my classmates, friends and family. Finally a special thanks to Helge for endless support and encouragement, and for being my always available personal tech-support.

Abstract

Organophosphate flame retardants (OPFRs) have received increasing attention as production has escalated, as a result of the polybrominated diphenyl ethers being phased out as flame retardants. The attention on adverse effects of OPFRs in living organisms and the environment has increased as several studies have indicated potential toxic effects as a result of exposure of OPFRs. Research on the occurrence of organophosphate flame retardants in air, dust, water and sediments, together with some metabolites in urine, are substantially studied. Research on OPFRs in foodstuffs as a pathway for human exposure is on the other hand less studied. Baby food is of special interest, since some of the OPFRs have suspected developmental effects. 49 baby foods were supposed to be examined for 19 OPFRs and 2 metabolites. Unfortunately labs were closed due to SARS-CoV-2, and the experimental work was not possible to complete. Only the extraction method development was able to be performed. One of the baby foods was used as example sample matrix for this purpose. Two different extraction protocols were tested with respectively ethyl acetate (EA) and Dichloromethane:Hexane (50:50) as the main solvent. The protocol where the extraction was executed with EA as the solvent showed considerably better recoveries and results than the extraction with DCM:Hex.

Liquid chromatography tandem mass spectrometry (LC-MS/MS) was used to analyze the OPFRs. Five of the 21 analyzed OPFRs showed concentrations above the estimated LOQ. Their concentrations ranged from 0.25-23.5 ng/g dw, where TCIPP showed the highest detected concentration (TCIPP > TnBP > TMP > TPP > TEP). The estimated LOD for all compounds ranged from 0.02-3.97 ng/g. Contamination of samples resulting in high blank values lead to difficulties to detect three of the OPFRs (EHDP, TEHP and TDCIPP). Recoveries ranged from 30.9-103%, with exception of EHDP, TEHP, TDCIPP, TTBP, IDPP and TCIPP. Detection of daughter fragments for each OPFR was obtained from the SRM detector. Structures for the daughter fragments were suggested together with a general fragmentation mechanism for OPFRs.

Sammendrag

Organofosfat flammehemmere (OPFR) har fått økende oppmerksomhet ettersom produksjonsvolumet har økt, som et resultat av at polybrominerte difenyl etere er faset ut som flammehemmere. Bevisstgjøring av risikoen for uheldige effekter etter eksponering av OPFR på levende organismer og miljøet har økt, ettersom flere studier har påvist potensielt toksiske effekter, som et resultat av eksponering for OPFR. Forskning på forekomsten av organofosfat flammehemmere i luft, støv, vann og sedimenter, sammen med noen metabolitter i urin er vesentlig forsket på, mens forskning på OPFR i mat som en rute for menneskelig eksponering er mindre forsket på. Babymat er spesielt interessant ettersom noen av OPFRene er mistenkt for å ha en effekt på menneskelig utvikling. 49 ulike varianter av babymat skulle bli analysert for 19 forskjellige typer OPFR og 2 metabolitter. Uheldigvis ble laboratoriene stengt på grunn av SARS-CoV-2, og det eksperimentelle arbeidet var ikke mulig å fullføre. Kun utvikling av ekstraksjonsmetoden ble mulig å gjennomføre. En av babymatprøvene ble brukt som eksempelmatris for metodeutviklingen. To ulike ekstraksjonsprotokoller ble testet med henholdsvis etylacetat (EA) og diklormetan:heksan (50:50) som hovedløsemiddel. Protokollen hvor etylacetat ble brukt som løsemiddel viste betraktelig bedre resultater enn ekstraksjonen med diklormetan:heksan. Væskekromatografi tandem massespektroskopi (LC-MS/MS) ble brukt for å analysere flammehemmerene. Fem av de 21 analyserte organofosfatene hadde konsentrasjoner over LOQ. De kvantifiserbare konsentrasjonene var mellom 0.25-23.5 ng/g dw, hvor TCIPP hadde den høyeste detekterte konsentrasjonen (TCIPP > TnBP > TMP > TPP > TEP). De estimerte grensene for deteksjon varierte fra 0.02-3.97 ng/g. Forurensning av prøvene resulterte i høye verdier for noen av blankprøvene, som førte til vanskeligheter med å detektere tre av stoffene (EHDP, TEHP og TDCIPP). Recoveries varierte fra 30.9-103%, med unntak av EHDP, TEHP, TDCIPP, TTBP, IDPP and TCIPP. Deteksjon av datterfragmenter for hver OPFR ble gjort med SRM-detektoren. Strukturer for datterfragmenter er foreslått sammen med en generell fragmenteringsmekanisme for OPFR.

Table of Contents

Preface	i
Abstract	iii
Sammendrag	v
Table of Contents	vii
List of Figures	xi
List of Tables	xiii
Abbreviations	xvi
1 Introduction	1
2 Theoretical Background	3
2.1 Flame retardants	3
2.2 Organophosphate flame retardants	3
2.2.1 Characteristics	10
2.2.2 History and use	10
2.2.3 Human and environmental exposure and effects	11
2.2.4 Study population: Baby foods	15
2.3 Previous studies	15
2.4 Analytical techniques	20
2.4.1 Sample preparation	20
2.4.2 Liquid chromatography	21
2.4.3 Liquid chromatography coupled to Mass spectrometer (LC-MS/MS)	21
2.4.4 Mass spectrometry	22
2.4.5 Ionization	23
2.4.6 Triple quadrupole analyzer	25
2.4.7 Collision energy and cone voltage	26
2.4.8 Fragmentation of organophosphate flame retardants	27
2.5 Quantitation and quality assurance	29
2.5.1 Retention Time (RT) and Relative Retention Time (RRT)	29
2.5.2 Limit of detection and limit of quantification	30
2.5.3 Internal Standard Method	30
2.5.4 Relative response ratio	31
2.5.5 Ion Ratio	31
2.5.6 Absolute and relative recovery	32
2.5.7 Matrix Effect	33

2.5.8	Coefficient of determination	33
3	Materials and method	35
3.1	Sample Collection	35
3.2	Chemicals	35
3.3	Sample preparation	36
3.3.1	Standards	36
3.4	Development of extraction technique	36
3.5	Instrumentation for Analysis	37
3.6	Data treatment	39
3.7	SRM Transitions and fragmentation	39
3.8	Experimental work disrupted by SARS-CoV-2	40
4	Results and discussion	43
4.1	Extraction method development	43
4.2	Recoveries	44
4.2.1	Precision	48
4.3	Ion ratios	50
4.4	Concentrations	52
4.5	Analysis	52
4.6	SRM Transitions	54
4.6.1	General fragmentation mechanism	54
4.6.2	TMP	56
4.6.3	TEP	58
4.6.4	TnPP	60
4.6.5	TnBP	62
4.6.6	TiBP	64
4.6.7	TBOEP	66
4.6.8	TEHP	68
4.6.9	TCEP	70
4.6.10	TCIPP	72
4.6.11	TDCIPP	74
4.6.12	TPP	76
4.6.13	DCrP	78
4.6.14	TMPP	80
4.6.15	EHDP	82
4.6.16	IDPP	84
4.6.17	BPDP	85
4.6.18	TTBPP	86
4.6.19	RDP	88
4.6.20	V6	90

4.6.21	BPA-BDPP	93
4.6.22	BBOEHEP	95
4.6.23	3OH-BOEP	97
4.6.24	DnBP	99
4.6.25	BCEP	101
4.6.26	BCIPP	103
4.6.27	BBOEP	105
4.7	Summary of OPFR fragmentation	107
4.8	Fragment detection	107
4.9	Further work and suggestions	113
5	Conclusion	114
	References	115
A	Appendix	127
A.1	Protocol for extraction of OPFRs from foodstuffs - Ethyl Acetate	127
A.2	Protocol for extraction of OPFRs from foodstuffs - Hexane:DCM	128

List of Figures

2.1	General structure of organophosphate flame retardants	10
2.2	Schematic description of the LC-MS/MS instrument. Reproduced from Giri (2020).	22
2.3	Schematic representation of the ESI(+) (reproduced from Lundanes (2014) page 87).	24
2.4	Schematic representation of the triple quadrupole mass analyzer (repro- duced from Dass (2007b) p.132)	26
2.5	Suggested fragmentation pathways for TMP and TEP by Bell et al. (1997).	27
2.6	Suggested fragmentation pathway for TCEP(a), TPP(b) and BPA-BDPP(c) by Rodil et al. (2005).	28
2.7	Suggested fragmentation rules for organophosphate esters by Schwarzen- berg et al. (2013).	28
4.1	General reaction mechanism for fragmentation of OPFRs. TEP is used as an example compound.	55
4.2	Optimized daughter spectrum for TMP at collision energy 18eV.	56
4.3	Suggested TMP daughter fragments.	57
4.4	Optimized daughter spectrum for TEP at collision energy 8eV.	58
4.5	Suggested TEP daughter fragments.	59
4.6	Optimized daughter spectrum for TnPP at collision energy 10eV.	60
4.7	Optimized daughter spectrum for TnPP at collision energy 38eV.	60
4.8	Suggested TnPP daughter fragments.	61
4.9	Optimized daughter spectrum for TnBP at collision energy 8eV.	62
4.10	Optimized daughter spectrum for TnBP at collision energy 44eV.	62
4.11	Suggested TnBP daughter fragments.	63
4.12	Optimized daughter spectrum for TiBP at collision energy 6eV.	64
4.13	Optimized daughter spectrum for TiBP at collision energy 42eV.	64
4.14	Suggested TiBP daughter fragments.	65
4.15	Optimized daughter spectrum for TBOEP at collision energy 16eV.	66
4.16	Suggested TBOEP daughter fragments.	67
4.17	Optimized daughter spectrum for TEHP at collision energy 6eV.	68
4.18	Suggested TEHP daughter fragments.	69
4.19	Optimized daughter spectrum for TCEP at collision energy 12eV.	70
4.20	Suggested TCEP daughter fragments.	71
4.21	Suggested TCEP daughter fragment at m/z 63.	71
4.22	Optimized daughter spectrum for TCIPP at collision energy 8eV.	72
4.23	Optimized daughter spectrum for TCIPP at collision energy 50eV.	72
4.24	Suggested TCIPP daughter fragments.	73
4.25	Optimized daughter spectrum for TDCIPP at collision energy 12eV.	74
4.26	Optimized daughter spectrum for TDCIPP at collision energy 32eV.	74

4.27	Suggested TDCIPP daughter fragments.	75
4.28	Optimized daughter spectrum for TPP at collision energy 24eV.	76
4.29	Suggested TPP daughter fragments.	77
4.30	Optimized daughter spectrum for DCrP at collision energy 22eV.	78
4.31	Suggested DCrP daughter fragments.	79
4.32	Optimized daughter spectrum for TMPP at collision energy 28eV.	80
4.33	Suggested TMPP daughter fragments.	81
4.34	Optimized daughter spectrum for EHDP at collision energy 10eV.	82
4.35	Suggested EHDP daughter fragments.	83
4.36	Alternative EHDP daughter fragments at m/z 344 and m/z 281.	83
4.37	Suggested IDPP daughter fragments.	84
4.38	Suggested BPDP daughter fragments.	85
4.39	Optimized daughter spectrum for TTBPP at collision energy 20eV.	86
4.40	Optimized daughter spectrum for TTBPP at collision energy 64eV.	86
4.41	Suggested TTBPP daughter fragments.	87
4.42	Optimized daughter spectrum for RDP at collision energy 18eV.	88
4.43	Optimized daughter spectrum for RDP at collision energy 40eV.	88
4.44	Optimized daughter spectrum for V6 at collision energy 18eV.	90
4.45	Optimized daughter spectrum for V6 at collision energy 28eV.	90
4.46	Optimized daughter spectrum for V6 at collision energy 50eV.	91
4.47	Suggested V6 daughter fragments.	92
4.48	Optimized daughter spectrum for BPA-BDPP at collision energy 32eV.	93
4.49	Optimized daughter spectrum for BPA-BDPP at collision energy 80eV.	93
4.50	Suggested BPA-BDPP daughter fragments.	94
4.51	Optimized daughter spectrum for BBOEHEP at collision energy 12eV.	95
4.52	Suggested BBOEHEP daughter fragments.	96
4.53	Optimized daughter spectrum for 3OH-BOEP at collision energy 18eV.	97
4.54	Suggested 3OH-BOEP daughter fragments.	98
4.55	Optimized daughter spectrum for DnBP at collision energy 4eV.	99
4.56	Suggested DnBP daughter fragments.	100
4.57	Optimized daughter spectrum for BCEP at collision energy 14eV.	101
4.58	Suggested BCEP daughter fragments.	102
4.59	Optimized daughter spectrum for BCIPP at collision energy 6eV.	103
4.60	Optimized daughter spectrum for BCIPP at collision energy 28eV.	103
4.61	Suggested BCIPP daughter fragments.	104
4.62	Optimized daughter spectrum for BBOEP at collision energy 14eV.	105
4.63	Suggested BBOEP daughter fragments.	106

List of Tables

2.1	OPFR compound, name(abbr.), CAS number, solubility factor, molecular formula and molecular weight for target analytes in this project.	5
2.2	Application and suspected toxic effects for each investigated OPFR. . . .	13
2.3	Overview of previous studies of detection of OPFRs. All studies analyzing foodstuffs are presented, in addition to a few other examples.	17
2.4	Summary of what studies have reported detection of which OPFRs in foodstuffs.	19
3.1	Gradient used for the mobile phase during the UHPLC-MC/MC. A is the aquatic phase(water with 0.1%v/v formic acid), while B is the organic phase(acetonitrile with 0.1%v/v formic acid).	38
3.2	Settings for UPLC-MS/MS analysis of organophosphate flame retardants. .	38
4.1	Relative recoveries of each target analyte from extraction protocol 1 (Appendix A.1) and extraction protocol 2 (Appendix A.2). (*) Indicate not acceptable recoveries, (**) indicate (RB>S), while (***) indicate (RB>MM or SP).	44
4.2	Absolute recoveries of each target analyte from extraction method 1 (Appendix A.1) and extraction 2 (Appendix A.2). (*) indicate recoveries that are not acceptable, either because of low recoveries, extremely high blanks, negative values or missing detection.	45
4.3	Statistics for OPFRs in triplicates of samples spiked prior to sample preparation to concentrations of 10 ppb TA. Mean and median area, standard deviation (STD) and relative standard deviation (RSD%) for absolute and relative values are presented. Calculations for EHDP and TDCIPP is excluded because of negative values as a result of high blank values.	49
4.4	Ion Ratio(IR), Retention time(RT) and Relative retention time(RRT) for target analytes and retention times for the internal standards. – refers to when only one fragment is detected for the compound.	51
4.5	Concentrations of OPFRs in ng/g dw together with the internal standard(IS) used and LOD (ng/g) for each OPFR. For the extraction with DCM:Hex only TEP-d15 showed usable results and was used as IS for all compounds.	52
4.6	SRM transitions for TMP.	56
4.7	SRM transitions for TEP.	58
4.8	SRM transitions for TnPP.	61
4.9	SRM transitions for TnBP.	63
4.10	SRM transitions for TiBP.	65
4.11	SRM transitions for TBOEP.	66
4.12	SRM transitions for TEHP.	68
4.13	SRM transitions for TCEP.	70

4.14	SRM transitions for TCIPP.	73
4.15	SRM transitions for TDCIPP.	75
4.16	SRM transitions for TPP.	76
4.17	SRM transitions for DCrP.	78
4.18	SRM transitions for TMPP.	80
4.19	SRM transitions for EHDP.	82
4.20	SRM transitions for BPDP.	85
4.21	SRM transitions for TTBPP.	87
4.22	SRM transitions for RDP.	88
4.23	Suggested daughter fragments for RDP.	89
4.24	SRM transitions for V6.	91
4.25	SRM transitions for BPA-BDPP.	94
4.26	SRM transitions for BBOEHEP.	95
4.27	SRM transitions for 3OH-BOEP.	97
4.28	SRM transitions for DnBP.	99
4.29	SRM transitions for BCEP.	101
4.30	SRM transitions for BCIPP.	104
4.31	SRM transitions for BBOEP.	105
4.32	Transitions for the OPFRs analyzed found in literature.	108
4.33	Daughter fragments detected in SRM for each analyze. (*) refers to the quantification ion, (**) refers to the confirmation ion and (***) refers to the ions where only one transition was detected with acceptable peaks. . .	111
A.1	Overview of internal standard (IS) and target analyte (TA) addition. . . .	129

Abbreviations

ACN	Acetonitrile
DC	Direct current
DCM	Dichloromethane
d-SPE	Dispersed solid phase extraction
EA	Ethyl acetate
ESI	Electrospray ionizer
FA	Formic acid
GC	Gas chromatography
HPLC	High pressure liquid chromatography
IS	Internal standard
IS-mix	Internal standard mixture
LC	Liquid chromatography
LC-MS	Liquid chromatography mass spectrometry
LC-MS/MS	Liquid chromatography tandem mass spectrometry
LLE	Liquid liquid extraction
LOD	Limit of detection
LOQ	Limit of quantification
ME	Matrix effect
MRM	Multiple reaction monitoring
MS	Mass spectrometry
MS/MS	Tandem mass spectrometry
OPFR	Organophosphorus flame retardants
PBDE	Polybrominated diphenyl ethers
PFAS	Polyfluoraklyl substances
PLE	Pressurized liquid extraction
PP	Poly propylene
RF	Radio frequency
RT	Retention time
RRT	Relative retention time
RSD	Relative standard deviation
SPE	Solid phase extraction
SRM	Selected reaction monitoring
TA	Target analyte
UPLC	Ultra performance liquid chromatography
QqQ	Triple Quadrupole mass analyzer
WWTP	Waste water treatment plants

Compounds

TMP	Trimethyl Phosphate
TEP	Triethyl Phosphate
TnPP	Tri- <i>n</i> -propyl Phosphate
TnBP	Tri- <i>n</i> -butyl Phosphate
TiBP	Triisobutyl Phosphate
TBOEP	Tris(2-butoxyethyl) Phosphate
TEHP	Tris(2-ethylhexyl) Phosphate
TCEP	Tris(2-chloroethyl) Phosphate
TCIPP	Tris(1-chloro-2-propyl) Phosphate
TDCIPP	Tris(1,3-dichloro-2-propyl) Phosphate
TPP	Triphenyl Phosphate
DCrP	Diphenyltolyl Phosphate
TMPP	Tritolyl Phosphate
EHDP	2-Ethylhexyldiphenyl Phosphate
IDPP	Isodecyl Diphenyl Phosphate
BPDP	Tert-Butylphenyldiphenyl Phosphate
TTBPP	Tris(4-tert-butylphenyl) Phosphate
RDP	Tetraphenylrecorcinol bis(diphenyl Phosphate)
V6	2,2-Bis(chloromethyl)-1,3-propandiol bis[bis(2-chloroethyl)] Phosphate
BPA-BDPP	Bisphenol A bis[(diphenyl) Phosphate]
DnBP	Di- <i>n</i> -butyl Phosphate
BCEP	Bis(2-chloroethyl) Phosphate
BCIPP	Bis(2-chloropropyl) Phosphate
BBOEP	Bis(2-butoxyethyl) Phosphate
BBOEHEP	Bis(2-butoxyethyl) hydroxyethyl Phosphate
3OH-TBOEP	Bis(2-butoxyethyl) (2-(3-hydroxybutoxy)ethyl) Phosphate

1 Introduction

Over the past 15 years the production and use of organophosphate flame retardants (OPFRs) in consumer products and plastics have continued to increase (Poma et al., 2018). This comes as a result after polybrominated diphenyl ethers (PBDEs), the previously most used flame retardants, were added to the list of Persistent Organic Pollutants (POPs) by the Stockholm Convention in 2009 (Boer, 2012; Castro-Jiménez et al., 2016). The addition to the POPs list lead to the banning of further production for some PBDEs, and highly restricted production and use for others (Zhao et al., 2019). Even though PBDEs had a known toxicity and high persistence in the environment it took time before they were banned and the phasing out started. The urge for a flame retardant replacement was obvious, and OPFRs were suggested as a good and promising replacement that could meet the increasing demand of flame retardants in the industry (Du et al., 2019). The OPFRs are supposedly a better alternative, still increasing in production volume. Nevertheless, release of OPFRs from the initial product to its environment is likely since the majority of the OPFRs are not covalently bound to the product. The OPFRs are suspected to elicit adverse health effects after prolonged exposure and to be persistent organic pollutants (Castorina et al., 2017; Blum et al., 2019; Li et al., 2019). A broader understanding of the human exposure routes is important to evaluate possible toxic effects.

In addition, no effective way of degradation or adsorption for complete elimination of the OPFRs in the environment exist (Yang et al., 2019). The compounds are even detected in Arctic and Antarctic waters and research on exposure routes and possible toxic effects on humans, animals and environment is needed.

For humans, inhalation of dust was long suspected and accepted to be the main contributor to exposure (Kademoglou et al., 2017). Nevertheless, studies have shown that dietary exposure of OPFRs are comparable with the ingestion from air and dust (Yadav et al., 2017). Research on OPFRs in foodstuffs is limited, and further investigation of these compounds in human dietary products is important to get a better understanding of human exposure of OPFRs. OPFRs can end up in foodstuffs by different routes, either by migration from food packaging, from instruments during food production, during storage, or processing (Wei et al., 2015; Ding et al., 2018; Poma et al., 2018).

For children and infants it is especially important to know if OPFRs are present in their foods. Research indicates that early life exposure of OPFRs can affect development of children in a variety of non-beneficial ways (Doherty et al., 2019).

The main aim of this thesis was supposed to be determination and quantification of OPFRs in a variety of baby foods. As a result of the SARS-CoV-2 outbreak, and the following closing of the university, the experimental work was significantly limited. The focus of the project has therefore been aimed more towards development of extraction techniques for OPFRs from complex matrices. Proposing structures for detected daughter fragments from the MS, and understanding how they break down has also become a major part of the practical work. This can be helpful in understanding how the OPFRs break down in nature and to some degree how they are metabolized. The theoretical part of the report remains somewhat similar as if the experimental work was carried out completely.

2 Theoretical Background

2.1 Flame retardants

Flame retardants are chemicals added to different materials to prevent fire and ignition during both production and use of materials or consumer products (Blum et al., 2019; van der Veen and de Boer, 2012). In addition, they minimize and delay spread of already started fires. To meet a continuously increasing industry, and to fulfil stringent safety standards, flame retardants are used more and more. The global consumption of flame retardants are expected to exceed 3.1 million tonnes by 2023, compared to a production of 1.7 million tonnes in 2008 (The Freedonia Group, 2011; McWilliams, 2018). Increased production often implicates increased exposure, and research on how the flame retardants spread, as well as the effects on humans and environment, is needed. Many halogenated flame retardants have proven persistent properties and have been in the spotlight and of concern for human and environmental health for over 40 years (van der Veen and de Boer, 2012). As OPFRs are considered an option for the phased out PBDEs, it is important that the OPFRs are less persistent and toxic than its precursor (van der Veen and de Boer, 2012).

Flame retardants act differently, and most of the phosphorus containing flame retardants works by counteracting the fire in the solid phase of the selected material. Still some may have a mechanism of action in the gas phase (van der Veen and de Boer, 2012). This means that the flame retardants either suppress chemical reactions in the actual flame, or are forming a layer protecting the surface of the material from heat and oxygen to reduce flammability (Speight and Speight, 2017).

2.2 Organophosphate flame retardants

OPFRs are classified as persistent organic chemicals (Castorina et al., 2017). They have a variety of beneficial properties as plasticizers and flame retardants, and are therefore used in everything from plastic, food packaging, furniture and electronics, to paint, lubricants, hydraulic fluids and building materials (Ding et al., 2018; Li et al., 2019; Marklund et al., 2005).

The OPFRs have a variety of different physical and chemical properties that make them behave different in the environment, and also to have different degrees of toxicity. When assessing the risks of OPFRs in humans and the environment, important factors to take into account are solubility, the octanol-water coefficient ($\log K_{ow}$), and vapour pressure.

The OPFRs treated in this project are mainly the additive type and are presented in Table 2.1. For the metabolites, chromatograms were only obtained for BBOEHEP and 3OH-BOEP, but fragmentation is predicted for all metabolites in Table 2.1 as MS-spectra were provided. The same accounts for BPDP.

In general the OPFRs are metabolized rather quickly in animals and humans, and establishing risks of metabolites and the compound itself is important (Bruchajzer et al., 2015). TEP (triethyl phosphate), TBP (tributyl phosphate) and TCEP (tri(2-chloroethyl)phosphate) are examples of more volatile OPFRs, that easier than heavier OPFRs, tend to discharge into the air and deposit on dust (Yang et al., 2019). Chlorinated OPFRs have, in addition to proposed carcinogenic effects, shown to be water soluble and therefore also posing a threat to aquatic environment and animals. Heavier OPFRs, like alkyl OPFRs and aryl OPFRs are more hydrophobic and have a greater affinity to soil and sediment (Yang et al., 2019). It is also stated that aryl OPFRs like TPP have a greater probability of causing adverse toxic effects than alkyl OPFRs (Du et al., 2015).

Table 2.1: OPFR compound, name(abbr.), CAS number, solubility factor, molecular formula and molecular weight for target analytes in this project.

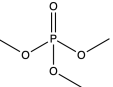
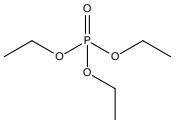
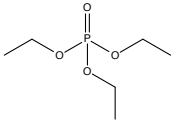
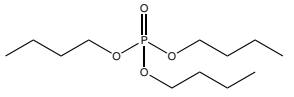
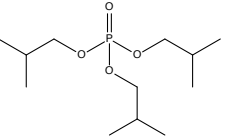
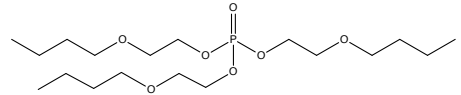
Structure	Name	CAS number	Log K_{ow}	Molecular formula	Molecular weight (g mol ⁻¹)
	Trimethyl Phosphate (TMP)	512-56-1	-0.60	C ₃ H ₉ O ₄ P	140.07
	Triethyl Phosphate (TEP)	78-40-0	0.87	C ₆ H ₁₅ O ₄ P	182.15
	Tri- <i>n</i> -propyl Phosphate (TnPP)	513-08-6	2.35	C ₁₉ H ₂₁ O ₄ P	224.23
	Tri- <i>n</i> -butyl Phosphate (TnBP)	126-73-8	3.82	C ₁₂ H ₂₇ O ₄ P	266.31
	Triisobutyl Phosphate (TiBP)	126-71-6	3.60	C ₁₂ H ₂₇ O ₄ P	266.31
	Tris(2-butoxyethyl) Phosphate (TBOEP)	78-51-3	3.00	C ₁₈ H ₃₉ O ₇ P	398.47

Table 2.1 continued from previous page

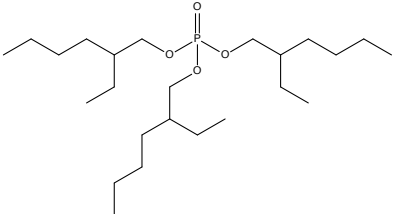
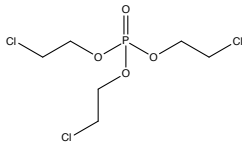
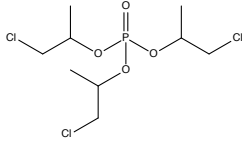
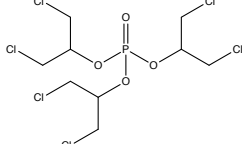
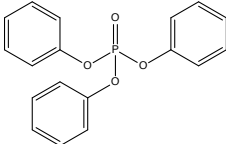
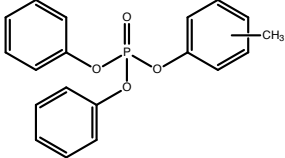
Structure	Name	CAS number	Log K_{ow}	Molecular formula	Molecular weight (g mol ⁻¹)
	Tris(2-ethylhexyl) Phosphate (TEHP)	78-42-2	9.49	C ₂₄ H ₅₁ O ₄ P	434.63
	Tris(2-chloroethyl) Phosphate (TCEP)	115-96-8	1.63	C ₆ H ₁₂ Cl ₃ O ₄ P	285.49
	Tris(1-chloro-2-propyl) Phosphate (TCIPP)	13674-84-5	2.89	C ₉ H ₁₈ Cl ₃ O ₄ P	327.57
	Tris(1,3-dichloro-2-propyl) Phosphate (TDCIPP)	13674-87-8	3.65	C ₉ H ₁₅ Cl ₆ O ₄ P	430.90
	Triphenyl Phosphate (TPP)	115-86-6	4.70	C ₁₈ H ₁₅ O ₄ P	326.28
	Diphenyltolyl Phosphate (DCrP)	26444-49	5.25	C ₁₉ H ₁₇ O ₄ P	340.32

Table 2.1 continued from previous page

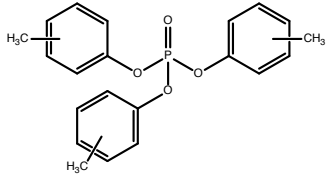
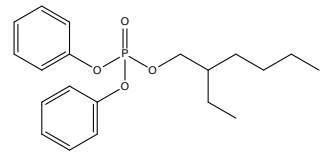
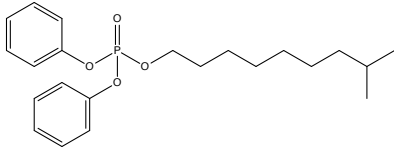
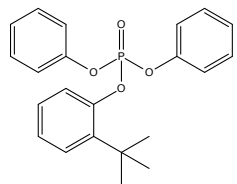
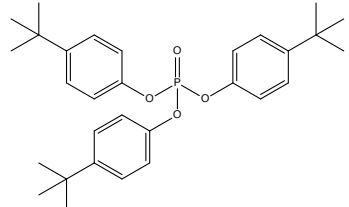
Structure	Name	CAS number	Log K_{ow}	Molecular formula	Molecular weight (g mol ⁻¹)
	Tritolyl Phosphate (TMPP)	1330-78-5	6.34	C ₂₁ H ₂₁ O ₄ P	368.37
	2-Ethylhexyldiphenyl Phosphate (EHDP)	1241-94-7	6.30	C ₂₀ H ₂₇ O ₄ P	362.40
	Isodecyl Diphenyl Phosphate (IDPP)	29761-21-5	7.28	C ₂₂ H ₃₁ O ₄ P	390.46
	Tert-Butylphenyldiphenyl Phosphate (BPDP)	56803-37-3	6.61	C ₂₂ H ₂₃ O ₄ P	382.40
	Tris(4-tert-butylphenyl) Phosphate (TTBPP)	78-33-1	10.43	C ₃₀ H ₃₉ O ₄ P	494.60

Table 2.1 continued from previous page

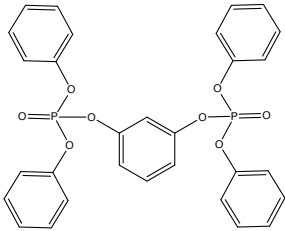
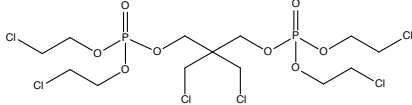
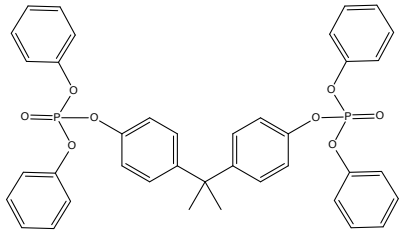
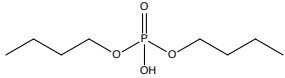
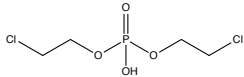
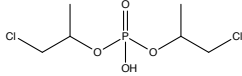
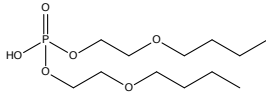
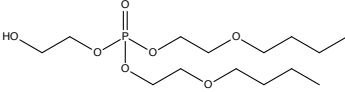
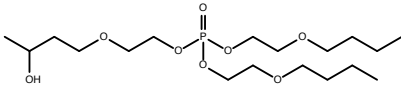
Structure	Name	CAS number	Log K_{ow}	Molecular formula	Molecular weight (g mol ⁻¹)
	Tetraphenylrecorcinol bis(diphenyl Phosphate) (RDP)	57583-54-7	7.41	C ₃₀ H ₂₄ O ₈ P ₂	574.45
	2,2-Bis(chloromethyl)-1,3-propanediol bis[bis(2-chloroethyl)] Phosphate (V6)	38051-10-4	3.31	C ₁₃ H ₂₄ Cl ₆ O ₈ P ₂	582.99
	Bisphenol A bis[(diphenyl) Phosphate] (BPA-BDPP)	5945-33-5	4.5	C ₃₉ H ₃₄ O ₈ P ₂	692.63
<i>Metabolites</i>					
	Di- <i>n</i> -butyl Phosphate (DnBP)	107-66-4	2.29	C ₈ H ₁₉ O ₄ P	210.21
	Bis(2-chloroethyl) Phosphate (BCEP)	3040-56-0	0.83	C ₄ H ₉ Cl ₂ O ₄ P	222.99

Table 2.1 continued from previous page

Structure	Name	CAS number	Log K_{ow}	Molecular formula	Molecular weight (g mol ⁻¹)
	Bis(2-chloropropyl) Phosphate (BCIPP)	789440-10-4	–	C ₆ H ₁₃ Cl ₂ O ₄ P	251.04
	Bis(2-butoxyethyl) Phosphate (BBOEP)	14260-97-0	1.74	C ₁₂ H ₂₇ O ₆ P	298.31
	Bis(2-butoxyethyl) hydroxyethyl Phosphate (BBOEHEP)	1477494-86-2	–	C ₁₄ H ₃₁ O ₇ P	342.37
	Bis(2-butoxyethyl) (2-(3-hydroxybutoxy)ethyl) Phosphate (3OH-BOEP)	1477494-87-3	–	C ₁₈ H ₃₉ O ₈ P	414.47

2.2.1 Characteristics

Three main groups of phosphorus flame retardants can be defined. These include inorganic, organic and halogen containing phosphorus flame retardants. Some of the OPFRs are not only used as flame retardants but also as plasticizers (Wei et al., 2015). The organic phosphorus flame retardants can further be categorized based on their general structure. Figure 2.1 show these three general structures, the phosphinates, the phosphonates and the organophosphate esters (Fu et al., 2017).

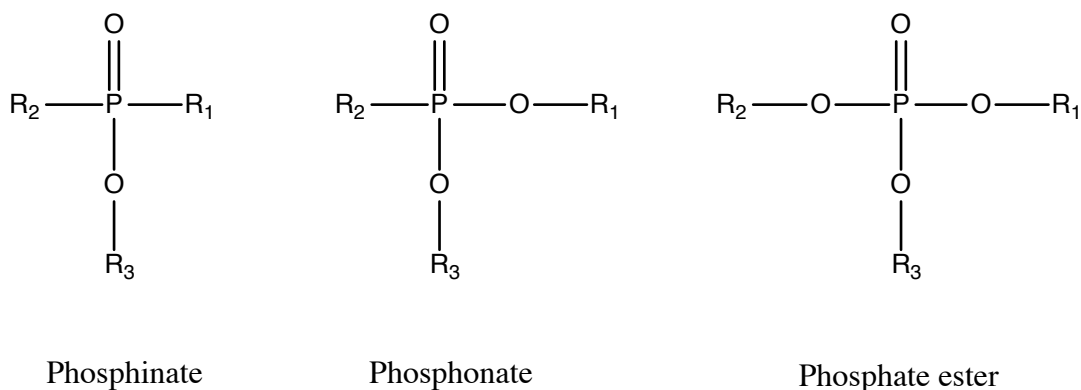


Figure 2.1: General structure of organophosphate flame retardants

The OPFRs can further be recognized as a reactive component or as additives (Weil and Levchik, 2017). A reactive component refers to OPFRs that are chemically bonded into a polymer, whereas the additive OPFRs are mixed into a polymer and not chemically bound. The reactive OPFRs have limited release during the lifetime of the product, while the additives may easier leach from the product and spread into the environment by leaching, abrasion or volatalization (van der Veen and de Boer, 2012; Marklund et al., 2005). Factors like time, temperature, pH, pressure and UV-light are all factors that can induce release of OPFRs. Migration from finished products is nevertheless only one of the pathways the OPFRs might use to reach humans and environment.

2.2.2 History and use

As the production of electronics and plastics drastically increased from the 1960s, the demand for plasticizers and flame retardants followed the exponential production growth. The use of flame retardants have continued to increase following the the increase in general industry and production. As a result of this the organophosphate esters (OPEs) are

considered high production-volume chemicals (Reemtsma et al., 2008).

The use of organophosphates as flame retardants and plasticizers is not new, and they have been used in consumer products since the 1940s (Muir, 1984). The compounds have also been of toxicological interest with studies regarding bio-accumulation and degradability since the late 1970s (Reemtsma et al., 2008; Du et al., 2019). Nevertheless, not much research on this was performed before the increasing usage and high environmental concentrations were reported (Du et al., 2019). Several studies on the pathways for release and the toxicological effects of the different OPFRs have been performed, but more research on this is still needed and desired (Du et al., 2019).

2.2.3 Human and environmental exposure and effects

As OPFRs are used a lot in industry, and in consumer products and plastics, continuous exposure to these flame retardants is both likely and probable. OPFRs have been detected and documented in a variety of different environments including air, water, soil, sediment, indoor dust, marine environments, freshwater biota, blood, urine and breast milk (Du et al., 2019; Marklund et al., 2003; Wang and Kannan, 2018; Saillenfait et al., 2018; Gibson et al., 2019). The compounds can end up exposing humans and environments by migration directly from products with the compounds incorporated, or from leakage and runoff from waste water treatment plants (WWTP), household discharge and industry (Cristale et al., 2016; Meyer and Bester, 2004; Wolschke et al., 2015).

Organophosphate pesticides are known to be neurotoxic. The OPFRs have in laboratories demonstrated neurotoxicity, and this, in combination with the structural similarities between the pesticides and flame retardants, is raising concerns about the toxicity of the OPFRs (Gibson et al., 2019). Human epidemiological studies have also been carried out, and exposure of OPFRs have been suspected to have a variety of adverse effects. Amongst these, WHO have reported neurotoxic effects as a result of exposure to TCEP, TnBP and TPP (Wei et al., 2015). TPP has also proven endocrine disrupting effects and TCEP has shown toxic effects in brain and kidney (Patisaul et al., 2013; Matthews et al., 1993). Other suspected effects as reproductive toxicity, carcinogenic effect, affected neurodevelopment and endocrine disruption can occur as a result of prolonged exposure and accumulation of the different OPFRs over time (Li et al., 2019; Dishaw et al., 2011;

Castorina et al., 2017). The interest and urge for more research on mapping the human and environmental exposure and accumulation is obvious and beneficial for both human and environmental health. It is worth mentioning that different OPFRs may cause very different effects. As an example, chlorinated OPFRs are more likely to be carcinogenic and persistent than the non-chlorinated OPFRs, while at the same time being more resistant to biodegradation. EHDP on the other hand, is approved for use in food packaging (Wei et al., 2015; Blum et al., 2019; Reemtsma et al., 2008).

A summary of the applications and suspected toxic effects for the OPFRs investigated in this project is presented in Table 2.2.

In conclusion RDP, BPA-BDPP and V6 are suggested to be the most suitable substitutes for the PBDEs, as well as TCEP and TCPP.

Table 2.2: Application and suspected toxic effects for each investigated OPFR.

Compound	Applications	Suspected toxic effects	References
TMP	Flame retardant, stabilizer, antioxidant	Neurotoxicity, reproductive toxicity, carcinogenic	European Chemical Agency (2020e)
TEP	Plasticizers, PVC, polyester resins, polyurethane foam	Adaptive liver response (Suspected only at very high direct doses)	European Chemical Agency (2020c) van der Veen and de Boer (2012) Wei et al. (2015) Sheftel (2000) Gumbmann et al. (1968)
ThPP	Plasticizer, floor covering, industrial processes	<i>No data</i>	European Chemical Agency (2020f)
ThBP	Plasticizer, hydraulic fluid, floor finish wax, lacquer, paint, glue, industrial processes, anti-foam agent	Neurotoxicity, carcinogenic	European Chemical Agency (2020b) van der Veen and de Boer (2012) Wei et al. (2015) Sheftel (2000) Berdasco and McCready (2011)
TiBP	Plasticizers, lubricant, concrete	<i>No data</i>	European Chemical Agency (2020d) van der Veen and de Boer (2012) Wei et al. (2015)
TBOEP	Flame retardant, plasticizer, hydraulic fluids, floor finish, wax, lacquer, paint, glue, rubber, anti-foam agent	Carcinogenic, reproductive toxic effects	Liu et al. (2012) van der Veen and de Boer (2012) Wei et al. (2015) Wang and Kannan (2018) Sheftel (2000)
TEHP	Flame retardant, plasticizer, fungus resistance, cellulose, paint, rubber, polyurethane foam	<i>Limited knowledge</i>	Du et al. (2019) van der Veen and de Boer (2012) Wei et al. (2015)
TCEP	Flame retardant, plasticizers, paint, glue, industrial processes, polyurethane foam	Carcinogenic, neurotoxicity, toxic effects in brain and kidney, endocrine disruption, reproductive toxicity	Yang et al. (2019) European Chemical Agency (2020h) Du et al. (2019) van der Veen and de Boer (2012) Wei et al. (2015) Wang and Kannan (2018) Kademoglou et al. (2017)
TCIPP	Flame retardant, plasticizers	Carcinogenic, neurotoxicity, endocrine disruption	Yang et al. (2019) European Chemical Agency (2020g) Liu et al. (2012) Du et al. (2019) van der Veen and de Boer (2012) Wei et al. (2015) Wang and Kannan (2018) Kademoglou et al. (2017)

Table 2.2 continued from previous page

Compound	Applications	Suspected toxic effects	References
TDCIPP	Flame retardant, plasticizers, paint, glue, lacquer polyurethane foam	Carcinogenic, neurotoxicity, endocrine disruption, developmental toxicity	Yang et al. (2019) Liu et al. (2012) Du et al. (2019) van der Veen and de Boer (2012) Wei et al. (2015) Wang and Kannan (2018) Cooper et al. (2011) Kademoglou et al. (2017)
TPP	Flame retardant, plasticizer, PVC, hydraulic fluids, lacquer, paint, glue, synthetic polymers polyurethane foam	Neurotoxicity, endocrine disruption, cardiotoxicity, developmental toxicity, reproductive toxic effects	Liu et al. (2012) Du et al. (2019) van der Veen and de Boer (2012) Wei et al. (2015) Cooper et al. (2011) Schang et al. (2016) Kademoglou et al. (2017)
DCrP	Flame retardant, textile coating, PVC, lubricants, adhesives, thermoplastics polyurethane	Minimal effects detected, <i>need more research</i>	European Chemical Agency (2020a) Brooke (2009) Hartwig and Commission (2016)
TMPP	Plasticizers, PVC, hydraulic fluids, cellulose, cutting oils, transmission fluids	Carcinogenic Neurotoxicity, endocrine disruption, reproductive toxicity, bioaccumulative	van der Veen and de Boer (2012) Wei et al. (2015) Schang et al. (2016)
EHDP	Flame retardant, plasticizers, food packaging, rubber, paint, rubber, photo films, adhesives hydraulic fluid	Toxic to aquatic organisms, approved for use in food packaging	Wei et al. (2015) Ballesteros-Gómez et al. (2015a) Schang et al. (2016)
IDPP	Plasticizer, flame retardant, PVC synthetic rubber, textiles, pigments toys, culinary products	Disrupting steroid production, cytotoxicity, male reproductive health	van der Veen and de Boer (2012) Schang et al. (2016) Kademoglou et al. (2017)
BPDP	Plasticizer, flame retardant	Lack of toxicological data	Schang et al. (2016)
TTBPP	Flame retardant	<i>Limited knowledge</i>	Guan et al. (2019)
RDP	Flame retardant, engineering plastics, electronics, PVC, paint	Non mutagenic, endocrine disruption	Ballesteros-Gómez et al. (2015b)
V6	Plasticizer, electronics	Increased thyroid weight	van der Veen and de Boer (2012)
BPA-BDPP	Plasticizer, electronics	Non mutagenic, minimal effect	van der Veen and de Boer (2012)

It is nevertheless important to state that the toxic effects presented in Table 2.2 are only suspected toxic effects based on studies on human cells and animals, and that as stated in Li et al. (2019) there is not enough studies on the toxicological effects to conclude with

the long term toxic effects OPFRs may have on humans. The degree of toxicity will also vary with dose and length of exposure.

2.2.4 Study population: Baby foods

As OPFRs are used in both production halls and in food packaging, the probability of OPFRs migrating to the food itself is evident. It is stated that OPFRs from foodstuffs contributes to human exposure of OPFRs (Wang and Kannan, 2018; Hou et al., 2016). Since small children are more easily affected, baby foods are of special interest. It is also indicated that early life exposure of OPFRs can have neurodevelopmental effects, affecting both behavioural and cognitive development (Doherty et al., 2019). Migration of the OPFRs from initial product to foodstuffs can happen during food production, processing (e.g. canning, packing) or during storage (Wei et al., 2015; Ding et al., 2018; Poma et al., 2018).

2.3 Previous studies

OPFRs have frequently been detected in air, dust, water and sediments, and human exposure from these matrices are well understood. Over the last years foodstuffs as a pathway for human exposure to OPFRs have been of increasing interest. Some OPFRs have been detected in a variety of foodstuffs over the last years, but research is still limited, and more knowledge is needed to outline the possible pathways for human exposure.

All studies found on determination and quantification of OPFRs in foodstuffs are summarized in Table 2.3. In Table 2.4 the OPFRs investigated by each study is summarized. It is evident that some OPFRs are more researched and detected than others. No studies reported investigation or detection of TTBPP, V6, BPA-BDPP or RDP in foodstuffs.

Zhang et al. (2016) detected six OPFRs in foodstuffs from China, including 75 common foods and 50 rice samples. The detected concentrations were varying from 0.004 ng/g to 287 ng/g. The amount of the different OPFRs detected sorted from most abundant is given as TCEP > TCIPP > TPP > TEHP > TBOEP > TDCIPP.

The detected order from most to least abundant of the OPFRs investigated in Zhao et al. (2019) is given as EHDP > TEP > TCEP > TCIPP > TPP > TEHP > TNBP

> TBOEP > TMPP, while the three most abundant OPFRs detected in foodstuffs and food packaging in Wang and Kannan (2018) are TBOEP > TnBP > TCIPP.

In Poma et al. (2018) the OPFRs were detected in order TPP > TCIPP > EHDP > TDCIPP > TEHP > TnBP > TCEP, while their previous study, Poma et al. (2017), detected OPFRs in foodstuffs in order EHDP > TPP > TDCIPP > TCEP > TCIPP, while TEHP, TnBP and TBOEP not was detected in the foodstuffs investigated.

All OPFRs investigated showed concentrations below LOQ in Xu et al. (2015). Nevertheless, the concentrations of TCEP > TPP even though TPP was more frequently detected.

TBOEP, TnBP, and TCIPP are the most abundant and common OPFRs to find in foodstuffs (Wang and Kannan, 2018). EHDP is allowed for use in food packaging so this may be a reason to expect detection of the compound, and why EHDP was the most abundant OPFR in Zhao et al. (2019).

TBOEP was not detected in Poma et al. (2017), and was one of the least detected in Zhao et al. (2019) and Zhang et al. (2016), while it was one of the most abundant OPFRs in Wang and Kannan (2018). Trends show that TCIPP is one of the most abundant OPFRs detected in all studies on foodstuffs except in Poma et al. (2017). As of now, Wang and Kannan (2018) has reported detection of the most OPFRs, having reported detection of 15 different OPFRs.

Table 2.3: Overview of previous studies of detection of OPFRs. All studies analyzing foodstuffs are presented, in addition to a few other examples.

Sample matrix	Analytical technique	Sample preparation/ solvents	Clean up	Column/ mobile phase	Parameters	Reference
Foodstuffs	GC-EI-MS	LLE with ACN d-SPE with QuE Z-Sep	SPE/Florisil -> DCM:Hex (1:1 v/v) and EtAc. Reconstituted in iso-octane:toluene(9:1) and iso-octane:EtAc(8:2)	HT-8 column (25 m x 0.22 mm, 0.25 μ m) He	R%: 33-71 % LOQ: 0.05-3 ng/g ww	Poma et al. (2017)
Foodstuffs	GC-EI-MS	UVAE/ MeCN:toluene (9:1)	SPE/Florisil ->MeCN -> Z-SEP/C18 ->d-SPE ->APS-> DCM:Hex	DB-5 column (15 m x 0.25 mm, 0.10 μ m) He	R%: 66-135 % RSD: 1-24 % LOQ: 1.4-3.6 ng/g dw	Xu et al. (2015)
Foodstuffs (Focus on rice)	GC-MS/MS(QqQ)	Food: Microwave-assisted extraction Acetone:Hex (1:1 v/v) Beverages: Ultrasonication Ethyl acetate	Reconstituted in iso-octane:EtOAc(1:1) SPE/Florisil eluted in Acetone:EtAc (3:7 v/v)	HP-5 capillary column (15 m x 250 μ m, 0.25 μ m)	R%: 97 \pm 13 % (rice) 53 \pm 14 % (foodstuffs) $R^2 > 0.99$	Zhang et al. (2016)
Foodstuffs (Only study with baby food included)	GC-EI-MS/MS(QqQ)	SLE/Acetone	Concentrated and reconstituted in <i>n</i> -Hex before Florisil (EtAc:n-Hex)	Zebtron semivolatile column (20 m x 0.18 mm, 0.18 μ m)	LOQ: 0.001-61.97 ng/g ww Blank: 1.6 pg/g -21.1 ng/g	Poma et al. (2018)
Foodstuffs (Including food packaging)	HPLC-ESI(+)-MS/MS(QqQ)	QuEChERS/ACN	Reconstituted in iso-octane:EtAc(8:2) d-SPE/reconstituted in Water:MeOH (4/6 v/v)	A Betasil C18 column (100 mm x 2.1 mm, 5 μ m)	$R^2 > 0.99$ LOD: 0.01-0.17 ng/g ww R%: 51.2-137 %	Wang and Kannan (2018)
Foodstuffs	UPLC-ESI(+)-MS/MS	QuEChERS/ACN	d-SPE/reconstituted in MeOH	Waters BEH C18 (2.1 mm x 100 mm, 1.7 μ m) VanGuard precolumn (C18, 2.1 mm x 5 mm, 1.7 μ m)	R%: 73-106% LOQ: 0.05-0.42 ng/g fw Blank: 0.18-4.4 ng/mL	Ding et al. (2018)
Milk powder	UPLC-ESI(+)-MS/MS	QuEChERS different solvents tested: ACN, ACN/0.5%FA(v/v), ACN/MeOH (3:1, v/v), 0.5%FA/ACN/MeOH(3:1, v/v) ACN/toluene (3:1, v/v)	PSA, GCB, C18	Different columns tested Phenomenex Kinetex PFP (50 mm x 3.5 mm, 2.6 μ m) Acquity UPLC BEH Phenyl (100 mm x 2.1 mm, 1.7 μ m) Acquity UPLC BEH C18 (100 mm x 2.1 mm, 1.7 μ m)	$R^2 > 0.99$ LOD: 0.1-0.25 ug/kg R%: 73.5-110.2%	Guo et al. (2016)
Foodstuffs	UPLC-APCI(+)-MS/MS	LLE with ultrasonication and centrifuging	d-SPE/reconstituted in MeOH	Waters Cortecs C18 column (50 mm x 2.1 mm, 1.6 μ m) Water:MeOH	LOQ: 0.01-0.36 ng/g ww R%: 40.8-135.9%	Zhao et al. (2019)
Yellow eel (freshwater)	GC/EI-MS	DCM:Hex (50:50 v/v) Ultrasonication and centrifuging Hex:Acetone (3:1, v/v)	SPE/Florisil eluted in EtAc Reconstituted in iso-octane			Malarvannan et al. (2015)

Table 2.3 continued from previous page

Sample matrix	Analytical technique	Sample preparation/ solvents	Clean up	Column/ mobile phase	Parameters	Reference
Fish	GC-FPD	PLE(pressurized liquid extraction) Water:ACN (90:10)	SPME(solid phase microextraction)	HP-5 capillary column (30 m x 0.32 mm, 0.25 μ m) He	$R^2 > 0.99$ LOD: 0.010-0.208 ng/g R%: 79.8-107.3 %	Gao et al. (2014)
Egg and liver	UPLC-MS/MS-APCI(+)	Ultrasonic extraction DCM:Hex (50:50 v/v)	d-SPE/reconstituted in MeOH	Waters Cortecs™ UPLC® C18 column (50 mm x 2.1 mm, 1.6 μ m)	LOQ: 0.06-0.29 ng/g (egg) 0.05-0.50 ng/g (liver) R%: 54-113 % $R^2 > 0.99$	Chu and Letcher (2015)
Dust	HPLC-ESI(+)-MS/MS	Ultrasonic extraction Acetone:toluene (1:1 v/v)	SPE/Acetone:toluene (1:1 v/v) reconstituted in MeOH	Luna C18 Phenomenex (150 mm x 3 mm, 3 μ m)		Brandsma et al. (2013b)
Fish	LC-QqLIT-MS	Ultrasonic extraction Acetone:hexane (1:1)	SPE/C18 and alumina cartridge	Purosphere Star RP-18 (125 mm x 2.0 mm, 5 μ m) Luna C18 Phenomenex guard column	LOD:0.34–11.6 ng/g lw LOQ: 1.12–38.8 ng/g lw R%: 45-115	Santín et al. (2016)
Sediment, sludge and dust	GC-EI-MS/MS	Ultrasonic extraction Ethyl acetate/cyclohexane (5:2, v/v)	SPE/Florisil Reconstituted in toluene	PDB-5MS (15 m x 0.25 mm, 0.10 μ m)	LOD: 1.9-60 μ g/kg (dust) 28-575 μ g/kg (sludge) 3.8-288 μ g/kg (dust) R%: 48-107 (dust) R%: 64 to 131 (sludge) R%: 78-108 (dusy)	Cristale and Lacorte (2013)
Herring gull eggs	LC-ESI(+)-MS/MS(QqQ)	Accelerated solvent extraction DCM:Hex (50:50)	SPE (DCM:Hex) reconstituted in methanol	Waters Xterra® phenyl column (2.1 mm x 100 mm, 3.5 μ m)	LOD:0.01 to 0.12 ng/mL LOQ: 0.06 to 0.20 ng/g R%: 89-104	Chen et al. (2012)

Table 2.4: Summary of what studies have reported detection of which OPFRs in foodstuffs.

Reference/ Compound	TMP	TEP	TnPP	TnBP	TiBP	TBOEP	TEHP	TCEP	TCIPP	TDCIPP	TPP	TMPP	DCrP	EHDPP	IDPP
Poma et al. (2017)						x	x	x	x	x	x			x	
Xu et al. (2015)			x	x			x	x		x	x			x	
Zhang et al. (2016)						x	x	x	x	x	x				
Poma et al. (2018)			x	x			x	x	x	x	x			x	
Wang and Kannan (2018)	x	x	x	x	x	x	x	x	x	x	x	x	x	x	x
Ding et al. (2018)	x	x		x		x	x	x	x	x	x		x		
Guo et al. (2016)	x	x		x		x	x	x	x		x		x		
Zhao et al. (2019)		x		x		x	x	x	x		x		x	x	

2.4 Analytical techniques

LC-ESI(+)-MS/MS has shown great results in detecting and quantification of organophosphorus flame retardants and is therefore the preferred method in this project (Chen et al., 2012; Yang et al., 2019). Before analyzing in UPLC, sample preparation needs to be performed. Samples from different matrices require different extraction processes, and the complexity of the matrices often makes this step a challenge. An overview of previous studies and the analytical techniques used are shown in Table 2.3.

2.4.1 Sample preparation

The aim of the sample preparation is to make a sample suitable for analysis by separating the target analytes from the matrix of the sample. The physical and chemical properties of both the matrix, and the target analytes, are important to take into consideration when choosing a sample preparation technique and what solvents to use (Pavlović et al., 2007). In modern analytical chemistry the extraction process can be one of the major challenges of analysis. Often because the target analytes are mixed in a complex matrix. It is nevertheless a very important step to perform sample analysis correctly. A variety of extraction techniques exist including liquid-liquid extraction (LLE), solid-liquid extraction (SLE) and solid-phase extraction (SPE) amongst others. (Lundanes, 2014)

Liquid-liquid extraction is an extraction technique where two immiscible solvents are used to transfer the targeted analytes into one of the solvent phases. Usually one of the phases is aqueous and the other is an organic non-polar solvent. Mixing and phase separation is as in all extraction processes important in LLE (Berk, 2018). Advantages of LLE includes it being easy to implement, and inexpensive (Humbert et al., 2014). All methods have its disadvantages, and for LLE this includes it being difficult to automate, and therefore time-consuming when analyzing large amounts of samples. Another inconvenience is the use of toxic solvents which is not uncommon, and that highly polar compounds can be difficult to extract. (Humbert et al., 2014)

For the extraction of OPFRs a variety of extraction techniques are presented in literature. In Brandsma et al. (2013a) several extraction techniques from different studies are presented, showing that LLE supported by ultrasonication is a commonly used technique,

often followed up by a clean-up step where use of SPE with a Florisil column was most frequently used. This can be seen in Table 2.3 where almost all studies used a form of filtration as a clean-up step. It is nevertheless also pointed out that use of filtration as a clean-up step may add an extra possibility for contamination.

2.4.2 Liquid chromatography

The ability to separate different analytes in a mixture is crucial to perform analysis in analytical chemistry, and liquid chromatography (LC) is the most widely used technique (Snyder and Dolan, 2017). There exists a variety of different liquid chromatography techniques and the most modern and used techniques today are High Performance Liquid Chromatography (HPLC) and Ultra High Performance Liquid Chromatography (UHPLC) (Lundanes, 2014). The popularity of liquid chromatography comes, amongst other things, from the technique being very versatile (Lores et al., 1999). Both food, environmental, pharmaceutical, cosmetic, biological and drug analysis are examples of LC applications (Niessen, 2006).

The basic principle behind this technique is utilizing the analytes' different affinity, and often polarity and weight, to a stationary phase of a column versus a mobile phase that flows through the column. This will separate the analytes, and thereby give them different retention times (RT) through the column (Lundanes, 2014; McMaster, 2005). UHPLC/HPLC is different than the original LC by including, and being able to analyze, smaller particles. Smaller particles have considerably larger surface area compared to volume, and higher pressure is needed to pump the mobile phase through the column. This made the technique both more efficient and giving more precise results in higher resolution. UHPLC can tolerate even higher pressure, smaller particles, and use shorter columns that is contributing to make the instrument even more effective and precise. Nevertheless, an instrument with higher pressure and higher sensitivity needs to be more robust and costs more. (Lundanes, 2014; McMaster, 2007)

2.4.3 Liquid chromatography coupled to Mass spectrometer (LC-MS/MS)

Liquid chromatography (LC) and mass spectrometry (MS) is frequently coupled together to optimize the analysis and thereby combine the physical separation from the LC, and

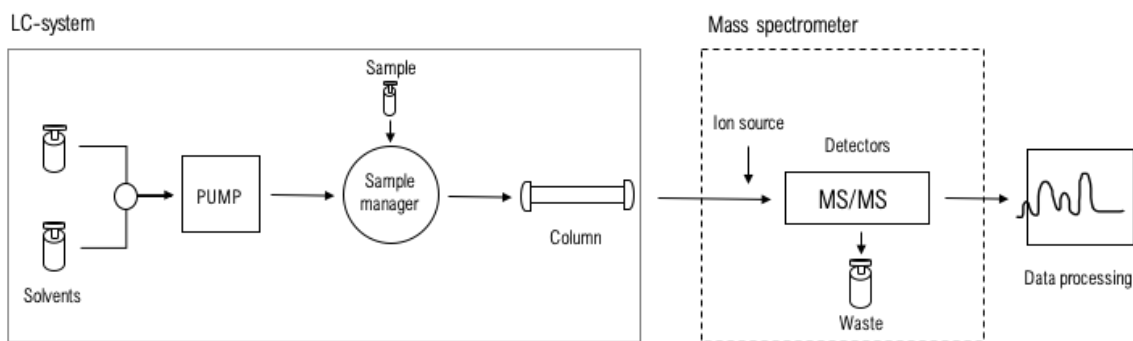


Figure 2.2: Schematic description of the LC-MS/MS instrument. Reproduced from Giri (2020).

the mass and structural analysis from the MS. This combination provides detailed data, making it possible to both qualify and quantify different compounds and their ions. The use of MS/MS in analysis is favorable because it enhances the noise suppression and minimizes the matrix interference. This comes as a result of the selection, collision and fragmentation of molecules in the quadrupoles in the instrument. UHPLC is more effective and less time consuming than regular LC and HPLC. This makes UHPLC-MS/MS a great combination instrument obtaining good resolution of peaks and both qualitative and quantitative information with very low limits of detection (LOD) and limits of quantification (). (Lundanes, 2014; McMaster, 2005; Van De Steene and Lambert, 2008; Skoog et al., 2003). A brief representation of the instrumentation of LC-MS/MS is presented in Figure 2.2.

2.4.4 Mass spectrometry

Mass spectrometry (MS) is a powerful analytical tool that is used to determine which ions are present in the sample. This is performed by measuring the mass to charge ratio of one or more analytes in a sample. Tandem mass spectrometry MS/MS combines two mass analyzers resulting in increased sensitivity. In addition to measure molecular weight, the MS/MS can identify characteristic fragments of the specified molecule by fragmenting the precursor ion. (Barceló and Petrovic, 2007; McMaster, 2005)

The mass spectrometer consists of three main components. First an ion source to ionize the molecules is needed. A mass analyzer to detect the ionized molecules comes next, before an ion detection system is necessary. When the ions pass through these components,

vacuum is obtained and the compounds are vaporized to ensure the ions pass through the system effectively without interference (Watson and Sparkman, 2007).

When using tandem MS (MS/MS), different application modes can be utilized. Selected reaction monitoring (SRM) is a targeted spectrometry technique that works like a filter where a chosen mass ion is selected to go through fragmentation and only a selected fragment is detected further (de Hoffmann, 1996). If the system is set to detect two or more daughter ions the term multiple reaction monitoring is used (MRM) (McMaster, 2005). The triple quadrupole analyzer (QqQ) is an example of an analyzer suited for SRM and MRM.

For organophosphate flame retardants, previous studies have indicated that GC-MS may have limited selectivity in complex matrices compared to LC-MS methods when determining OPFRs. This is because other phosphorus compounds from the same matrix may co-elute with the target analytes (Guo et al., 2016).

2.4.5 Ionization

To use a mass spectrometer the sample of interest needs to be both in gas form, and ionized. This is done by an ionizer, and is also an important part when connecting the LC and the MS. Without the interfacing ionizer, the devices would be incompatible. This is because the LC operates with high pressurized liquid and the MS analyzers operates under vacuum and therefore requires the input to be gaseous. The interface makes the transition between the devices possible, and is a part of the inlet system of the MS. (Watson and Sparkman, 2007; Lundanes, 2014)

Different ionization methods exists, and properties such as size and polarity is taken into account when choosing the preferred ionization method. The most used interfaces are electrospray ionization (ESI), atmospheric pressure photoionization (APPI), atmospheric pressure chemical ionization (APCI) and inductively coupled plasma ionization (ICP) (Lundanes, 2014). In this project an electrospray ionizer (ESI) is used as the interface and ion source to ionize the analytes. ESI can be carried out in atmospheric pressure and can be used on both neutral, acidic and basic compounds, though mainly on compounds with polar groups (Lundanes, 2014).

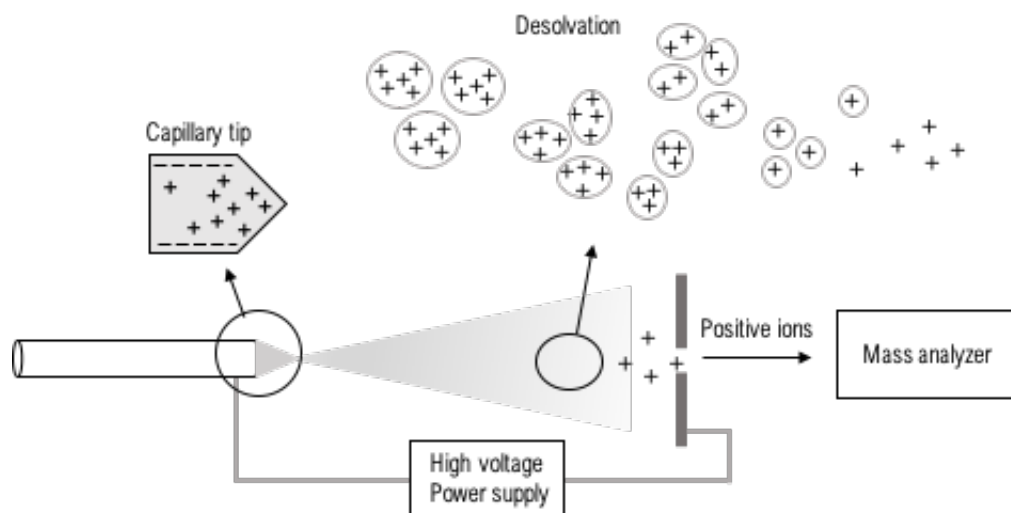
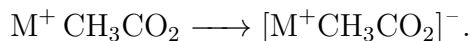


Figure 2.3: Schematic representation of the ESI(+) (reproduced from Lundanes (2014) page 87).

The ESI process begins with the inlet where in example the eluent from a chromatographic system is led into a capillary. Application of high voltage (typically +5 or -5 kV) to the capillary follows. A nebulizing gas like N_2 is introduced at the outlet of the capillary mixing with the inlet to create droplets. These droplets are highly charged and the droplets burst into smaller droplets when the surface tension of the drops is exceeded by the repulsive forces on the inside of the drop (Lundanes, 2014). As this happens repetitively the liquid inlet is transformed to a gaseous phase that further can be analyzed by mass analyzers. A representation of this is shown in Figure 2.3 with ESI(+) as the example.

Detection of the ions can be performed in either positive (ESI(+)) or negative mode (ESI(-)), creating respectively negative or positive ions. Determination of what mode to use depends highly on the structure of the molecules to be analyzed.

Examples of formation of different adduct ions formed by ESI is presented below. In positive mode ESI the most common adduct formation is the $M^+H^+ \longrightarrow [M^+H]^+$, nevertheless other adduct formations can occur (Kruve and Kaupmees, 2017; Cech and Enke, 2001). Examples of these are the sodium adduct, $M^+Na^+ \longrightarrow [M^+Na]^+$, the potassium adduct, $M^+K^+ \longrightarrow [M^+K]^+$, and the ammonium adduct $M^+NH_4^+ \longrightarrow [M^+NH_4]^+$. For negative mode ESI negative ions will be formed and adduct ions can include $M^+H^- \longrightarrow [M^+H]^-$, $M^+^{35}Cl^- \longrightarrow [M^+^{35}Cl]^-$, $M^+^{79}Br^- \longrightarrow [M^+^{79}Br]^-$ and



The mechanism of ionization and m/z can further be described with ESI(+) as an examples. The cations need a place to bind, and the larger the molecules are, the more places exists for cations to place. Single charged ions, m/z are the same as mass plus cation ($[M+H]^+$). Larger molecules facilitate multiple charged ions since the molecules have more sites for the cations to bind. If an atom has two H^+ ions bound in different sites, corresponding to a charge (z) of two, the m/z will be half of what it would have been if only one H^+ was bound to the molecule. This is useful when analyzing very high mass molecules, bringing them down within the range of the mass spectrometer.

2.4.6 Triple quadrupole analyzer

A variety of mass analyzers exist including Time-of-Flight (ToF) analyzers, Ion Trap analyzer, FTMS Analyzer (mass spectrometer with Fourier transform data acquisition) and the Triple quadrupole analyzer (QqQ) (Lundanes, 2014). The triple quadrupole analyzer is used for analysis in this project.

A quadrupole is made up of four parallel rods arranged evenly around a central axis. An oscillating field is created by applying a specific direct current (DC) and radio frequency (RF) to the rods. When the two diagonal pairs of rods have positively applied DC and RF, an oscillating electrical field is created. The ions generated through ionization carry an electrical charge, and when these ions enter the central axis of the rods they start oscillating in both x- and y-directions. If the ions are not stable in both the x- and y-directions they will collide with the rods and hence not be detected. The stability of the ion trajectories in this oscillating field is dependant on the m/z and is in that way used to separate the ions base on their m/z . Only ions with a specified m/z manage to pass through the rods when a chosen DC and RF are applied, and by varying the DC and RF obtaining a whole mass spectra is possible. (de Hoffmann and Stroobant, 2007; Lundanes, 2014).

The triple quadrupole (QqQ) is a mass analyzer that consists of three quadrupoles placed after one another. The first and the third quadrupole acts as mass filters while the second quadrupole functions as a collision cell. In the first quadrupole (Q_1), only the desired

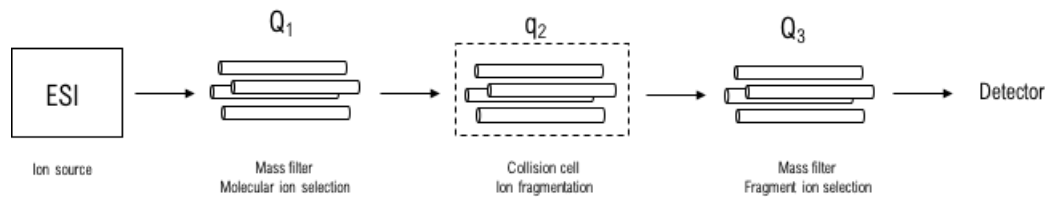


Figure 2.4: Schematic representation of the triple quadrupole mass analyzer (reproduced from Dass (2007b) p.132)

molecular ion is filtered through based on m/z . In the collision cell (q_2), ion fragmentation takes place, while the third quadrupole (Q_3) acts as another m/z filter where only selected fragments can pass through and be detected. A Selected-Reaction-Monitoring (SRM) can be used to acquire quantitative and specific data from the analysis and to detect ions with selected m/z . This method works well with the QqQ mass analyzer since monitoring of a precursor-product ion is performed. (McMaster, 2005; de Hoffmann and Stroobant, 2007; Lundanes, 2014)

2.4.7 Collision energy and cone voltage

Collision energy is the principal source of variation in the MS/MS spectrum of a given ion (Neta et al., 2009). The collision energy refers to the energy applied in the second quadrupole to fragment the ions by collision induced dissociation (CID) (Douglas, 1998). Ions pass through the first quadrupole into the collision cell where the ions undergo collisional excitation followed by dissociation (Douglas, 1998). The applied electrical potential to the collision cell will contribute to increase the kinetic energy of the ions and allow them to collide with a neutral gas ion like argon or nitrogen. The kinetic energy of the ions can in some degree convert into internal energy that contributes and leads to fragmentation and bond breakage (Sleno and Volmer, 2004).

High collision energies refers to energies in keV and can be used with a tandem sector and time-of-flight instrument, while low energies in the eV range are mostly used in triple quadrupole instruments and in ion trapping devices (Sleno and Volmer, 2004). In this project low energies under 100eV are applied as the collision energy. Nevertheless, energies ranging from 2 eV to 100 eV show different molecular fragmentation of the compounds.

Increasing collision energies can induce increasing degrees of fragmentation. Trends also

indicate that increasing collision energy is required for fragmentation of ions with increasing mass. (Neta et al., 2009)

2.4.8 Fragmentation of organophosphate flame retardants

For OPFRs the m/z of daughter ions, specifically the quantifier and qualifier ion, are presented in a variety of literature (see Table 4.32). The structure of the fragments and the fragmentation pathways are not as well reported. Suggested fragmentation patterns for organophosphate esters are nevertheless presented in Schwarzenberg et al. (2013), Bell et al. (1997) and Rodil et al. (2005) and these are used as inspiration for the OPFR fragments presented in Section 4.6.

Bell et al. (1997) have suggested fragmentation pathways for TMP and TEP as shown in Figure 2.5a and Figure 2.5b. This pattern can be utilized for other OPFRs as well, but for heavier and more complex molecules like TPP and the halogen containing OPFRs, other fragmentation pathways are suggested. Rodil et al. (2005) have suggested pathways for TCEP, TPP and BPA-BDPP, as shown in Figure 2.6.

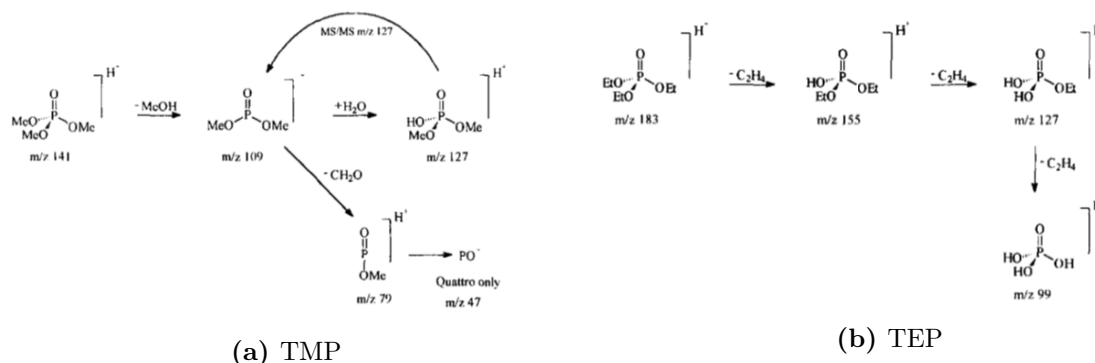


Figure 2.5: Suggested fragmentation pathways for TMP and TEP by Bell et al. (1997).

A set of rules, and an identification tree, for fragmentation of organophosphorus esters is suggested by Schwarzenberg et al. (2013) in Figure 2.7. This pattern shows similarities to the fragmentation pattern suggested and presented by Bell et al. (1997) for TEP and TMP.

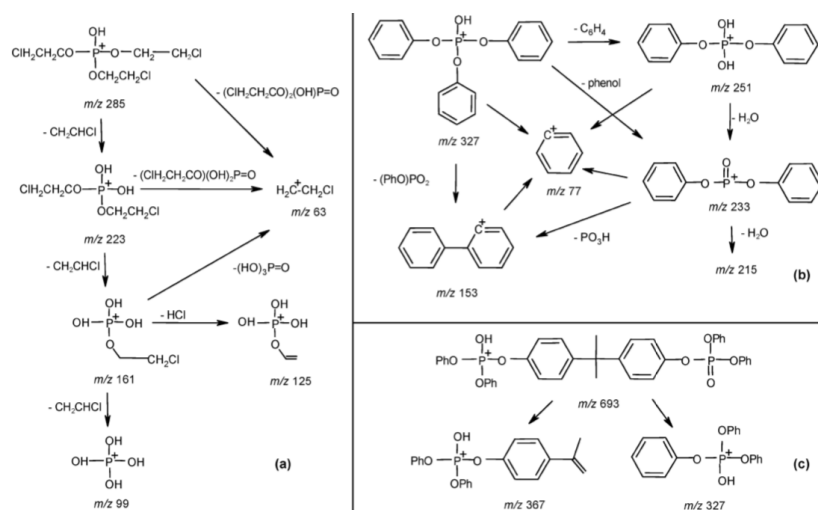


Figure 2.6: Suggested fragmentation pathway for TCEP(a), TPP(b) and BPA-BDPP(c) by Rodil et al. (2005).

Phosphates		Loss order
$R_1R_2R_3P$ 	If: $R_1=R_2=R_3 > \text{CH}_3$	1 - Loss of (R_1-1) 2 - Loss of (R_2-1) 3 - Loss of (R_3-1) 4 - Loss of H_2O 5 - Loss of H_2O
$MMMP$ 	If: $M_1=M_2=M_3=\text{CH}_3$ M=Methyl	1 - Loss of $(M_1\text{OH})$ 2 - Add/Loss of H_2O 3 - Loss of CH_2O 4 - Loss of CH_3OH

Figure 2.7: Suggested fragmentation rules for organophosphate esters by Schwarzenberg et al. (2013).

The suggested fragmentation pathways from Bell et al. (1997) and Rodil et al. (2005), will together with the rules proposed by Schwarzenberg et al. (2013) pose the suggested fragmentation of the OPFRs in this project that is presented in Section 4.

2.5 Quantitation and quality assurance

For some compounds several m/z fragments are obtained from the MS, and a quantifier ion need to be determined for every target analyte. The quantifier ion can be chosen by abundance as a higher abundance correlates with higher selectivity. Also the R^2 -value from the created calibration curves can be taken into account, together with the abundance, when choosing a quantifier ion. The quantifier ion is also used to quantify the analyte, and together with the confirmation ion, ion ratios can be calculated (as shown in Section 2.5.5).

2.5.1 Retention Time (RT) and Relative Retention Time (RRT)

The retention time (RT) of a compound is a measure of the elution time of a compound, which refers to the time from the injection to the elution (Lundanes, 2014). Several factors affect the retention time, among these are the injection method, flow rate, temperature, and the composition of the stationary and mobile phase. Since the retention time can differ between chromatographic systems the value of the RT is not universal. To make the retention times comparable and to compensate and correct for the fluctuations and variations from the different systems, the relative retention time (RRT) can be calculated as shown in Equation (2.1).

$$RRT = \frac{RT_a}{RT_i} \quad (2.1)$$

This value uses the relationship between the retention time of the analyte (RT_a) and the retention time of the corresponding internal standard (RT_i) to calculate a universal ratio, called the relative retention time, for the specific analyte under the specified conditions (e.g. same IS and mobile phase). This corrects for fluctuations and makes the retention times comparable since the relationship between the analyte and the internal standard always will be constant as they both are affected by the same fluctuations of the

chromatographic system they pass through.

2.5.2 Limit of detection and limit of quantification

To detect and quantify analytes with great accuracy a limit of detection (LOD) and a limit of quantification (LOQ) is defined and can further be estimated by calculation. LOD is defined as the smallest amount of an analyte in a sample that can be detected but not necessarily quantified. The smallest amount of an analyte in a sample that with precision and reliability can be quantified is called the LOQ (Dass, 2007a).

There are several approaches to find and estimate these values. The signal to noise ratio (S/N) can be utilized as a measure of the detection and quantification limits. The LOD is often set to three times the noise, $S/N \geq 3$. When the signal to noise ratio reach 10, quantification is obtainable and the LOQ is reached (Lundanes, 2014; Dass, 2007a). It should be noted that the LOD and LOQ is specific for each analyte, and is different in different systems.

The limit of quantification can also be determined as the lowest concentration detected in the calibration curve. Calculation of the LOD will then follow Equation (2.2)

$$LOD = \frac{LOQ}{3}. \quad (2.2)$$

2.5.3 Internal Standard Method

The internal standard method is frequently used to quantify analytes in chromatography, at the same time as it ensures an increased reproducibility and accuracy of the analysis. A known concentration of an internal standard is added during sample preparation. The ratio between the added concentration and the response from analysis can be used for quantification to correct errors as loss of analyte during extraction, variations in analysis conditions and matrix effects.

An internal standard (IS) is often an isotope-labeled analog of the actual analyte, often deuterated or ^{13}C (Wieling, 2002). A requirement for the internal standard is that it only has a slightly different retention time from the analyte, but at the same time being easily distinguishable in the chromatograms (Wang et al., 2007). Similar behavior in the system,

as well as possessing similar physical and chemical properties is also a requirement for the internal standard. It should also be stable, and thus not react, during sample preparation and analysis for accurate and stable measurements (Lundanes, 2014). These properties corresponds well to isotope-labeled compounds and their corresponding non-labeled compound. By choosing the right internal standard for the experiment, inaccuracies and loss during sample preparation and instrumental analysis can be corrected for.

A calibration curve can be created for every target analyte by using the internal standard method. Samples are prepared with varying concentrations of the target analyte while the internal standard concentration is held constant. The ratio between peak area of the analyte and the internal standard is plotted against the concentration of the analyte. (Skoog et al., 2003; Lundanes, 2014)

2.5.4 Relative response ratio

The relative response ratio (RR) can be calculated as a factor between the response of the analyte and the response of the internal standard. This can be used to compensate for loss during sample preparation and instrumental analysis. This is utilizable as the concentration of the internal standard is known, and the behavior of the IS is similar to the analyte. The ratio is calculated as shown in Equation (2.3), where A_i represents area of the chosen analyte, while A_{IS} represents the area of the chosen internal standard in the same sample. Subtraction of the blank signals from the samples is done to obtain corrected ratios.

$$\text{Relative response ratio} = \frac{A_i}{A_{IS}} \quad (2.3)$$

2.5.5 Ion Ratio

Ion ratio (IR) refers to a confirmation parameter that ensures additional confirmation of the target analytes. This ratio is unique for each analyte in a sample matrix. Dividing the area of the confirmation ion by the area of the quantification ion gives the value of the IR. This is shown in Equation (2.4).

$$\text{IR}\% = \frac{A_{\text{confirmation ion}}}{A_{\text{quantification ion}}} \cdot 100 \quad (2.4)$$

2.5.6 Absolute and relative recovery

To measure the efficiency of the extraction process, recoveries can be calculated. By comparing signals from samples with the same, and known, concentration of target analyte where the TA have been added at respectively the beginning and the end of the extraction process, the absolute recovery can be determined as in Equation (2.5)(Caban et al., 2012).

$$\text{Absolute recovery}\% = \frac{A_{\text{SP}}}{A_{\text{MM}}} \cdot 100 \quad (2.5)$$

Where A_{SP} refers to the area of the pre-extraction spiked sample, and A_{MM} refers to the area of the post-extraction spiked sample.

Comparing the ratio of the samples with target analyte added pre-extraction and post-extraction shows the relative recovery. Losses of target analyte during sample preparation is compensated for when calculating the relative recovery making it a corrected form of recovery as calculated in Equation (2.6).

$$\text{Relative recovery}\% = \frac{RR_{\text{SP}}}{RR_{\text{MM}}} \cdot 100 \quad (2.6)$$

Where RR_{SP} refers to the relative response ratio of the pre-extraction spiked sample and RR_{MM} refers to the post-extraction spiked sample. This can also be presented as in Equation (2.7)

$$\text{Relative recovery}\% = \frac{A_{\text{SP}}/A_{\text{IS}_{\text{SP}}}}{A_{\text{MM}}/A_{\text{IS}_{\text{MM}}}} \cdot 100 \quad (2.7)$$

Where A_{SP} refers to the area of the pre-extraction spiked sample, $A_{\text{IS}_{\text{SP}}}$ refers to the area of the internal standard in the pre-extraction spiked sample, A_{MM} refers to the area of the post-extraction spiked sample and $A_{\text{IS}_{\text{MM}}}$ refers to the area of the internal standard in the post-extraction spiked sample.

To correct for contamination, the area of the reagent blank sample is subtracted from both the spiked, non-spiked and matrix match samples.

2.5.7 Matrix Effect

When developing a LC-MS method, evaluation of the matrix effects (ME) is an important part to determine the impact on the accuracy and reproducibility of the method. In LC-MS (and LC-MS/MS) co-eluting compounds from the matrix can affect both the ionization efficiency and reproducibility, causing suppression or enhancement of signals. This is a common error that can impact the quantification in LC-MS and is therefore an important parameter to evaluate. (Van De Steene and Lambert, 2008)

There exist a variety of approaches to calculate the matrix effect. One method to calculate the matrix effect percentage is presented in Equation (2.8) where an instrumental response of the analyte is compared to the response of a post-extraction spiked sample.

$$\%ME = \frac{A_{MM} - A_{RB}}{A_{Solvent_{TA}} - 1} \cdot 100 \quad (2.8)$$

A_{MM} refers to the area of the post-extraction spiked matrix match sample (MM), while A_{RB} refers to the area of the reagent blank. $A_{Solvent_{TA}}$ is the area of the target analyte at a concentration corresponding to the MM in an instrument standard solvent solution. To compensate for matrix effects labeled internal standards can be used since the ratio between the area of the peaks should be constant (Van De Steene and Lambert, 2008).

If the %ME is equal to 100% there is no matrix effect. Ionization suppression can be considered when $ME < 100\%$, while $\%ME > 100\%$ indicates an ionization enhancement.

2.5.8 Coefficient of determination

Calibration curves that show the relationship between the response ratio (analyte/internal standard) and the concentrations (analyte/internal standards) need to be established to use the coefficient of determination as a parameter. These curves are created using the MS-signals from samples with known concentrations of internal standard solutions and known concentrations of the analyte. The concentration range of the curve should prefer-

ably cover the expected concentration in the unknown samples. This can further be used to predict concentrations of analytes. Linear regression is performed on the data to create a linear slope. The slope provides a coefficient of determination (R^2) that can be an indicator of how good representation the linear regression is of the data set. The correlation increases as the R^2 approaches 1, and a R^2 value over 0.99 indicate minimal variations in the quality of the analysis. Equation (2.9) shows the calculation of the coefficient of determination.

$$R^2 = 1 - \frac{\sum(y_i - f_i)^2}{\sum(y_i - \bar{y})^2} \quad (2.9)$$

y_i refers to a value from the data set, while f_i is the correlated value from the fitted model. The mean value of the detected data is represented as \bar{y} .

Quantification of precision in experimental work is important and this can be done by calculating repeatability and reproducibility. Measuring the variation of the instrumentation under equal conditions for the same sample gives an indication of the repeatability of the experiment. (Skoog et al., 2003)

Standard deviation (STD) is an often used parameter to measure the variation in a data set, and can therefore be calculated to determine repeatability. Calculation follows Equation (2.10).

$$STD = \sqrt{\frac{\sum_{i=1}^n (x_i - \bar{x})^2}{n - 1}} \quad (2.10)$$

Where x_n refers to value n in the data set, and \bar{x} refers to the mean value of the data set.

The relative standard deviation (RSD) gives an indication of the quantity of the standard deviation in comparison with the values and mean of the data set. It is therefore a great parameter to measure precision and repeatability. The RSD is calculated by dividing the STD by the mean value of the data set and multiplying it by 100 to get the value represented in percent (see Equation (2.11)).

$$\%RSD = \frac{STD}{\bar{x}} \cdot 100 \quad (2.11)$$

3 Materials and method

As mentioned in the introduction the experimental work was disrupted and forced to be changed as a result of SARS-CoV-2. For further description of the changes see Section 3.8.

3.1 Sample Collection

49 different baby foods from a variety of producers was bought from a local grocery store. This included milk replacements (both powders and liquids), porridge, dinners, snacks, bars, smoothies and purees. Both dry food, wet food, and food containing meat, chicken, fish, vegetables, fruits, dairy and grains were supposed to be analyzed. Both glass, aluminium, lined cardboard and different plastics were used as original containers for the foodstuffs.

When preparing the samples for analysis, all samples were transferred to 50 mL (polypropylene) PP tubes and freeze dried for 72 hours to ensure complete dryness of the samples. Approximately 1.0 grams of each food sample were further transferred to a 15 mL PP tube. When weighing out the samples a clean metal spoon, pre-washed in methanol and dried on clean aluminium foil in a fume hood, were used for each sample to avoid contamination.

3.2 Chemicals

Standards of all organophosphate esters, were bought from Chiron AS (Trondheim, Norway). This included Trimethyl Phosphate (TMP), Triethyl Phosphate (TEP), Tri-*n*-propyl Phosphate (TnPP), Tri-*n*-butyl Phosphate (TnBP), Tri-isobutyl Phosphate (TiBP), Tris(2-butoxyethyl) Phosphate (TBOEP), Tris(2-ethylhexyl) Phosphate (TEHP), Tris(2-chloroethyl) Phosphate (TCEP), Tris(1-chloro-2-propyl) Phosphate (TCIPP), Tris(1,3-dichloro-2-propyl) Phosphate (TDCIPP), Triphenyl Phosphate (TPP), Tritolyl Phosphate (TMPP), Diphenyltolyl Phosphate (DCrP), 2-Ethylhexyldiphenyl Phosphate (EHDP), Isodecyl Diphenyl Phosphate (IDPP), Tert-Butylphenyldiphenyl Phosphate (BPDP), Tris(4-tert-butylphenyl) Phosphate (TTBPP), Tetraphenylrecorcinol-bis(diphenyl Phosphate) (RDP), 2,2-Bis(chloromethyl)-1,3-propandiol-bis[bis(2-chloroethyl)] Phosphate (V6), Bisphenol A bis[(diphenyl) Phosphate] (BPA-BDPP), Di-*n*-butyl Phosphate (DPhP), Bis(2-

chloroethyl) Phosphate (BCEP), Bis(2-chloropropyl)hydrogen Phosphate(BCIPP), Bis(2-butoxyethyl) Phosphate (BBOEP), Bis(2-butoxyethyl) hydroxyethyl Phosphate (BBOE-HEP), Bis(2-butoxyethyl) hydroxy-2-butoxyethyl Phosphate (3OH-TBOEP).

The isotope labeled internal standards were also purchased from Chiron AS (Trondheim, Norway) and included Triethyl Phosphate -d15 (TEP-d15), Tri-*n*-butyl Phosphate -d27 (TnBP-d27), Tris(2-chloroethyl) Phosphate -d12 (TCEP-d12) and Tris(1,3-dichloro-2-propyl) Phosphate -d15 (TDCIPP-d15).

3.3 Sample preparation

3.3.1 Standards

Triethyl Phosphate -d15 (TEP-d15), Tri-*n*-butyl Phosphate -d27 (TnBP-d27), Tris(2-chloroethyl) Phosphate -d12 (TCEP-d12) and Tris(1,3-dichloro-2-propyl) Phosphate -d15 (TDCIPP-d15) were used as internal standards (IS) for the analysis of the OPFRs. A 1 ppm mixture of these four internal standards were made. 10 μ L of the finished 1 ppm internal standard mixture was added to all samples.

The matrix match samples and the spiked samples were also spiked with a 1 ppm target analyte standard mix (TA mix). The 25 standards was divided mixed into two 1ppm TA mixes, TA mix A and TA mix B. To get a final concentration of 1 ppb in the vial with total volume of 1mL, 10 μ L of both TA mixes were added to the spiked samples and the matrix match samples, respectively before and after the extraction procedure.

3.4 Development of extraction technique

A variation of extraction techniques of organophosphate flame retardants (OPFRs) are presented in literature (Table 2.3). Two different protocols were tested as described in Appendix A.1 and Appendix A.2.

Different extraction techniques and solvents were tested to optimize the extraction of the organophosphate flame retardants. The first extraction technique that was tested used ethylacetate to extract the OPFRs. To try to optimize the extraction, and further improve the recoveries, an extraction using dichloromethane and hexane as major solvents were

carried out. The test of each protocol was carried out with one reagent blank sample (RB), three sample samples (S), four spiked samples (SP) and two matrix match samples (MM). For both extraction protocols roughly 1 g of *Nestle min Havregrøt med Mango og Banan* was added in all tubes except the RB samples.

An integration method for OPFRs in foodstuffs was carried out experimentally using MassLynx and TargetLynx software packages (Waters, USA). The results were further processed in Microsoft Excel and recoveries were calculated. Results showed that the largest and most non-polar compounds were harder to extract from the matrix. Therefore a new extraction optimization experiment was carried out. The procedure described above was used as a base, but in the two first extractions the solvent was changed from ethylacetate to 50:50 DCM:Hexane (Appendix A.2).

3.5 Instrumentation for Analysis

A Acquity UHPLC system (Waters, Milford, USA) was used to perform the analysis of the OPFRs. The columns used were a Kinetex C18 column (30 x 2.1 mm, 1.3 μm , 100Å Phenomenex) serially connected to a C18 Phenomenex guard column. For elution of the analytes the aquatic phase (A) consisted of LC-grade water with 0.1% (v/v) formic acid, while the organic phase (B) was acetonitrile with 0.1% (v/v) formic acid. Run time of the analysis was 5 minutes, and the injection volume was set to 2 μL . The flow rate was set to 0.4 $\mu\text{L}/\text{min}$, and the separation was performed with gradient elution following Table 3.1. Xevo TQ-s, Triple Quadrupole Mass Analyzer (QqQ) including ZSpray ESI function (Waters, Milford, USA) was used in SRM mode. ESI(+) with a capillary voltage of 2.8kV was used for analysis of all OPFRs. Ionization and desolvation temperatures were set to respectively 150°C and 350°C. All instrumental parameters are presented in Table 3.2.

Table 3.1: Gradient used for the mobile phase during the UHPLC-MC/MC. A is the aquatic phase(water with 0.1%v/v formic acid), while B is the organic phase(acetonitrile with 0.1%v/v formic acid).

Time [min]	Flow [mL/min]	%A	%B	Curve
Initislized	0.4	75	25	Initialized
1.00	0.4	75	25	6
2.50	0.4	0	100	6
3.50	0.4	0	100	6
4.00	0.4	75	25	6
5.00	0.4	75	25	6

Table 3.2: Settings for UPLC-MS/MS analysis of organophosphate flame retardants.

Settings	
Polarity	ESI(+)
Capillary	2.8 kV
Cone voltage	50 V
Source offset	80 V
Source temperature	150 C
Desolvation temperature	350 C
Desolvation gas flow	1000 L/hr
Cone	150 L/hr
Nebuliser	6.0 bar
Collision gas flow	0.15 mL/min

3.6 Data treatment

MassLynx and TargetLynx software packages (Waters, USA) were used to acquire data from the LC-MS/MS. Further processing of the data was performed in Microsoft Excel. Concentrations were calculated based on the relative area ratios of the spiked samples using the internal standard with the closest retention time to the target analyte. The calculations were further based on the spiked samples. In these samples a known concentration of 10 ppb was added to the samples in the beginning of the sample preparation, making it possible to utilize this knowledge to calculate the concentrations in the samples. To ensure a measure of 10 ppb in the spikes sample, the area of the non-spiked sample was subtracted from the spiked sample. The pre-spiked samples are used to calculate the concentrations as it mimics the process the whole sample undergoes better than the matrix match samples where the TA is added at the end of the sample preparation.

Quantification of the target analytes were then accomplished based on the internal standard method, and by utilizing matrix-matched calibration standards prepared by fortifying target analytes into the specified matrices prior to extraction (Asimakopoulos et al., 2014, 2016).

3.7 SRM Transitions and fragmentation

To obtain transitions for daughter fragments for each target OPFR, standards of each analyte (5ng/mL) were infused into the mass analyzer. The first quadrupole of the QqQ analyzer were set to only allow the molecular ion through, while the third quadrupole were set to scan for all possible daughter fragments. IntelliStart software (Waters) suggested daughter fragments and provided mass spectra with different collision energies for each target analyte.

Molecular ions and fragmentation ions were compared to literature and structures from fragmentation are suggested in Section 4.6.

Suggested structures for the daughter fragments were created in ChemDraw Professional 16.0. The fragments were created according to the daughter ions obtained from the SRM for each OPFR. The pathways presented in Section 2.4.8 were used to predict the structure of the daughter ions as far as possible.

3.8 Experimental work disrupted by SARS-CoV-2

As SARS-CoV-2 arrived mid March 2020, the whole university, and thereby also all laboratories, were closed. The pandemic interrupted this project in a way that the experimental work was disrupted and not able to be completed. A more theoretical approach, and structural determination of the daughter fragments detected in the MS became included in the project. No data from the 49 original samples were obtained and evaluation and determination of OPFR concentrations in the different baby food samples were not feasible.

Data was only obtained from the extraction method development, and these experiments ended up being the only lab work carried out completely. For the rest of the 49 samples that were supposed to be analyzed, the experimental work was disrupted by closing of labs after the day after all samples were finished freeze dried and weighed out. The extraction was supposed to be carried out by following the extraction protocol from Appendix A.1 with minor adjustments. An additional round of extraction with ethyl acetate was supposed to be carried out, making it four in total. A 30 minute sonication was also presumed to be added for each addition of ethyl acetate, instead of only 10 minutes of sonicating after the first addition of ethyl acetate.

A calibration curve was supposed to be made by preparing solutions of the TA with different concentrations, mixed with a constant concentration of the internal standard mix. For example, solutions of the TA would be prepared in the following concentrations: 0.1, 0.2, 0.5, 1, 2, 5, 10, 20, 25 and 50 ppb, while the IS would be added to a 10 ppb concentration in all samples. The solvents used would be the same as the instrumental solvents, ACN:MQ-water. The same gradient program as described in Table 3.1 would be used to run the samples. The curve was further supposed to be constructed by plotting the peak area ratio against the analyte concentration. A linear regression would be made to find the best fit linear line. As described in Section 2.5.8 a satisfactory coefficient of determination would be $R^2 > 0.998$, which describes great correlation and minimal variations when it comes to the quality of the analysis, meaning that the input values explain the variation of the data set.

Matrix effects were also supposed to be calculated, but no analysis of a sample with

only the target analyte in the instrument solvents was able to be performed. Matrix effects would have been calculated for each analyte following Equation (2.8). Negative values would indicate ion suppression possibly caused by interfering co-eluent. To observe matrix effects when investigating and analyzing trace organic compounds in complex matrices is expected due to the low concentrations of the target analytes and the complex matrices containing possibly interfering compounds.

Calculations of the concentration of each target analyte in each baby food were supposed to be performed and presented. The values were supposed to be compared to other studies and relationships between concentrations, type of baby food and their packaging were supposed to be established.

For calculation of precision quadruplicates of samples with the same amount of added TA was supposed to be analyzed. This would have been performed with three different concentrations, and analyzed by calculating the mean, median, standard deviation and relative standard deviation.

4 Results and discussion

4.1 Extraction method development

To properly analyze different chemicals in a variety of matrices, an optimized extraction method need to be developed and tested. The extraction is seen as one of the most complex steps in analysis performed in complex matrices like foodstuffs. Not many studies have reported OPFRs in foodstuffs (see Table 2.4 and Table 2.3) and several use the same extraction technique with minor differences. The use of dichloromethane and hexane as solvents is also widespread when analyzing OPFRs both in foodstuffs and more researched matrices like dust, air, water, urine and fish. When testing extraction and calculating recoveries the extraction following Appendix A.1 showed significantly better recoveries and clearer peaks in the chromatograms than Appendix A.2, even though DCM and hexane are by far more used for extraction of OPFRs than ethyl acetate.

In this project two similar protocols for extraction with different solvents were tested. The protocol in Appendix A.1 was followed, and until the reconstitution in the LC-vials no issues had arrived. In this last step, the reconstituting, the liquid coagulated and became foggy. The vials were stored in the refrigerator overnight, and the liquid had then separated into layers and with some precipitation. The vials were centrifuged for a total of 30 minutes at 4000 rpm to gather the precipitates before the vials again were refrigerated overnight. Then, clear layers and bubbles of lipids were visible. The lipids or precipitates were pipetted out, and clear liquid was carefully transferred into new vials for analysis.

After the data analysis, the results showed that the largest and most non-polar compounds were harder to extract from the matrix. Therefore a new extraction optimalization experiment was carried out. The procedure described in Appendix A.1 was used as a base, but in the two first extractions the solvent was changed from ethylacetate to 50:50 DCM:Hexane.

When following the protocol presented in Appendix A.2 more attention was paid to the reconstitution step, as this was where the issues had arrived when following the first protocol. The samples became slightly foggy when reconstituting after extraction with DCM:Hex, but after being stored in the refrigerator overnight precipitants had formed a

thin layer at the bottom of the vial. This made it possible to easily transfer clean samples into new vials.

After testing the two protocols, it was evident that the extraction carried out with only ethyl acetate showed better recoveries and extracted more of the target analytes from the matrix. This discovery was quite a surprise as many previous studies have used DCM:Hex as the main solvent as shown in Table 2.3. The results were therefore expected to be better than the first tested protocol. This may come as a result of different factors. Firstly, most previous studies have used SPE as a clean-up step. This was not tested in this project. Secondly, some of the most troubling compounds to extract and detect are the least reported ones. A reason for the frequent use of DCM:Hex may be its known use in extraction of polychlorinated biphenyls (PCBs) and polyfluoralkyl substances (PFAS). This may also be a reason why most extraction techniques and solvents used are similar for the OPFRs and these substances. Also many of the previous studies used DCM:Hex as the only extraction solvent, and did not have one round of extraction with ethyl acetate or another solvent, which may have affected the extraction.

4.2 Recoveries

Relative recoveries are presented in Table 4.1 and is calculated as presented Equation (2.7), while absolute recoveries are shown in Table 4.2 and is calculated as described in Equation (2.5).

Table 4.1: Relative recoveries of each target analyte from extraction protocol 1 (Appendix A.1) and extraction protocol 2 (Appendix A.2). (*) Indicate not acceptable recoveries, (**) indicate (RB>S), while (***) indicate (RB>MM or SP).

Compound	RR% Extraction 1	RR% Extraction 2
TMP	48.7	114
TEP	85.4	159
TnPP	83.0	63.0
TnBP	96.4	18.9
TiBP	89.4	24.7
TBOEP	103	4.3 (*)
TEHP	1.9 (**)	3.7 (*)
TCEP	89.1	21.9

Table 4.1 continued from previous page

TCIPP	4.4 (*)	(***)
TDCIPP	(***)	(***)
TPP	72.3	49.9
DCrP	65.4	6.9 (*)
TMPP	36.3	4.1 (*)
EHDP	(***)	(***)
IDPP	9.8 (*)	(***)
TTBPP	3.0 (**)	2.2 (*)
RDP	70.3	3.8 (*)
V6	127	2.8 (*)
BPA-BDPP	30.9	4.8 (*)
<i>Metabolites</i>		
BBOEHEP	123	109
3OH-TBOEP	143	107

Table 4.2: Absolute recoveries of each target analyte from extraction method 1 (Appendix A.1) and extraction 2 (Appendix A.2). (*) indicate recoveries that are not acceptable, either because of low recoveries, extremely high blanks, negative values or missing detection.

Compound	Abs.R% Extraction 1	Abs.R% Extraction 2
TMP	21.3	8.3
TEP	36.3	10.2
TnPP	39.6	3.0 (*)
TnBP	28.0	0.8 (*)
TiBP	27.2	1.4 (*)
TBOEP	32.2	0.2 (*)
TEHP	0.5 (*)	3.7 (*)
TCEP	42.3	0.3 (*)
TCIPP	121	2.2 (*)
TDCIPP	(*)	81.4
TPP	22.3	3.1 (*)
DCrP	20.3	0.4 (*)
TMPP	11.4	0.2 (*)
EHDP	(*)	(*)
IDPP	3.9 (*)	(*)
TTBPP	0.7 (*)	0.1 (*)
RDP	21.6	0.2 (*)

Table 4.2 continued from previous page

V6	39.2	0.2 (*)
BPA-BDPP	9.4	0.3 (*)
<hr/>		
<i>Metabolites</i>		
BBOEHEP	54.2	2.9 (*)
3OH-TBOEP	44.6	6.9 (*)
<hr/>		
<i>Internal standards</i>		
TEP-d15	41.8	6.9 (*)
TnBP-d27	31.1	(*)
TCEP-d12	59.7	(*)
TDCIPP-d15	23.3	(*)

Low absolute recoveries, as all compounds showed while following the protocol in Appendix A.2, indicate that only a small fraction of the target analytes is present in the samples after the sample preparation procedure. The absolute recoveries for the extraction with DCM:Hex were extremely low, and this indicates that the extraction is not working as anticipated. Nevertheless relative recoveries were calculated compensating for the loss of analyte during the extraction process, but also these recoveries showed unsatisfactory results.

For the compounds showing good recoveries the area of the different samples typically showed the order MM > SP > S > RB.

For the extraction with DCM:Hex, 12 out of 21 compounds showed not acceptable relative recoveries. The compounds where the area of reagent blank sample (RB) exceeded the area of the post spiked matrix match (MM) were considered the most challenging compounds. In addition to the compounds being challenging to analyze after extraction with DCM:Hex, the internal standards did also show bad results possibly due to instability. Only TEP-d15 was possible to use as internal standard for the extraction with DCM:Hex, and was therefore used for all compounds. This may have been a contributor to the bad recoveries as the TEP-d15 internal standard has significantly different physical and chemical properties, and retention time, than many of the analyzed OPFRs.

6 compounds did not yield acceptable relative recoveries from the extraction with ethyl acetate. Unacceptable recoveries obtained from following the extraction protocol with EA

(Appendix A.1) are described. For TEHP a negative recovery was calculated and $MM > SP > RB > S$. For TCIPP $SP > MM$ also leading to not great results. For TDCIPP $RB > S > MM > SP$, and for EHDP $RB > MM > S > SP$, while for IDPP $MM > > SP$ and TTBPP $RB > S$. This somewhat odd orders of areas can in example come as a result of contamination of the samples from sample preparation, or contamination from the instrument. For the extraction following the protocol presented in Appendix A.2 similar tendencies were observed. Blank contamination is pointed out in both Poma et al. (2018) and Brandsma et al. (2013a) as one of the major challenges when analyzing OPFRs. This comes as a result of the OPFRs existence in both indoor dust, plastics and also possibly in the instruments.

Some compounds show high relative recoveries ($>150\%$) which may lead to overestimating the concentration of the target analyte in the sample. This might lead to an increase in the risk of critical errors in the quantification.

Most of the OPFRs had relatively low absolute recoveries (below 40%), which indicates loss of sample during sample preparation. This can in example come as a result of poor extraction efficiency. Low absolute recoveries can also come as a result of the target analytes binding to the matrix of sample. As the target analytes are detected air and dust, and also is different plastics, contamination resulting in higher recoveries should be taken into consideration.

When calculating the relative recoveries the loss of analyte during sample preparation is compensated for. This is because the relative recoveries are calculated relative to an internal standard as described in Equation (2.7). Most of the relative recoveries are substantially better than the absolute recoveries, indicating that the efficiency of the sample preparation might be better than first anticipated.

To obtain the most correct relative recoveries, an internal standard similar to the target analyte should be utilized as they would be affected similarly by fluctuations in the process and system. Differences between the internal standard and the target analyte may result in the TA and IS responding differently to the fluctuations making the recoveries less reliable. In this project only four deuterated internal standards were available. The 21 target analytes were corrected with the internal standard with the closest retention time

to the analyte. The retention times for the analytes ranged from 0,29 to 3,29 minutes (presented in Table 4.4) while the internal standards retention times ranged from 0,57 to 2,26 minutes making it likely and probable that some of the 21 analyzed compounds did not match perfectly with the IS closest to their retention time. The IS and TA may therefore, in some cases, have been affected differently by the fluctuations in the system and by the extraction process. To avoid this more target analyte specific internal standards could be used to better replicate the behaviour of more of the target analytes. Another possibility is to use ^{13}C internal standards instead of the deuterated standards. The ^{13}C standard behave even more similar to the target analytes than the deuterated standards. The deuterated standards tend to induce differences between the TA and the IS when it comes to reaction rates, hydrophobicities and interactions, while the ^{13}C standards often have more similar properties (Tan et al., 2012).

Nevertheless contamination during the process, and in the instrument may have been a contributor to the bad recoveries.

4.2.1 Precision

Precision can be estimated by evaluating replicates of the same sample. This often applies to samples with addition of the same known amount of a target analyte. Further analyzing the variations of these similar samples give an indication of the precision. This is often done by calculating the standard deviation and relative standard deviation of the data set calculated as described in Equation (2.10).

Analyzing triplicates or quadruplicates of spiked samples in different concentrations obtained from an optimized samples preparation protocol should have been done to evaluate precision, but was not able to be carried out as a result of SARS-CoV-2 restrictions. Mean area, medians, standard deviations and relative standard deviation (RSD) would have been presented in a table for the QA/QC.

Since the extraction method development was carried out with spiked triplicates mean area, medians, standard deviations and relative standard deviation (RSD) were calculated from the method development and is presented in Table 4.3. The calculations were done by using the results obtained from the extraction using only ethyl acetate as the extraction

solvent.

Table 4.3: Statistics for OPFRs in triplicates of samples spiked prior to sample preparation to concentrations of 10 ppb TA. Mean and median area, standard deviation (STD) and relative standard deviation (RSD%) for absolute and relative values are presented. Calculations for EHDP and TDCIPP is excluded because of negative values as a result of high blank values.

Compound	Absolute values				Relative values			
	Mean	Median	STD	RSD%	Mean	Median	STD	RSD%
TMP	16239	18112	3891	24.0	0.30	0.30	0.03	9.54
TEP	18414	20068	5218	28.3	0.33	0.33	0.05	16.0
TnPP	3806	3919	1301	34.2	5.03	5.10	1.05	20.8
TnBP	31127	30388	7549	24.3	0.16	0.15	0.02	14.1
TiBP	24450	23910	6183	25.3	0.13	0.13	0.02	13.6
TBOEP	58118	56965	16849	29.0	0.47	0.47	0.07	14.1
TEHP	1078	1066	284	26.3	0.01	0.01	0.002	26.6
TCEP	6577	6767	1876	28.5	8.74	8.80	1.29	14.8
TCIPP	13336	13681	3983	29.9	4.73	4.89	3.36	71.1
TDCIPP	–	–	–	–	–	–	–	–
TPP	84724	80779	19257	22.7	0.48	0.49	0.08	15.9
DCrP	9036	8893	1924	21.3	0.05	0.05	0.01	11.1
TMPP	24573	23646	6473	26.3	0.14	0.14	0.02	14.5
EHDP	–	–	–	–	–	–	–	–
IDPP	2152	1951	682	31.7	0.01	0.01	0.003	27.4
TTBPP	953	986	144	15.2	0.01	0.01	0.002	33.9
RDP	9928	9441	1719	17.3	0.06	0.06	0.01	14.9
V6	13714	13308	2888	21.1	0.08	0.08	0.01	18.1
BPA-BDPP	18057	18299	1543	8.54	0.10	0.11	0.02	16.3
<i>Metabolites</i>								
BBOEHEP	3836	3717	812	21.2	5.01	5.19	0.62	12.4
3OH-TBOEP	21585	20206	5213	24.2	0.12	0.12	0.02	14.5

RSD calculated with relative values were for some of the samples relatively high, which may be a result of the use of only four different internal standards making it likely that some of them do not match perfectly. These differences can, in addition to matrix effects, result in losses and different interactions during sample preparation.

The relative standard deviation for the absolute values varied from 8,54% to 34,2%. Acceptable values for the RSD should preferably be under 15%, but a maximum of 20% can be accepted. If a maximum of 20% is accepted TTBPP, RDP and BPA-BDPP show acceptable RSD% for the absolute values. The majority of the RSD% for the absolute values show results around 20-30%. High relative standard deviations and low precision can come as a result of different factors including differences in extraction efficiency, variations in temperature, different interactions with the matrix and non-homogeneous samples. Also inaccuracy in addition of IS and TA to the samples may have affected the RSD%.

For the relative values, values corrected by use of an internal standard, most OPFRs showed significantly better RSD. Only TTBPP, TEHP, IDPP, TCIPP and TnPP show RSD% above 20 %, while the remaining 14 OPFRs possible to calculate precision for showed acceptable RSD % with values lower than 20 %.

Since only four different internal standards were used for all 21 OPFRs, this may be an explanation for high RDS %. As mentioned small differences in retention time can lead to significant ion enhancement or ion suppression leading to weaker RSD %.

Low precision can for instance be a result of variations during sample preparations, non-homogeneous samples and fluctuations in temperature. If lab work was able to be finished, triplicates with concentrations of in example 25 ppb and 50 ppb would have be analyzed in addition to triplicates of 10 ppb.

4.3 Ion ratios

Ion ratios are calculated as presented in Equation (2.4) in Section 2.5.5 and presented in Table 4.4 together with retention times (RT) and relative retention times (RRT) calculated as in Equation (2.1) in Section 2.5.1. All values were considered acceptable.

Table 4.4: Ion Ratio(IR), Retention time(RT) and Relative retention time(RRT) for target analytes and retention times for the internal standards. – refers to when only one fragment is detected for the compound.

Compound	Ion Ratio (%)	RT	RRT
TMP	18.1	0.29	0.49
TEP	81.0	0.60	1.05
TnPP	86.1	1.88	1.25
TnBP	79.2	2.28	1.01
TiBP	79.2	2.28	1.01
TBOEP	97.6	2.38	1.05
TEHP	6.45	3.29	1.49
TCEP	38.4	1.53	1.01
TCIPP	–	1.99	0.90
TDCIPP	–	2.22	1.00
TPP	98.2	2.28	1.01
DCrP	98.2	2.37	1.07
TMPP	30.5	2.54	1.15
EHDP	–	2.64	1.19
IDPP	91.9	2.78	1.26
TTBPP	60.8	3.04	1.38
RDP	98.1	2.54	1.12
V6	–	2.04	0.91
BPA-BDPP	9.91	2.76	1.22
BBOEHEP	30.0	1.82	1.21
3OH-TBOEP	97.9	1.97	0.87
<i>Internal standards</i>			
TEP-d15		0.57	
TnBP-d27		2.26	
TCEP-d12		1.5	
TDCIPP-d15		2.21	

4.4 Concentrations

Concentrations of the different OPFRs and metabolites were calculated from the extraction with EA and are presented in Table 4.5.

Table 4.5: Concentrations of OPFRs in ng/g dw together with the internal standard (IS) used and LOD (ng/g) for each OPFR. For the extraction with DCM:Hex only TEP-d15 showed usable results and was used as IS for all compounds.

Compound	IS used	Concentration	LOD
TMP	TEP-d15	2.33	0.22
TEP	TEP-d15	0.25	0.02
TnPP	TCEP-d12	< LOQ	0.19
TnBP	TnBP-d27	2.67	0.24
TiBP	TnBP-d27	< LOD	0.13
TBOEP	TnBP-d27	< LOD	3.97
TEHP	TnBP-d27	–	3.21
TCEP	TCEP-d12	< LOD	0.20
TCIPP	TDCIPP-d15	23.5	0.12
TDCIPP	TDCIPP-d15	–	–
TPP	TnBP-d27	1.00	0.09
DCrP	TnBP-d27	< LOD	1.21
TMPP	TnBP-d27	< LOD	0.87
EHDP	TnBP-d27	–	2.33
IDPP	TnBP-d27	< LOQ	2.45
TTBPP	TnBP-d27	< LOD	3.72
RDP	TnBP-d27	< LOQ	0.11
V6	TnBP-d27	< LOD	0.02
BPA-BDPP	TnBP-d27	< LOD	0.29
BBOEHEP	TCEP-d12	< LOQ	0.68
3OH-TBOEP	TnBP-d27	< LOD	0.22

Detected concentrations ranged from 0.25 ng/g to 23.5 ng/g, while LOD ranged from 0.02-3.97 ng/g corresponding to LOQ ranging from 0.07-13.2 ng/g which is comparable to what found in previous studies as shown in Table 2.3. Also TCIPP showed the highest concentration which also corresponds to what was detected in previous studies of OPFRs in foodstuffs. TCIPP have a variety of suspected toxic effects which makes it important to determine the extent of its presence in foodstuffs.

4.5 Analysis

For TMP, TEP, TnPP, TnBP, TiBP, TBOEP, TCEP, TPP, TMPP, RDP, V6, BPA-BDPP, BBOEHEP, 3OH-TBOEP recoveries ranged from 48.1-143%. The compounds that were challenging to analyze in this project tended to have very high blank values (RB>MM), and corresponding bad or negative recoveries. In literature the blank values reported are

not that high, but the issue of contamination and high blank values is pointed out in example in Poma et al. (2018) and Brandsma et al. (2013a). The compounds considered most challenging to analyze in this project were TEHP, TCIPP, TDCIPP, EHDP, IDPP and TTBPP. For IDPP only one study on foodstuff reports detection, while for TTBPP no studies of my knowledge on OPFRs with foodstuffs as the matrix have detected the compound. Neither V6, BPA-BDPP, RDP or any of the metabolites are reported to be detected in studies of OPFRs in foodstuffs. Nevertheless TEHP, TCIPP and TDCIP are more frequently detected and reported as shown in Table 2.4. The reasons why we did not manage to obtain acceptable recoveries for these compounds may be related to contamination during the extraction, contamination of the instrument or a not optimized extraction method.

The trouble with high blank values is as mentioned pointed out in Poma et al. (2018) where it is stated that contamination is reported as one of the biggest issues when analyzing OPFRs because of their presence in dust. Repeatedly cleaning the working space and all laboratory equipment with in example acetone, and evaporation done in a fumehood in combination with all glass equipment precleaned with *n*-hexane and dried for 2.5 hours in 300°C was tested and found helpful in Poma et al. (2018). Contamination in all steps of sample preparation and analysis is extremely important since OPFRs inevitably is present in indoor air and in dust. Brandsma et al. (2013a) did a worldwide interlaboratory study of OPFR analysis where monitoring of blank values were an important part of the study. Variations between laboratories were reported, and also which compounds causing the highest blank values. Overall TnBP, TiBP, TBOEP and TCIPP were reported to show the highest blank values. TCIPP was the only compound with corresponding high blanks as reported in Brandsma et al. (2013a). Nevertheless the issue of contamination is inevitably one of the most challenging parts of analyzing OPFRs. Use of clean room, if available, and avoiding use of plastic and rubber was suggested as possible methods to avoid contamination from dust.

Contamination in all steps from sample preparation to UPLC-MS/MS analysis are important to take into consideration. Contamination of the instrument, and OPFRs used in parts of the instrument, may have affected the blanks to show very high peaks, and can therefore not be excluded as reasons for high blank values.

All data obtained in this project originates from what was supposed to be the method development. This can have affected the results in a variety of ways. In example was the sample preparation and extraction done for the first time when preparing the samples analyzed. Familiarity with the method can affect both precision in pipetting technique and awareness on contamination. Also familiarity with the software for processing of the data is favorable to ensure correct calculations.

4.6 SRM Transitions

SRM Transitions for 26 OPFRs was obtained from the MS instrument by use of Waters IntelliStart software. Suggested structure of the daughter fragments is presented together with the transitions and the the optimized MS-spectrum at the collision energy that best show all detected fragments in Sections 4.6.2 to 4.6.23. A suggested general mechanism for the fragmentation is also presented in Section 4.6.1. A summary of the detected SRM transitions is nevertheless presented in Table 4.33, while the SRM transitions found in literature is presented in Table 4.32. The advantage of the triple quadrupole in this matter is the ability to do rapid screenings, and that it also facilitates consecutive fragmentation.

4.6.1 General fragmentation mechanism

Many of the OPFRs tend to fragment through the same pattern. The suggested general mechanism for fragmentation is shown in Section 4.6.1 and made by utilizing the proposed fragmentation patterns from Bell et al. (1997) and Schwarzenberg et al. (2013) presented in Section 2.4.8. The pattern shows that most OPFRs fragment by breaking the ester bonds which result in breaking off one chain after another until the protonated phosphoric acid at m/z 99 is formed.

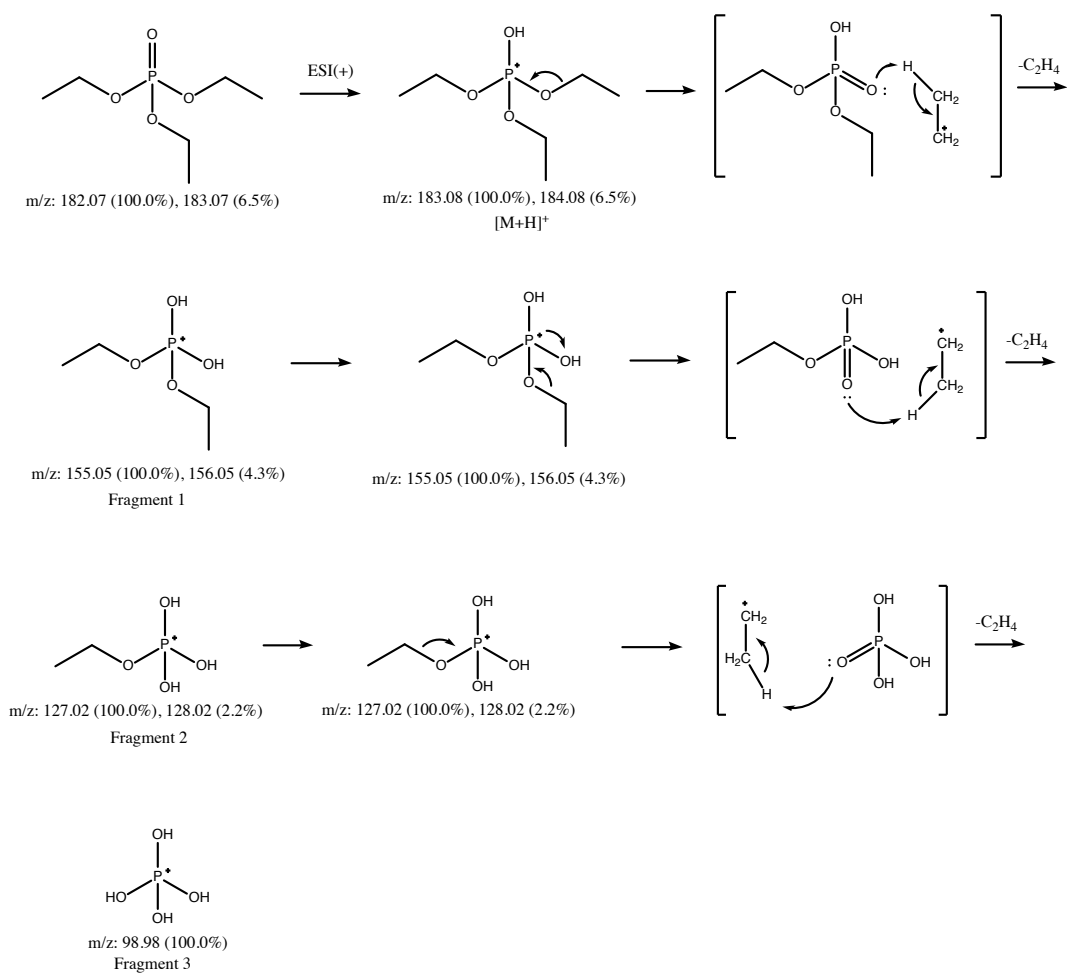


Figure 4.1: General reaction mechanism for fragmentation of OPFRs. TEP is used as an example compound.

4.6.2 TMP

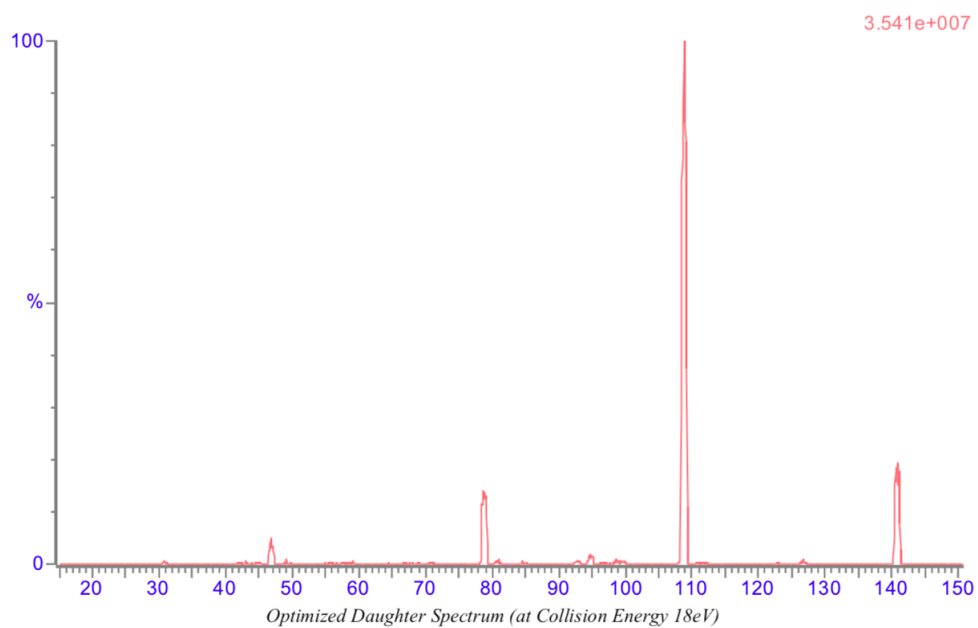


Figure 4.2: Optimized daughter spectrum for TMP at collision energy 18eV.

Compound	Formula/Mass		Parent m/z	Cone Voltage	Daughters	Collision Energy	Ion Mode
TMP	C ₃ H ₉ O ₄ P	1	140.86	32	108.86	16	ES+
		2	140.86	32	78.90	22	ES+
		3	140.86	32	46.98	14	ES+
		4	140.86	32	94.82	18	ES+

Table 4.6: SRM transitions for TMP.

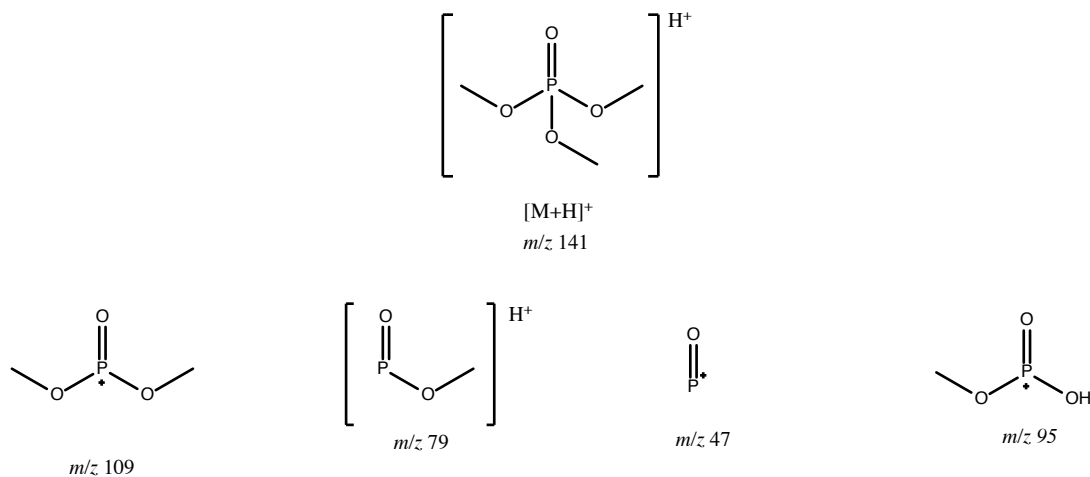


Figure 4.3: Suggested TMP daughter fragments.

Both the molecular ion and fragment 1, 2 and 3 are clearly visible in the spectra with optimized collision energy at 18eV. The daughter ion with m/z 95 shows the lowest abundance of the fragments, and the fragmentation of this may therefore be the most uncertain of the fragments since it neither follows the mechanism suggested in Section 4.6.1 or is clearly visible in the spectra of 18 eV or in spectra with collision energy of 14, 16 or 22 eV. It is neither reported as one of the daughter fragments in Table 4.32 which also may be an indicator of its uncertainty.

4.6.3 TEP

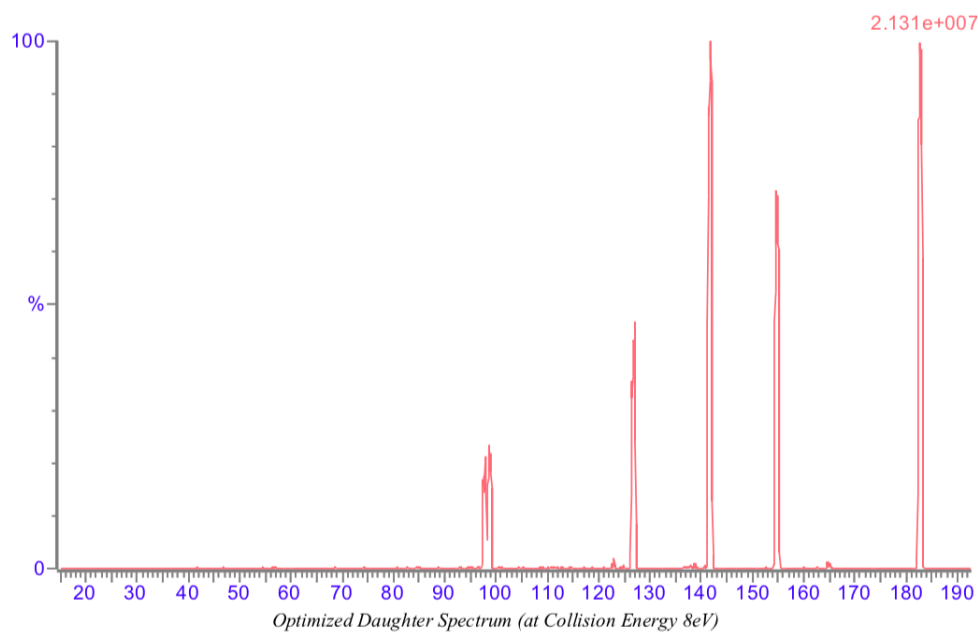


Figure 4.4: Optimized daughter spectrum for TEP at collision energy 8eV.

Compound	Formula/Mass		Parent m/z	Cone Voltage	Daughters	Collision Energy	Ion Mode
TEP	C ₆ H ₁₅ O ₄ P	1	182.85	22	98.65	18	ES+
		2	182.85	22	141.80	6	ES+
		3	182.85	22	126.85	10	ES+
		4	182.85	22	154.86	8	ES+

Table 4.7: SRM transitions for TEP.

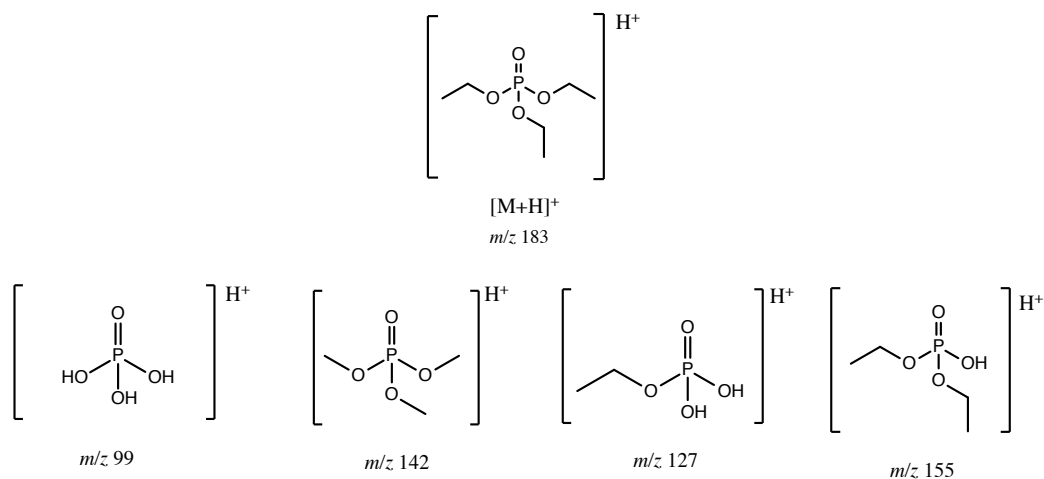


Figure 4.5: Suggested TEP daughter fragments.

In the spectrum for TEP all daughters from Table 4.12 are clearly visible with minimal noise. The suggested breakdown mechanism for TEP is shown in Section 4.6.1 and include mechanism for daughter fragments at m/z 155, 127 and 99. The fragment at 142 is neither a part of the suggested breakdown mechanism, nor presented in literature (Table 4.32). Most literature only presents the qualifier and quantifier ions, and for TEP the qualifier and quantifier ion is most often presented as the m/z at 155 and 127. In this experiment the m/z at 155 and 127 do also have the largest areas after integration, and are chosen as respectively the qualifier and quantifier ion.

4.6.4 TnPP

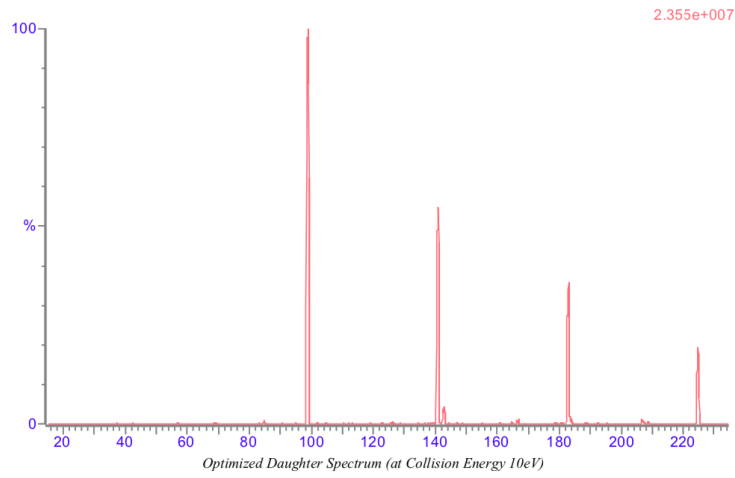


Figure 4.6: Optimized daughter spectrum for TnPP at collision energy 10eV.

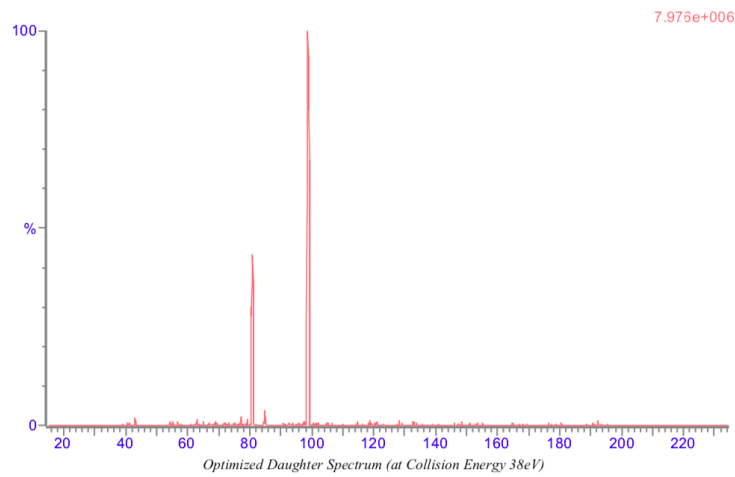


Figure 4.7: Optimized daughter spectrum for TnPP at collision energy 38eV.

Compound	Formula/Mass		Parent m/z	Cone Voltage	Daughters	Collision Energy	Ion Mode
TnPP	C ₉ H ₂₁ O ₄ P	1	224.89	10	98.83	16	ES+
		2	224.89	10	140.87	10	ES+
		3	224.89	10	84.80	18	ES+
		4	224.89	10	80.83	38	ES+

Table 4.8: SRM transitions for TnPP.

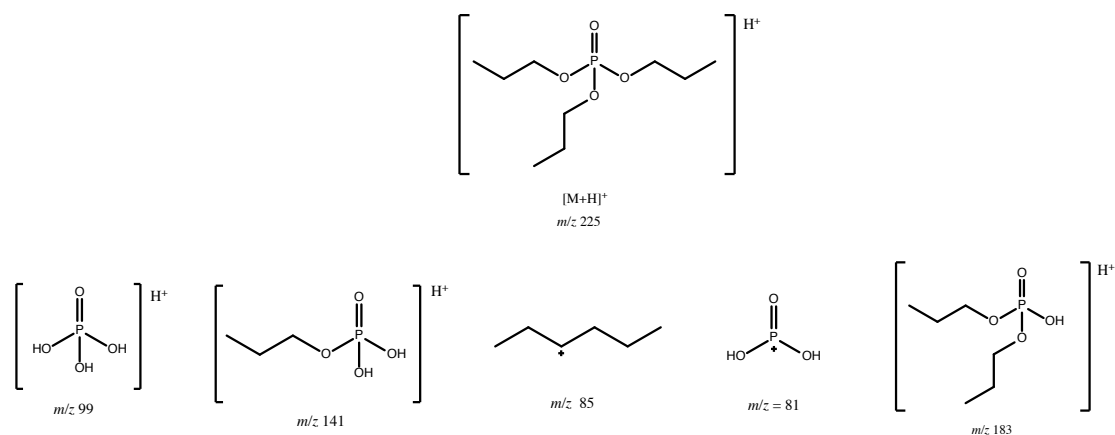


Figure 4.8: Suggested TnPP daughter fragments.

For TnPP only the daughter ions at m/z 99 and 141 follows the suggested general mechanism from Section 4.6.1. The fragment with m/z 85 was difficult to predict since following the steps of the suggested fragmentation mechanism does not lead to a m/z 85 fragment. In the spectra provided from the MS no clear peak is shown at m/z 85, while the m/z 81 only is visible as a clear peak when the collision energy is set to 38 eV. This is relatively high compared to the spectrum obtained at 10eV, making it more possible to form fragments that are not the evident suggestions by following Section 4.6.1. The suggested fragment at m/z 85 is a merge of the two consecutive losses from the molecular ion at m/z 225 to m/z 183 and further to m/z 141. Loss of water from the protonated phosphoric acid at m/z 99 likely forms the m/z 81 at higher collision energies, and is an example on how fragmentation can occur after consecutively releasing the three alkyl chains.

In the spectrum at 10eV another peak has relatively high abundance at around m/z 183. Even though it is not detected as a daughter fragment in the SRM, it is presented as a daughter fragment in multiple articles (Table 4.32) and fits well with the breakdown pattern. The structure for a daughter ion at m/z 183 is therefore suggested in Figure 4.8 as it likely is a daughter ion from TnPP.

4.6.5 TnBP

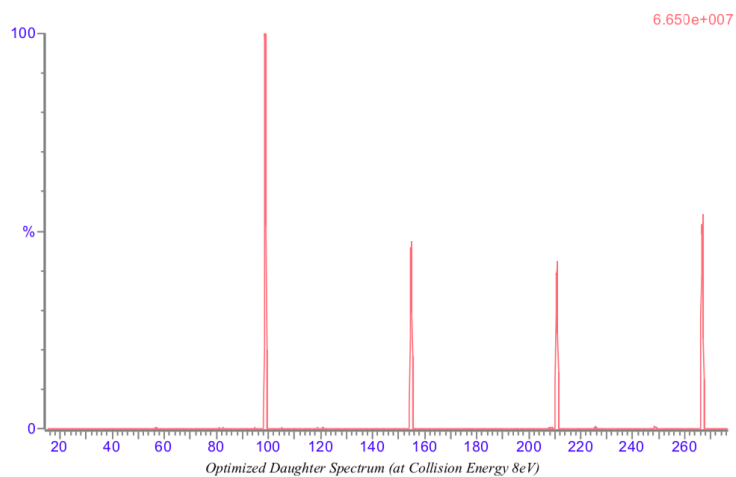


Figure 4.9: Optimized daughter spectrum for TnBP at collision energy 8eV.

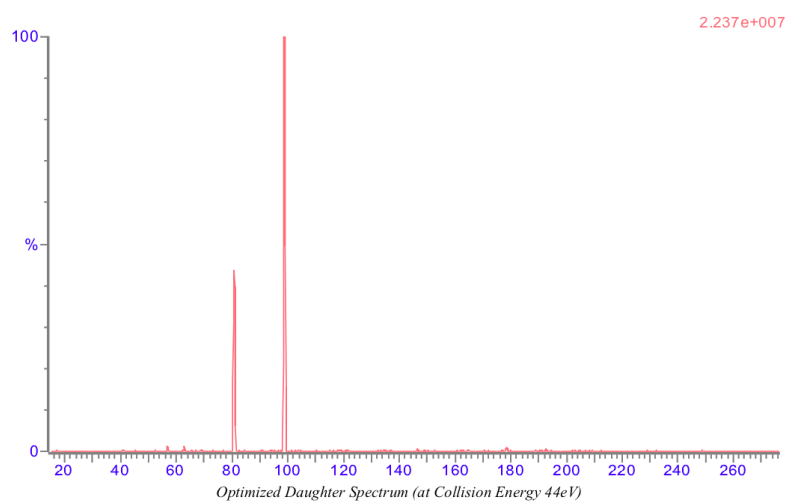


Figure 4.10: Optimized daughter spectrum for TnBP at collision energy 44eV.

Compound	Formula/Mass		Parent m/z	Cone Voltage	Daughters	Collision Energy	Ion Mode
TnBP	C ₁₂ H ₂₇ O ₄ P	1	266.88	10	98.76	14	ES+
		2	266.88	10	154.84	8	ES+
		3	266.88	10	210.92	6	ES+
		4	266.88	10	80.82	44	ES+

Table 4.9: SRM transitions for TnBP.

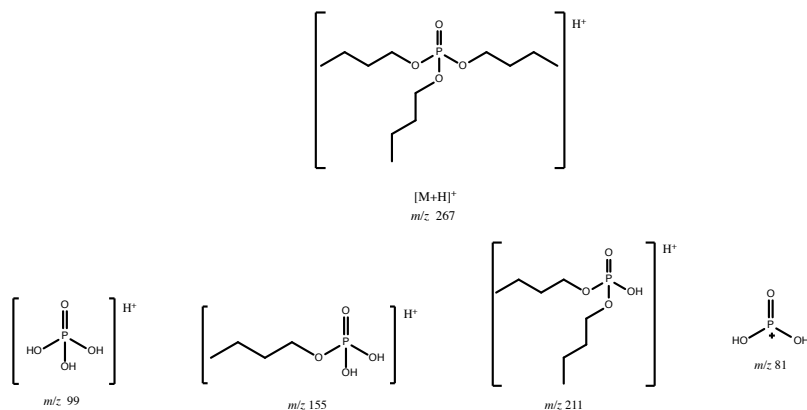


Figure 4.11: Suggested TnBP daughter fragments.

Both the molecular ion at m/z 267 and the daughter fragments at m/z 99, m/z 155 and m/z 211 are visible with abundance of around 50% and up in the spectrum obtained at 8eV. The suggested fragments presented in Figure 4.11 follows the general mechanism for fragmentation (see Section 4.6.1). The fragment at m/z 81 was as in Section 4.6.4 only visible in the spectrum with highest collision energy (here 44eV), where rearrangement and smaller molecules is more probable. The ion at m/z 81, with a loss of 18 Da is as in Section 4.6.4 proposed to be the loss of water from the protonated phosphoric acid at m/z 99 when collision energies are higher.

4.6.6 TiBP

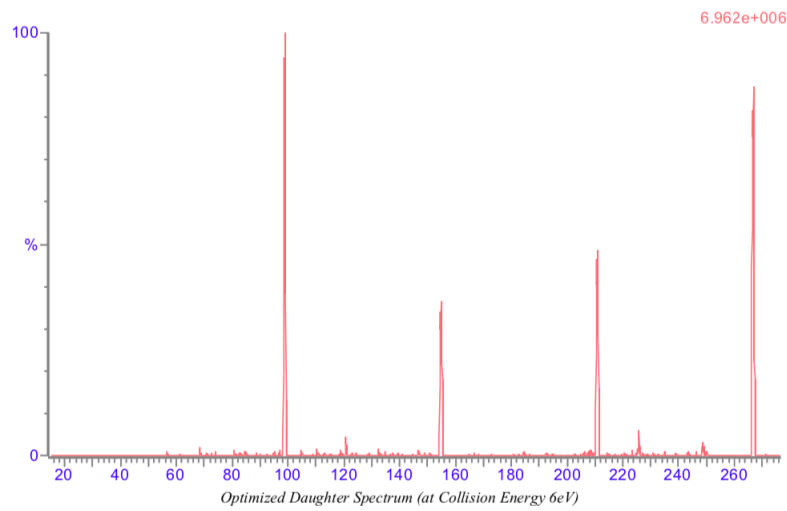


Figure 4.12: Optimized daughter spectrum for TiBP at collision energy 6eV.

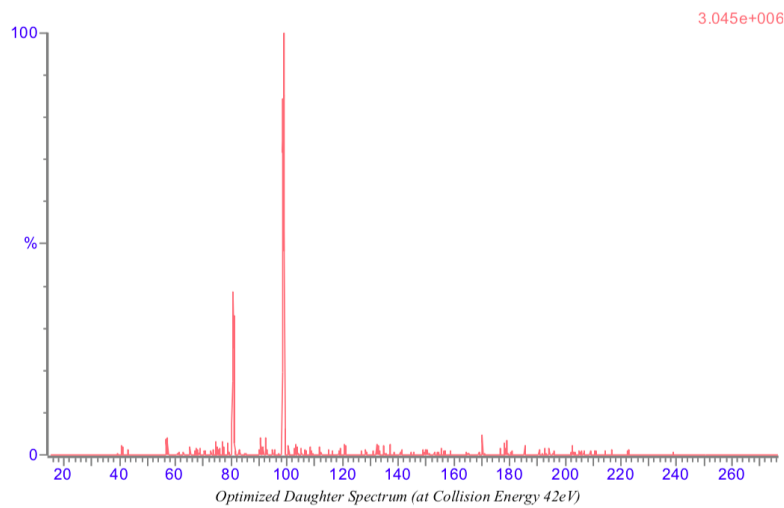


Figure 4.13: Optimized daughter spectrum for TiBP at collision energy 42eV.

Compound	Formula/Mass		Parent m/z	Cone Voltage	Daughters	Collision Energy	Ion Mode
TiBP	C ₁₂ H ₂₇ O ₄ P	1	266.88	14	98.82	14	ES+
		2	266.88	14	210.92	6	ES+
		3	266.88	14	154.84	6	ES+
		4	266.88	14	80.83	42	ES+

Table 4.10: SRM transitions for TiBP.

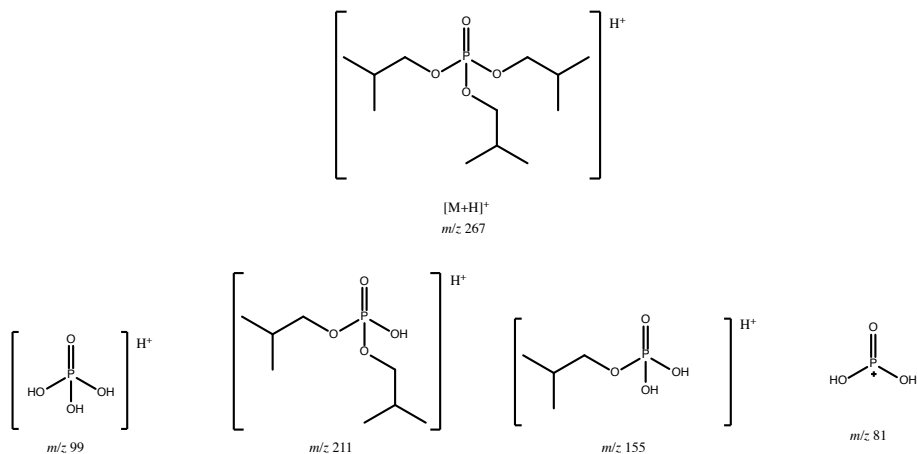


Figure 4.14: Suggested TiBP daughter fragments.

The suggested structures of the daughter ions for TiBP are presented in Figure 4.14. The daughter ions at m/z 99, 211 and 155 correlate to the daughter ions from Section 4.6.5 and works well with the suggested general fragmentation mechanism for the OPFRs. As in Section 4.6.5 and Section 4.6.4 the m/z 81 daughter is only visible when the collision energy is higher, like in Figure 4.13 where the collision energy is 42eV compared to 6eV in Figure 4.12 where all other daughter ions and the molecular ion is visible with abundance from around 40% and up. The m/z 81 is suggested to be the the same m/z 81 as in TnPP and TnBP.

4.6.7 TBOEP

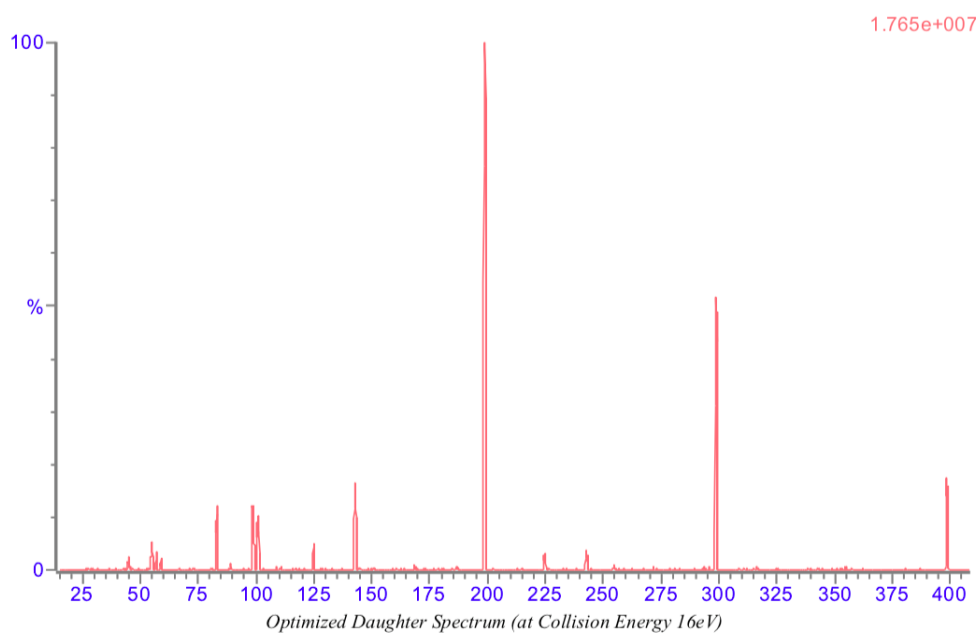


Figure 4.15: Optimized daughter spectrum for TBOEP at collision energy 16eV.

Compound	Formula/Mass		Parent m/z	Cone Voltage	Daughters	Collision Energy	Ion Mode
TBOEP	C ₁₈ H ₃₉ O ₇ P	1	398.89	12	298.89	10	ES+
		2	398.89	12	198.82	14	ES+
		3	398.89	12	98.82	26	ES+
		4	398.89	12	142.81	16	ES+

Table 4.11: SRM transitions for TBOEP.

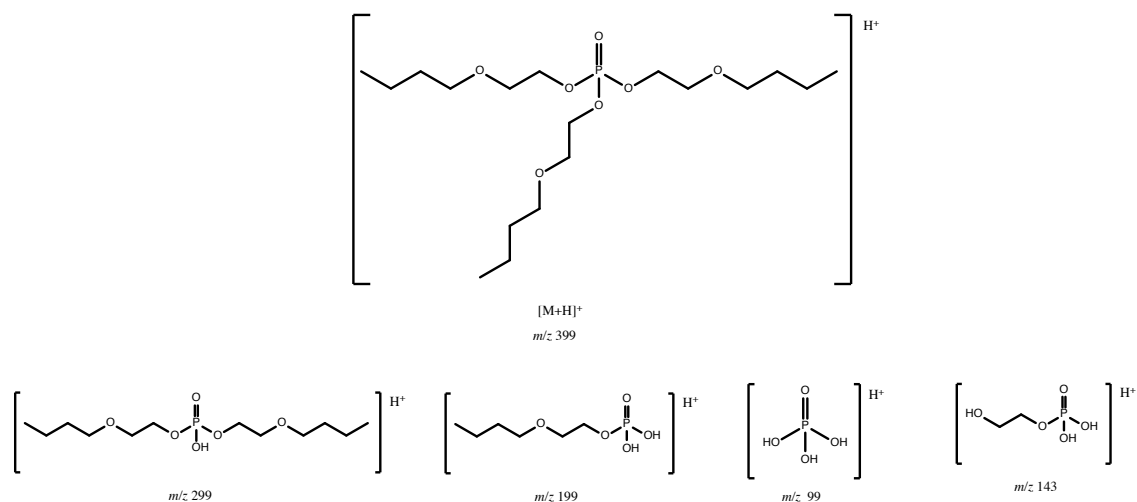


Figure 4.16: Suggested TBOEP daughter fragments.

For TBOEP the structure of all detected daughter ions could be suggested by following the general mechanism from Section 4.6.1. The ions at m/z 299, 199 and 99 are all products of sequential losses of the butoxyethyl group. This happens three times leading to m/z 99 which is the protonated phosphoric acid. The fourth daughter ion at m/z 143 is a fragmentation where the fragment at m/z 199 again is fragmented, but instead of breaking off the whole butoxyethyl group, the molecule is fragmented at the oxygen that is not a part of the phosphate. All fragments are visible in the spectrum obtained at collision energy 16eV.

4.6.8 TEHP

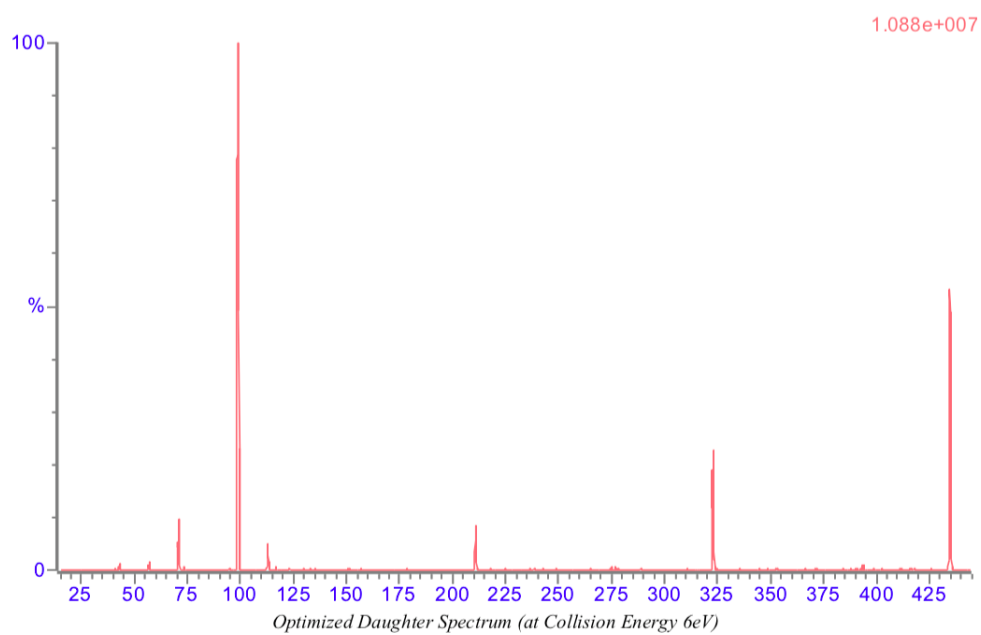


Figure 4.17: Optimized daughter spectrum for TEHP at collision energy 6eV.

Compound	Formula/Mass		Parent m/z	Cone Voltage	Daughters	Collision Energy	Ion Mode
TEHP	C ₂₄ H ₅₁ O ₄ P	1	434.94	24	98.82	12	ES+
		2	434.94	24	322.96	4	ES+
		3	434.94	24	70.95	8	ES+
		4	434.94	24	210.92	6	ES+

Table 4.12: SRM transitions for TEHP.

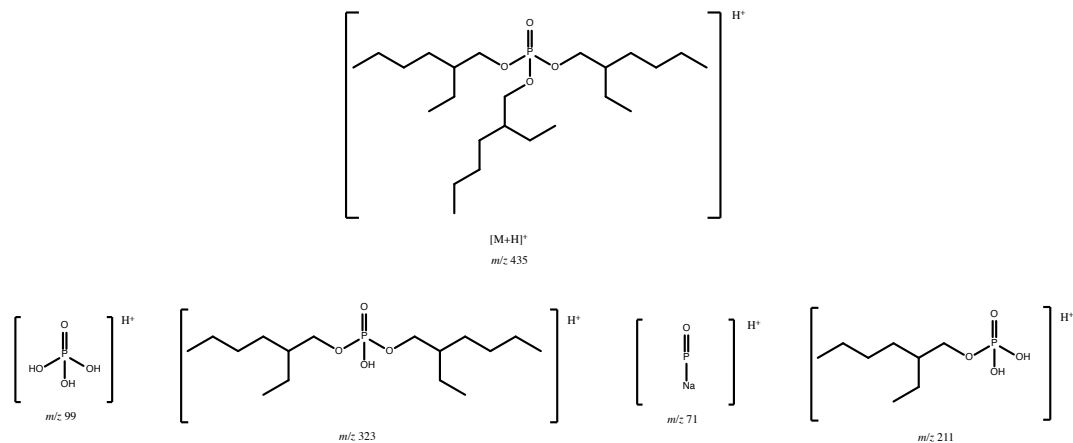


Figure 4.18: Suggested TEHP daughter fragments.

The fragment at m/z 323, m/z 211 and m/z follows the suggested fragmentation pathways from Figure 2.7 by three similar consecutive losses of the alkyl chains. The daughter ion at m/z 71 is proposed to be an adduct formed with sodium as shown in Section 2.4.5.

4.6.9 TCEP

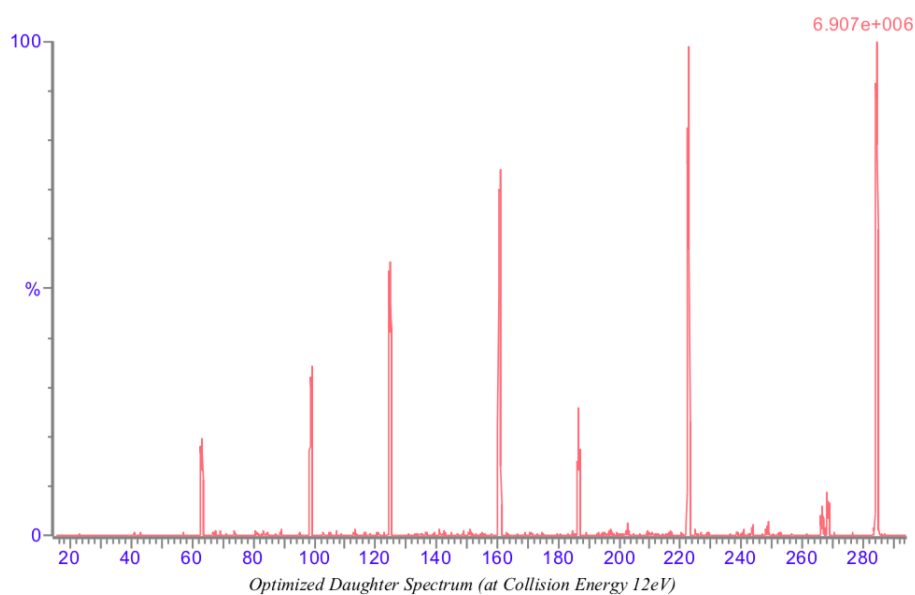


Figure 4.19: Optimized daughter spectrum for TCEP at collision energy 12eV.

Compound	Formula/Mass		Parent m/z	Cone Voltage	Daughters	Collision Energy	Ion Mode
TCEP	C ₆ H ₁₂ Cl ₃ O ₄ P	1	284.67	16	98.82	22	ES+
		2	284.67	16	222.73	12	ES+
		3	284.67	16	160.74	14	ES+
		4	284.67	16	124.81	14	ES+

Table 4.13: SRM transitions for TCEP.

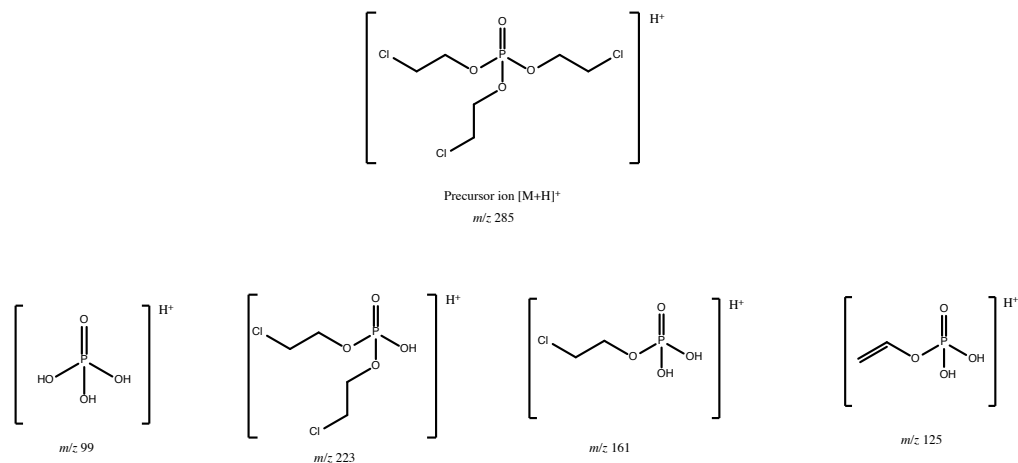


Figure 4.20: Suggested TCEP daughter fragments.

At optimized collision energy 12eV all fragments are clearly visible with good separation. The fragments at m/z 99, m/z 223 and m/z 161 follow the proposed pathway of fragmentation by three similar consecutive losses of one branches with m/z 62. The suggested structure of m/z 125, a protonated phosphoric acid monoethenylester, may be formed by loss of HCl from the daughter at m/z 161. In the spectrum presented in Figure 4.19 a peak is also visible at a little over m/z 60. This may be the compound suggested in Figure 4.21, as a charge migration process can follow the McLafferty rearrangements, that causes the similar consecutive losses at the C-O bonds. This can lead to a positive charge on the fragmented chloroalkyl groups making it detectable. The visible peak at m/z 63, may be the suggested in Figure 2.6 (a) even though it is not detected as a daughter in the SRM.

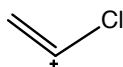


Figure 4.21: Suggested TCEP daughter fragment at m/z 63.

4.6.10 TCIPP

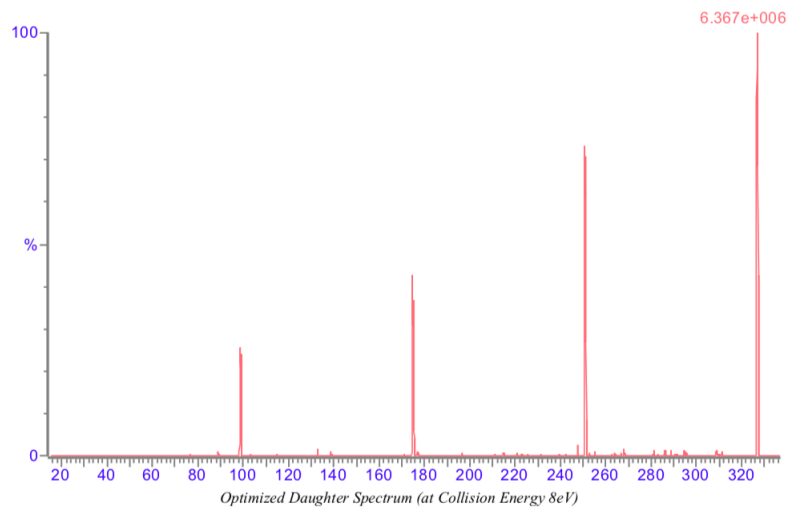


Figure 4.22: Optimized daughter spectrum for TCIPP at collision energy 8eV.

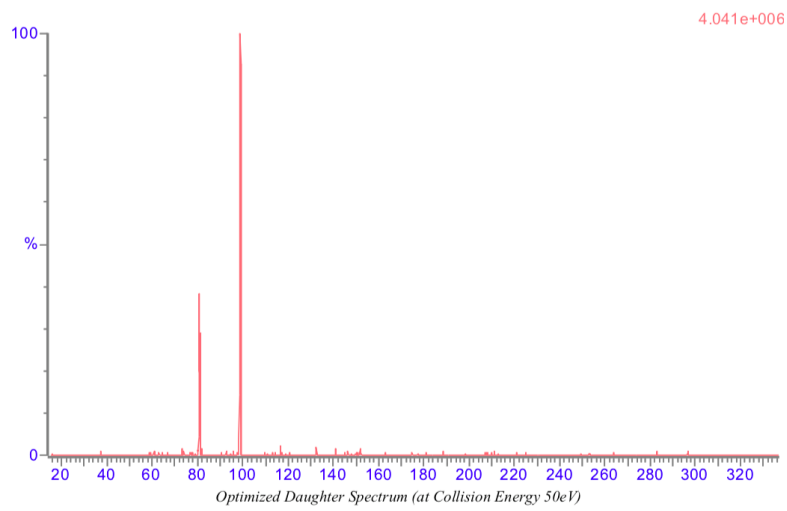


Figure 4.23: Optimized daughter spectrum for TCIPP at collision energy 50eV.

Compound	Formula/Mass		Parent m/z	Cone Voltage	Daughters	Collision Energy	Ion Mode
2020_TCIPP	326	1	327.10	2	98.94	20	ES+
		2	327.10	2	175.02	12	ES+
		3	327.10	2	251.01	8	ES+
		4	327.10	2	80.97	50	ES+

Table 4.14: SRM transitions for TCIPP.

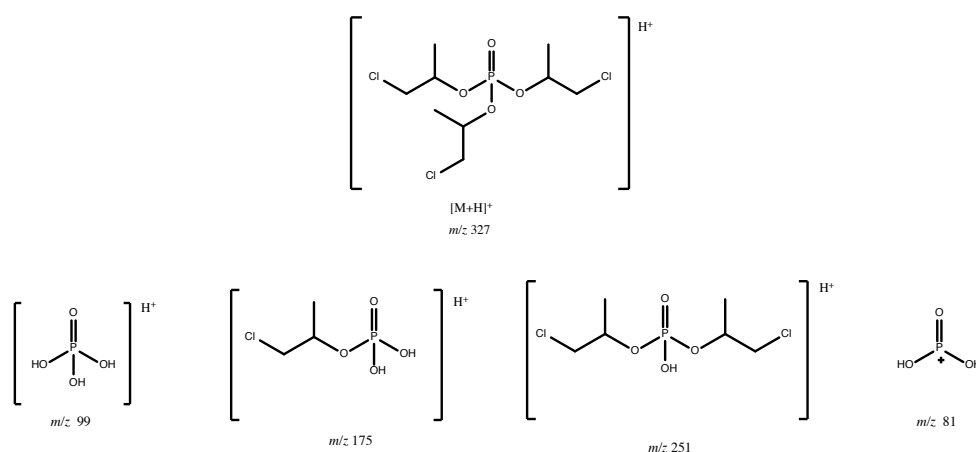


Figure 4.24: Suggested TCIPP daughter fragments.

TCIPP follows the suggested fragmentation pathway from Figure 2.7 leading to three consecutive losses of 76 Da. Here this represents the fragmentation of the three chloroalkyl chains, leading to the detected daughters at m/z 251, m/z 175 and m/z 99. The fragment at m/z 81 is also here a result of water elimination from the m/z 99. It is only visible at a higher collision energy where the molecular ion at m/z 327 and the two heaviest daughters at m/z 251 and m/z 175 no longer is visible. Obtaining multiple spectra at different collision energies is important to get a full picture of possible ways for fragmentation and rearrangement, even though the fragments only visible at high collision energies often are less likely to be dominant amongst the other fragments.

4.6.11 TDCIPP

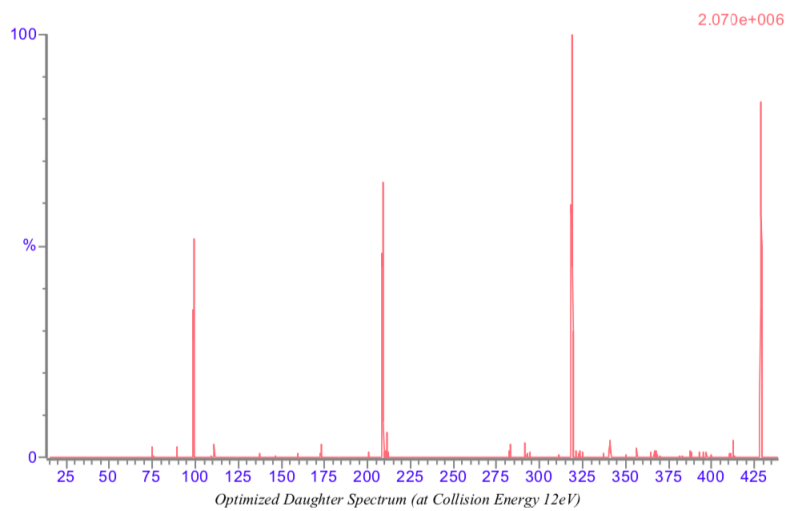


Figure 4.25: Optimized daughter spectrum for TDCIPP at collision energy 12eV.

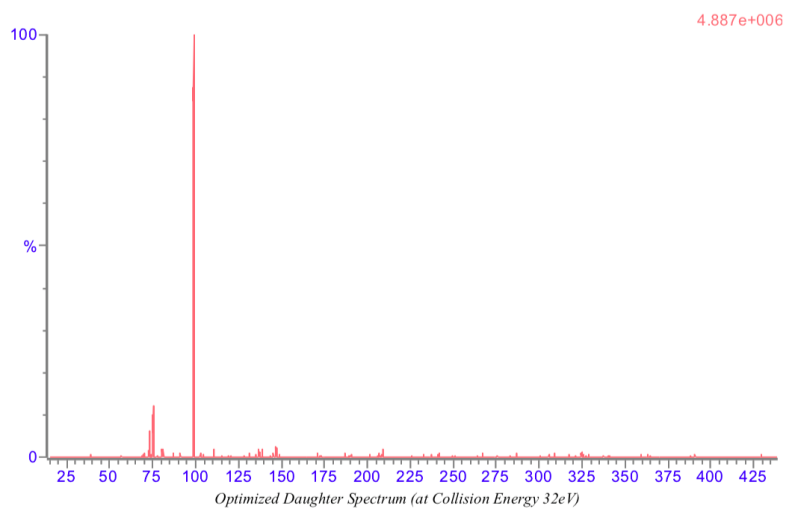


Figure 4.26: Optimized daughter spectrum for TDCIPP at collision energy 32eV.

Compound	Formula/Mass		Parent m/z	Cone Voltage	Daughters	Collision Energy	Ion Mode
2020_TDCIPP	C ₉ H ₁₅ Cl ₆ O ₄ P	1	428.98	28	98.93	22	ES+
		2	428.98	28	208.96	16	ES+
		3	428.98	28	318.94	12	ES+
		4	428.98	28	74.98	32	ES+

Table 4.15: SRM transitions for TDCIPP.

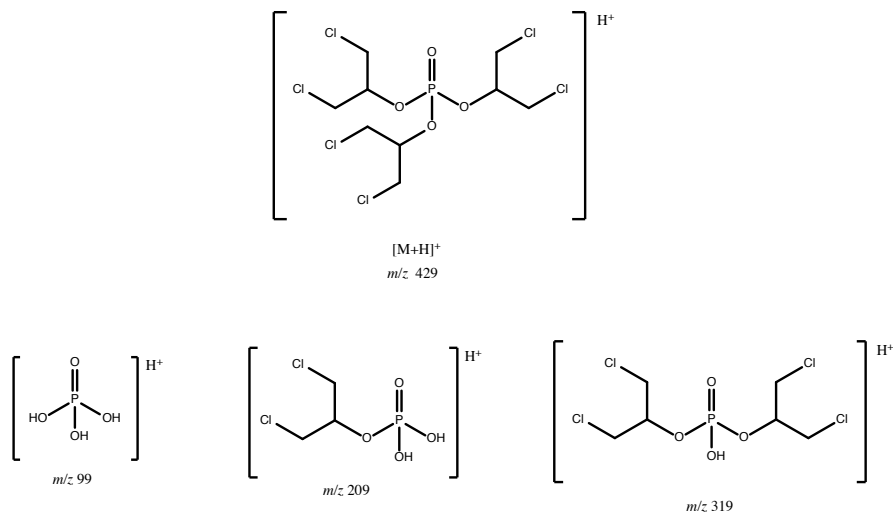


Figure 4.27: Suggested TDCIPP daughter fragments.

The fragmentation of TDCIPP mainly follows the suggested pathway for fragmentation of OPFRs from Figure 2.7. This accounts for the structural elucidation of m/z 319, m/z 209 and the protonated phosphoric acid at m/z 99. The fragment detected as the fourth daughter at m/z 75 is as the m/z 81 from TCIPP, TiBP, TnBP and TnPP only visible in the spectrum when collision energy is risen and possibilities for rearrangement increased. It is not possible to predict the structure for the m/z 75 by following the general mechanism or by breaking bonds within the compound, and therefore no structure is suggested for the m/z 75.

4.6.12 TPP

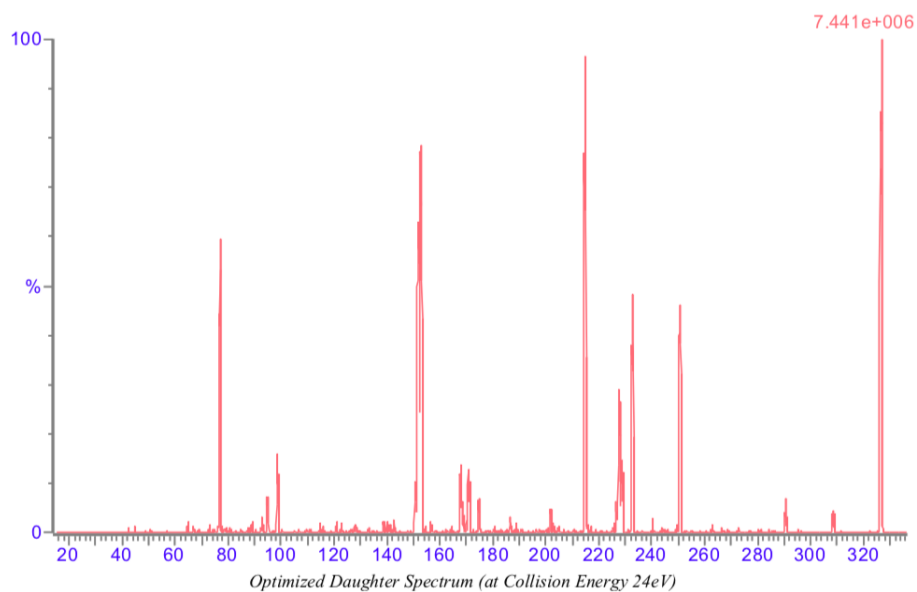


Figure 4.28: Optimized daughter spectrum for TPP at collision energy 24eV.

Compound	Formula/Mass		Parent m/z	Cone Voltage	Daughters	Collision Energy	Ion Mode
TPP	C ₁₈ H ₁₅ O ₄ P	1	326.72	38	151.96	32	ES+
		2	326.72	38	76.92	32	ES+
		3	326.72	38	214.79	24	ES+
		4	326.72	38	250.79	28	ES+

Table 4.16: SRM transitions for TPP.

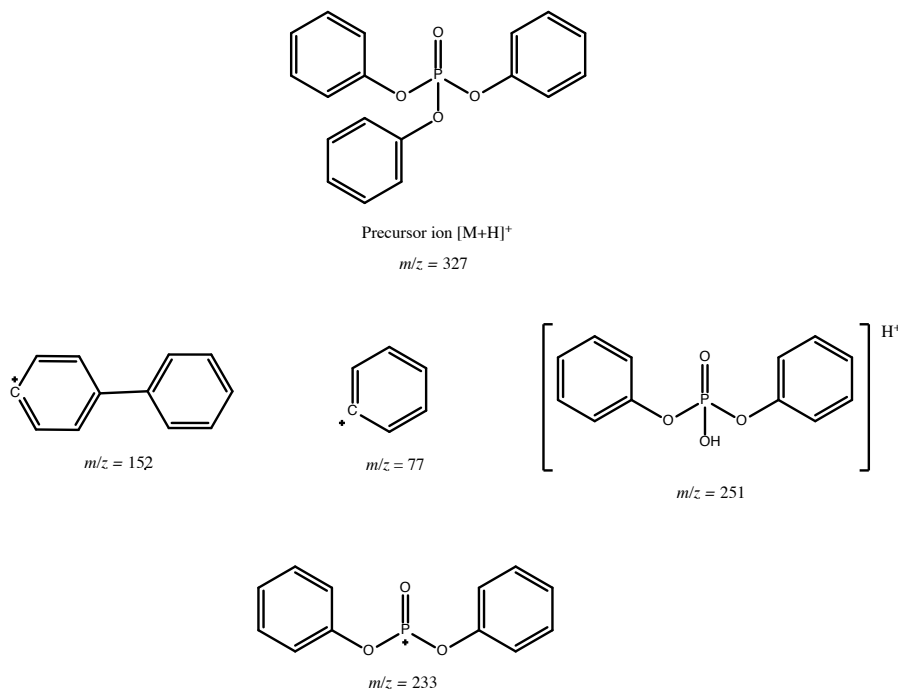


Figure 4.29: Suggested TPP daughter fragments.

For TPP the fragmentation does not follow the fragmentation pattern suggested with the McLafferty rearrangements for more than the daughter ion at m/z 251. The m/z 152 may be a result of a rearrangement from the molecular ion at m/z 327 (Rodil et al., 2005). Also the m/z 77 ion may be formed by breaking off the molecular ion, or the m/z 152. The structure of m/z 215 is harder to predict, but Rodil et al. (2005) suggests it can be formed by two consecutive losses of water from the m/z 251 or loss of water from a predicted ion with m/z 233 formed by losing a phenol from the molecular ion. Also, Lorenzo et al. (2016) suggests the molecular formula for the peak at m/z 215 to be $C_{12}H_8O_2P^+$ which supports Rodil et al. (2005) in the suggested loss from $C_{12}H_{10}O_3P^+$ at m/z 233. The m/z 233 is proposed in literature, and the peak at 233 is visible in the optimized daughter spectrum for TPP at collision energy 24eV, and the structure is therefore included in Figure 4.29.

4.6.13 DCrP

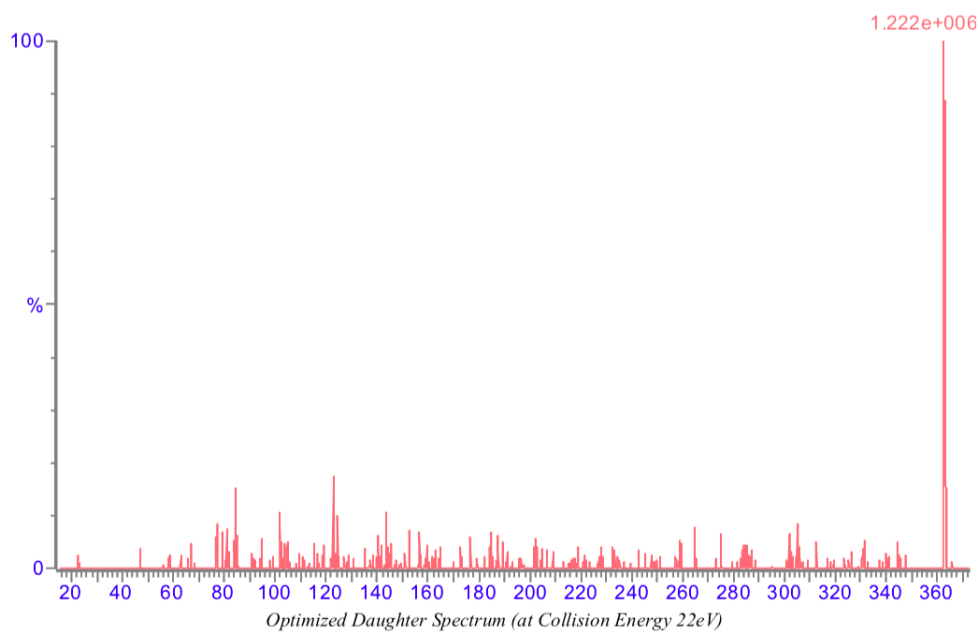


Figure 4.30: Optimized daughter spectrum for DCrP at collision energy 22eV.

Compound	Formula/Mass		Parent m/z	Cone Voltage	Daughters	Collision Energy	Ion Mode
DPhP_DCrP	C19H17O4P	1	362.99	6	102.11	24	ES+
		2	362.99	6	77.06	22	ES+
		3	362.99	6	123.23	22	ES+
		4	362.99	6	84.22	22	ES+

Table 4.17: SRM transitions for DCrP.

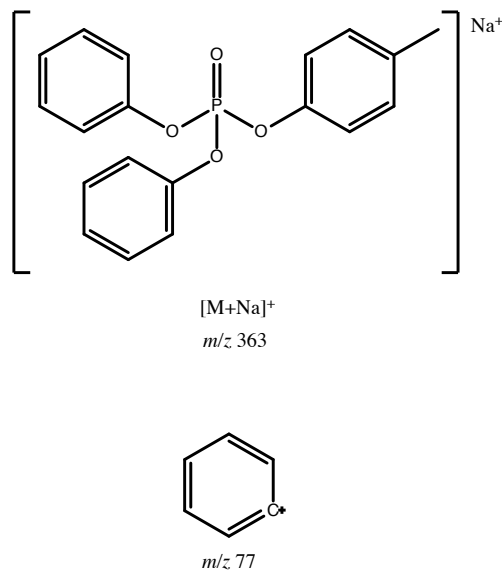


Figure 4.31: Suggested DCrP daughter fragments.

For DCrP only the molecular ion at m/z 363 is clearly visible. The molecular weight of DCrP is 340.32 g/mol which can indicate that the molecular ion has a positive sodium ion instead of a proton. The fragment at m/z 77 is suggested as the same m/z 77 fragment suggested for TPP (Figure 4.29). The fragments at m/z 102, m/z 123 and m/z 84 are difficult to predict as they do not follow the suggested general mechanism of fragmentation, nor is possible to create by breaking any bonds within the compound. This can indicate more complex rearrangements that are harder to predict. The peaks at m/z 102, m/z 123 and m/z 84 is also show low abundance <20%.

4.6.14 TMPP

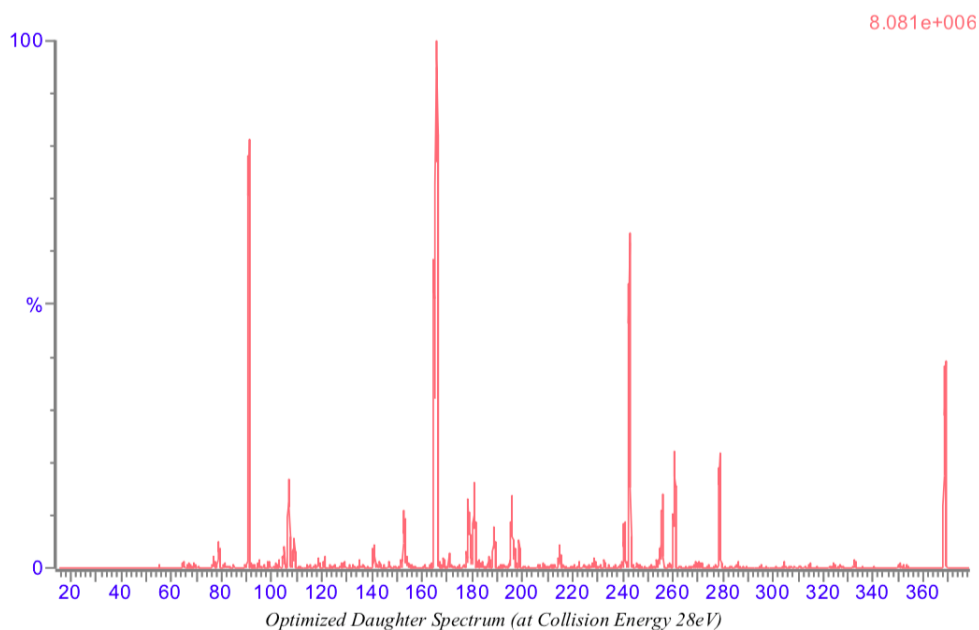


Figure 4.32: Optimized daughter spectrum for TMPP at collision energy 28eV.

Compound	Formula/Mass		Parent m/z	Cone Voltage	Daughters	Collision Energy	Ion Mode
TMPP	C ₂₁ H ₂₁ O ₄ P	1	368.77	30	165.10	38	ES+
		2	368.77	30	90.90	38	ES+
		3	368.77	30	242.83	28	ES+

Table 4.18: SRM transitions for TMPP.

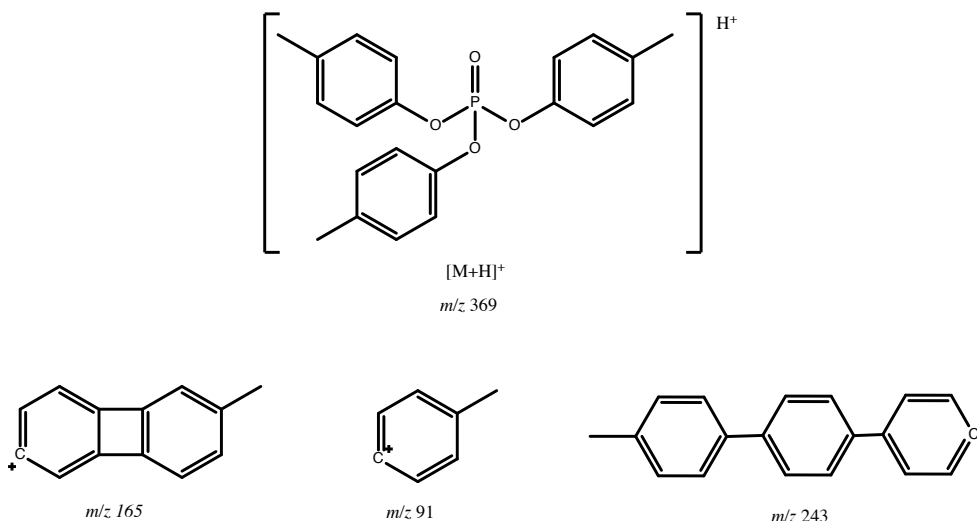


Figure 4.33: Suggested TMPP daughter fragments.

The structures of the daughter fragments for TMPP is difficult to predict with certainty as they do not follow the consecutive losses from breaking the C-O bonds. The optimized spectrum at collision energy 28eV shows the molecular ion and the three daughter ions at abundances over 40%. Some noise is also visible at different parts of the spectrum which may indicate that other ions also may be formed. For the three daughter fragments detected, the structures are suggested with inspiration from the fragmentation of TPP from Rodil et al. (2005) (also rendered in Figure 2.6).

4.6.15 EHDP

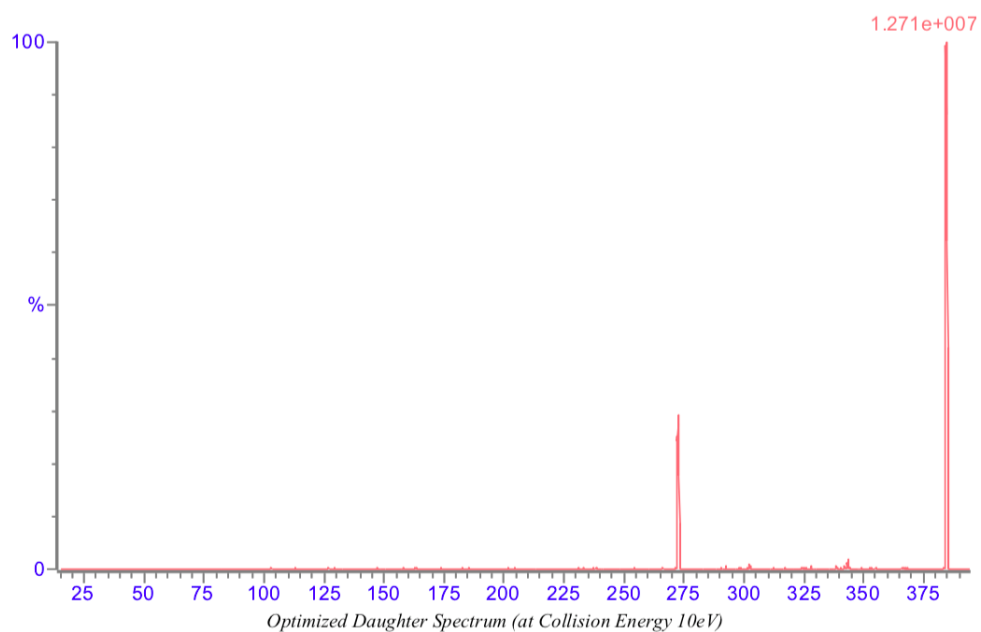


Figure 4.34: Optimized daughter spectrum for EHDP at collision energy 10eV.

Compound	Formula/Mass		Parent m/z	Cone Voltage	Daughters	Collision Energy	Ion Mode
EHDP	362.4	1	384.73	40	272.71	14	ES+
		2	384.73	40	280.76	20	ES+
		3	384.73	40	343.61	10	ES+

Table 4.19: SRM transitions for EHDP.

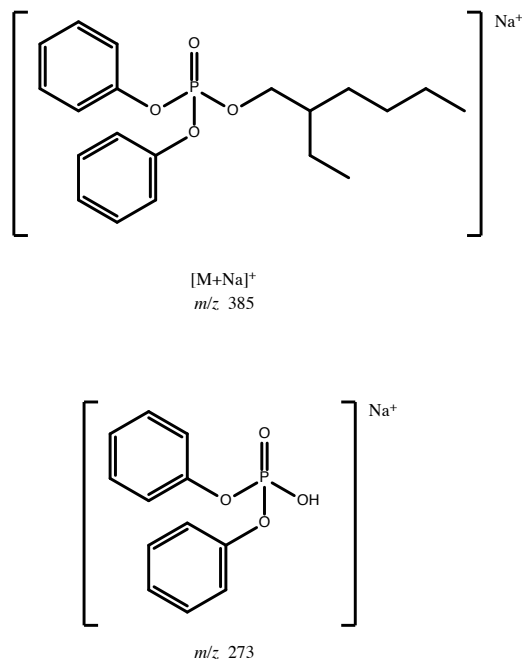


Figure 4.35: Suggested EHDP daughter fragments.

EHDP has a molecular mass of 362 g/mol, while the detected molecular ion is m/z 385. This can indicate that as in DCrP the positive charge comes from a sodium ion. In the spectrum presented in Figure 4.34 only the molecular ion at m/z 385 and the daughter fragment at m/z 273 is clearly visible. The fragmentation creating the m/z 273 follows the protocol in Figure 2.7 by breaking the C-O bond leading to fragmentation of an ethylhexyl fragment. The fragments at m/z 281 and m/z 344 are detected as daughters in the SRM but is not clearly visible in any of the spectrum provided from the MS/MS. Their structures does not follow the general pattern for fragmentation but alternative fragments are nevertheless suggested in Figure 4.36.

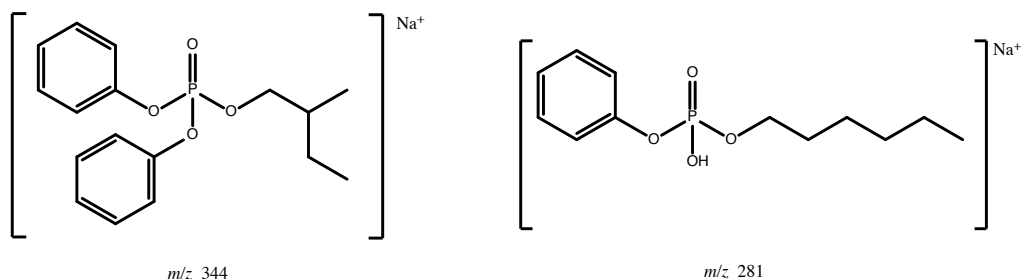


Figure 4.36: Alternative EHDP daughter fragments at m/z 344 and m/z 281.

4.6.16 IDPP

No SRM or spectra was obtained from IDPP. Nevertheless possible daughter fragments are suggested based on the proposed general mechanism for fragmentation and the different fragmentation patterns presented in Section 2.4.8. Structures are suggested for ions at m/z 315, m/z 251, m/z 175, m/z 77, m/z 99 and m/z 239 in addition to the molecular ion at m/z 391.

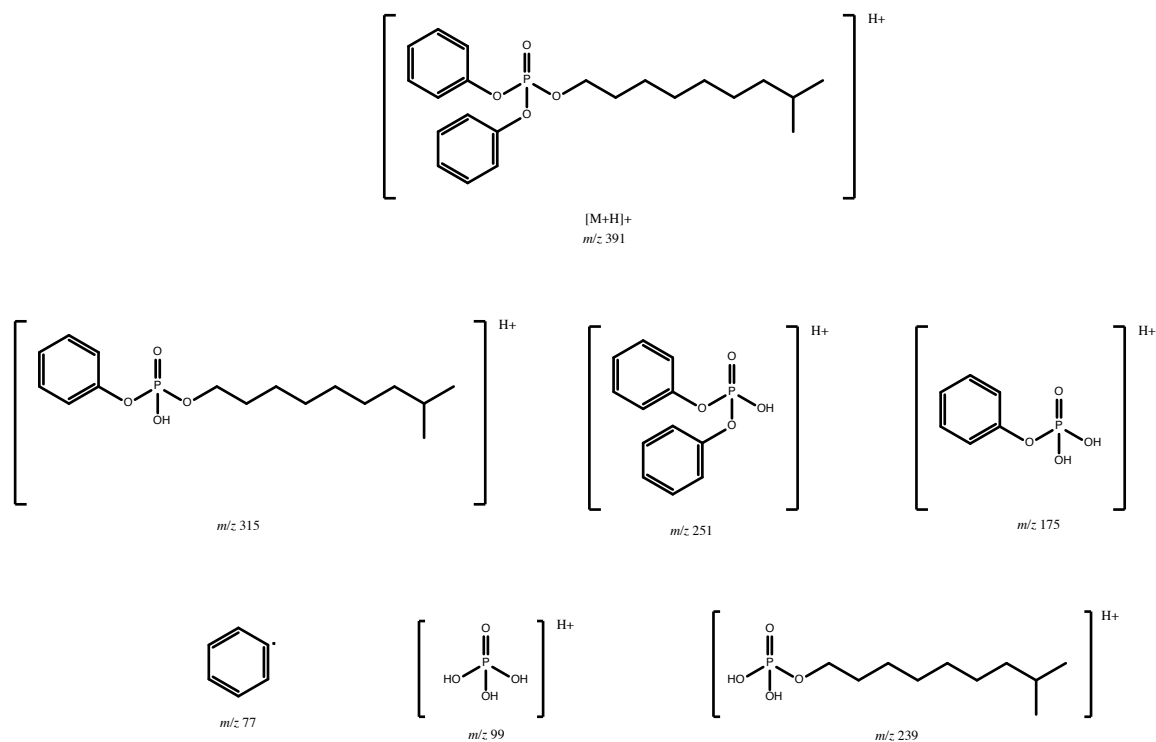


Figure 4.37: Suggested IDPP daughter fragments.

4.6.17 BPDP

As for IDPP, no spectra or daughters detected in SRM was obtained for BPDP. Possible daughter fragments are presented in Figure 4.38 and are suggested by following the presented general mechanism for fragmentation and the different fragmentation patterns presented in Section 2.4.8. Structures are suggested for ions at m/z 307, m/z 175, m/z 251, m/z 231, m/z 99 and m/z 77 in addition to the molecular ion at m/z 383.

Compound	Formula/Mass	Parent m/z	Cone Voltage	Daughters	Collision Energy	Ion Mode
2020_BPDP	C ₂₂ H ₂₃ O ₄ P			No transitions found.		

Table 4.20: SRM transitions for BPDP.

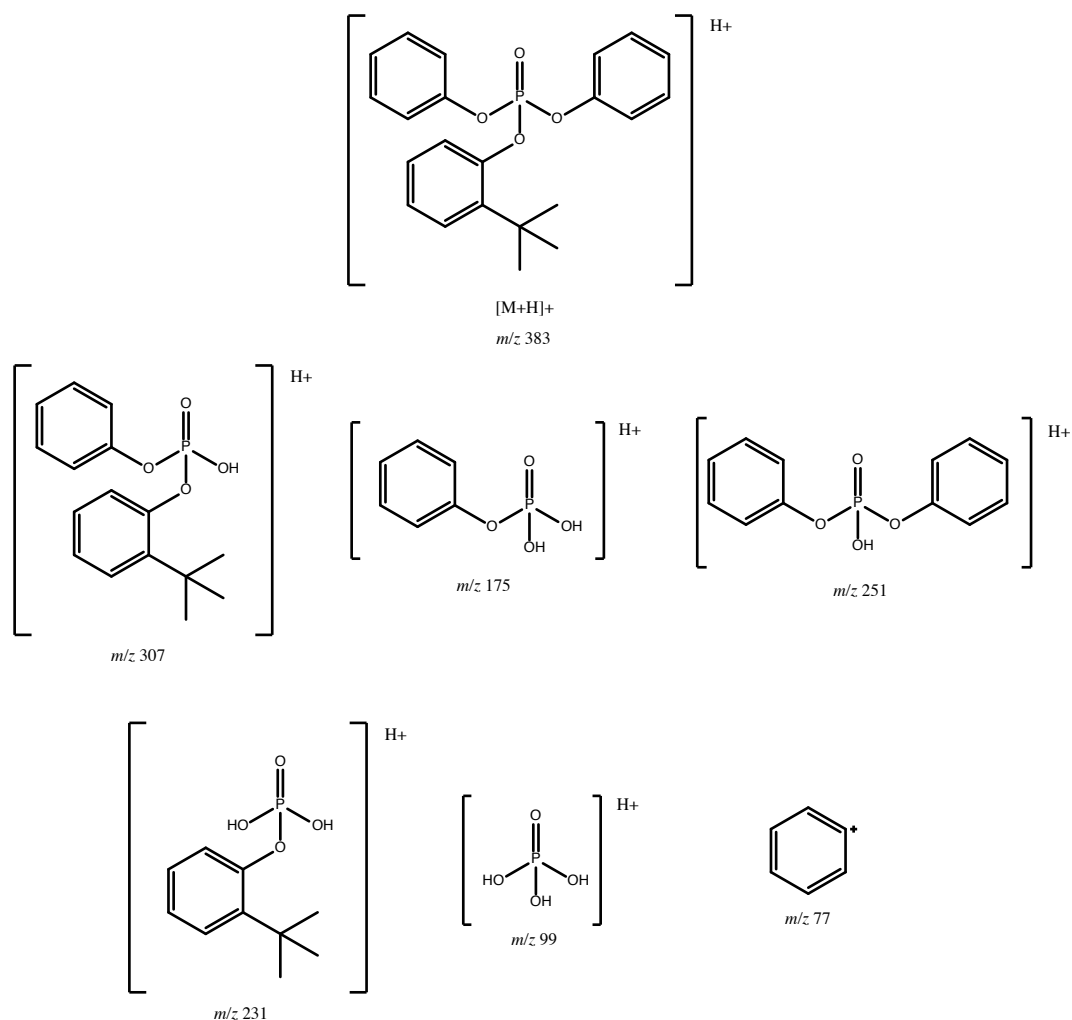


Figure 4.38: Suggested BPDP daughter fragments.

4.6.18 TTBPP

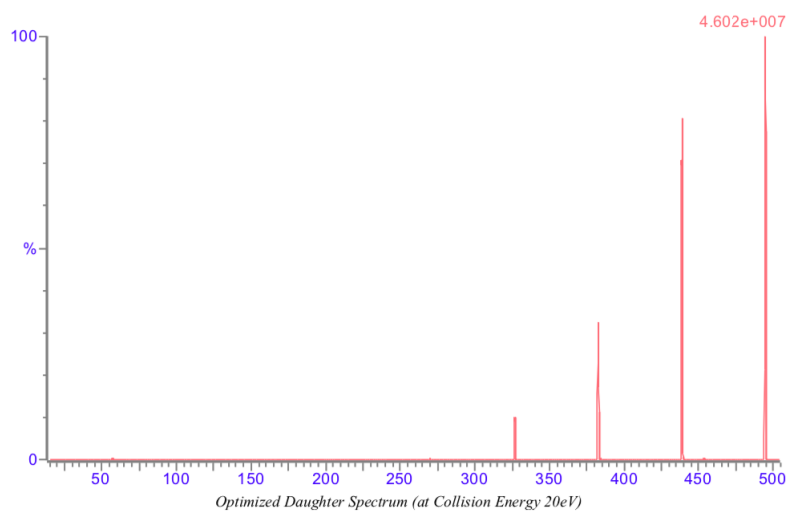


Figure 4.39: Optimized daughter spectrum for TTBPP at collision energy 20eV.

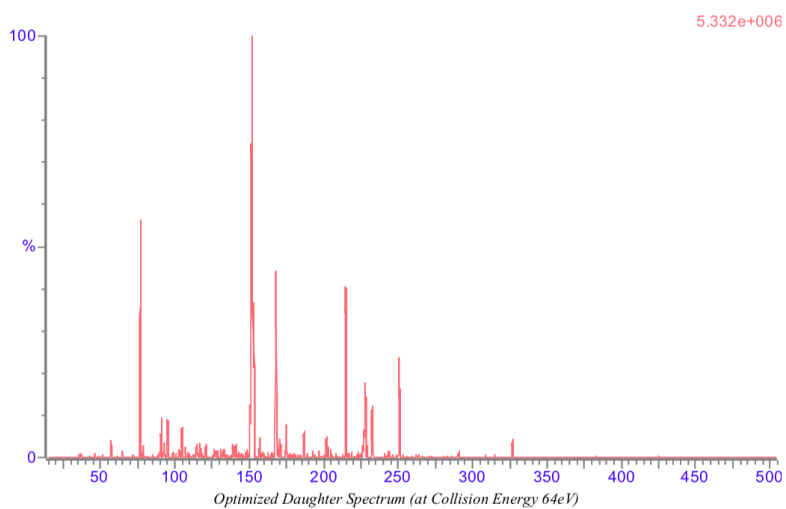


Figure 4.40: Optimized daughter spectrum for TTBPP at collision energy 64eV.

Compound	Formula/Mass		Parent m/z	Cone Voltage	Daughters	Collision Energy	Ion Mode
TTBPP	C ₃₀ H ₃₉ O ₄ P	1	494.78	62	326.77	32	ES+
		2	494.78	62	438.82	20	ES+
		3	494.78	62	382.79	26	ES+
		4	494.78	62	151.97	64	ES+

Table 4.21: SRM transitions for TTBPP.

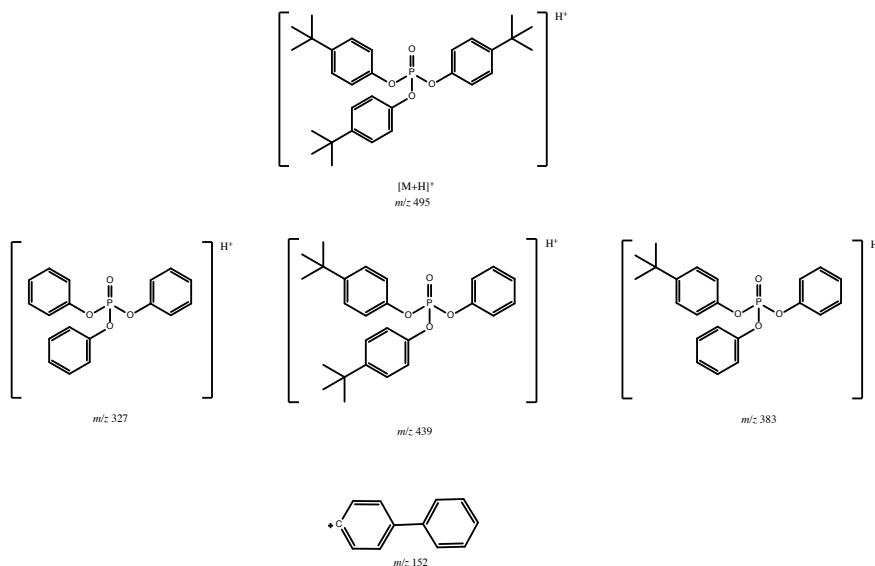


Figure 4.41: Suggested TTBPP daughter fragments.

The molecular ion for TTBPP at m/z 495 is clearly visible in a clean spectrum together with suggested daughter ions at m/z 327, m/z 439 and m/z 383 at collision energy 20eV. The fourth detected daughter ion at m/z 152 is only visible and detected when collision energy is increased to 64eV. This also increases the probability of rearrangements that does not only consist of fragments created by clean breakage of covalent bonds. The suggested structure of m/z 152 is the same variant as suggested structure for m/z 165 for TMPP and the m/z 152 for TPP. As the fragment at m/z 327 is the molecular ion for TPP, the structure for a similar m/z may also be the same.

4.6.19 RDP

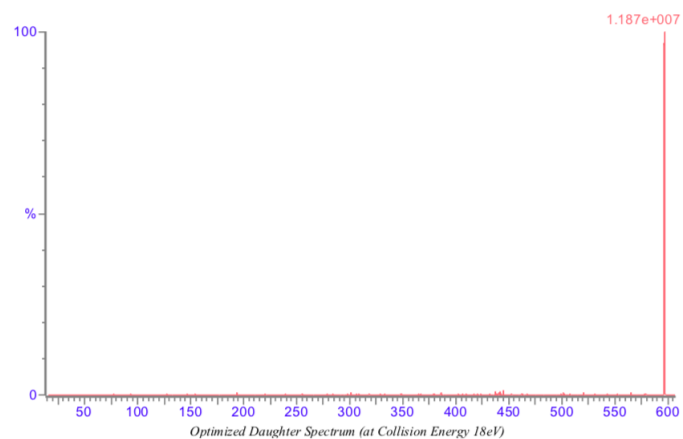


Figure 4.42: Optimized daughter spectrum for RDP at collision energy 18eV.

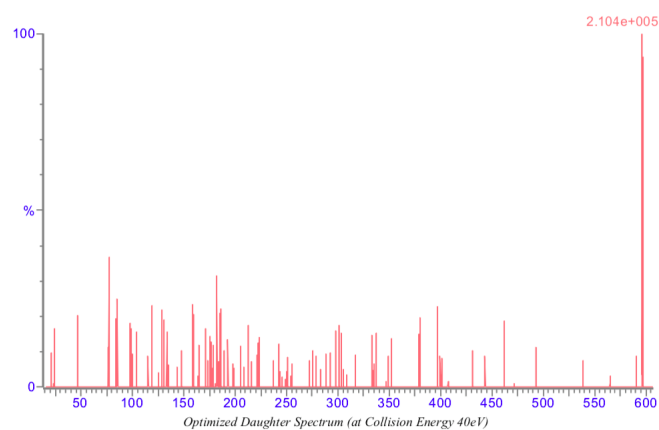


Figure 4.43: Optimized daughter spectrum for RDP at collision energy 40eV.

Compound	Formula/Mass	Parent m/z	Cone Voltage	Daughters	Collision Energy	Ion Mode	
TPRBDDP_RDP	C30H24O8P2	1	597.00	10	441.21	18	ES+
		2	597.00	10	23.14	30	ES+
		3	597.00	10	77.06	40	ES+

Table 4.22: SRM transitions for RDP.

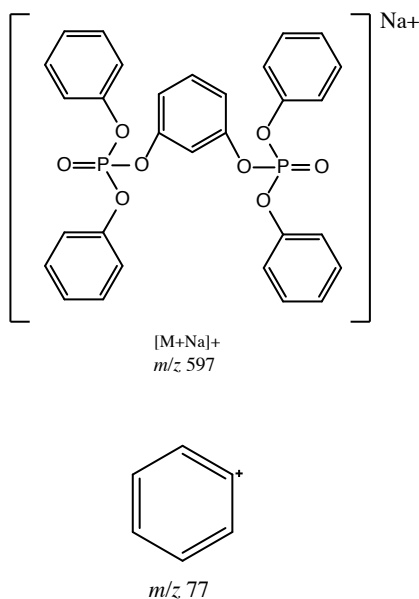


Table 4.23: Suggested daughter fragments for RDP.

For RDP the molecular ion detected at m/z 597 is most probably an adduct ion with sodium. The molecular mass of RDP is 574 g/mol which corresponds to an increase in molecular weight of 23 to the detected m/z 597 ion. Only the detected daughter ion at m/z 77 was clearly possible to predict. As the spectra in Figure 4.42 and Figure 4.43 show, only the molecular ion at m/z 597 is clearly visible. The noisy spectrum in Figure 4.43 at collision energy 40eV may indicate formation of several different daughter fragments, and since following suggested fragmentation mechanism or breaking any bonds in the molecule leads to formation of an ion at m/z 441 the structure is not suggested. The fragment at m/z 23 may be the sodium cation.

4.6.20 V6

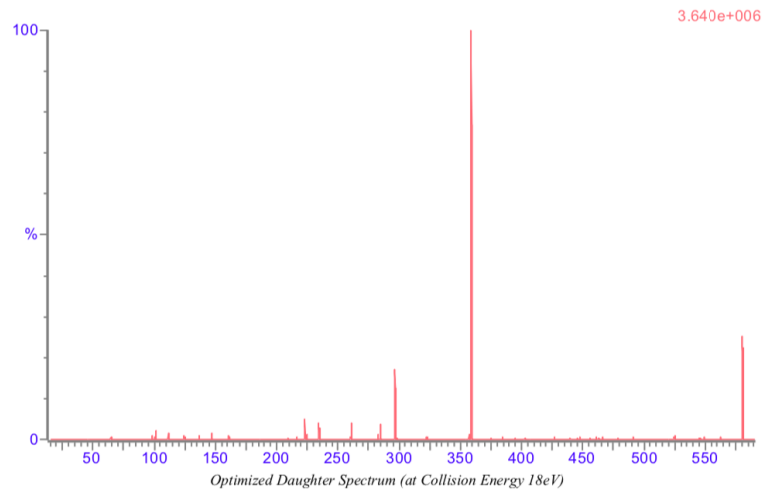


Figure 4.44: Optimized daughter spectrum for V6 at collision energy 18eV.

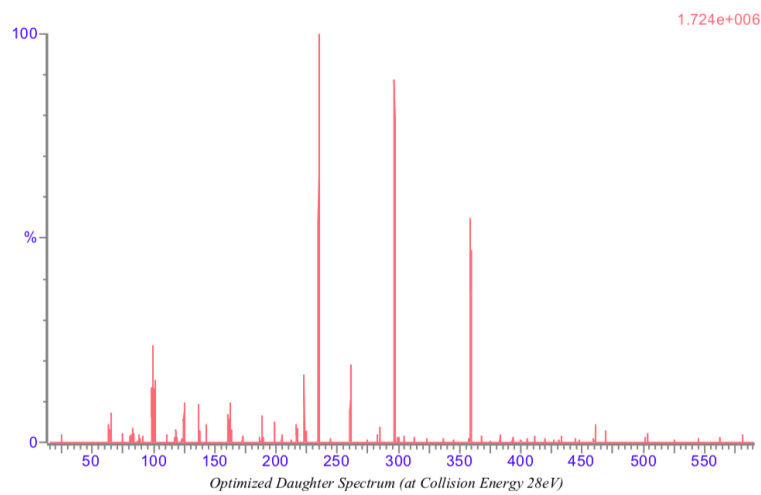


Figure 4.45: Optimized daughter spectrum for V6 at collision energy 28eV.

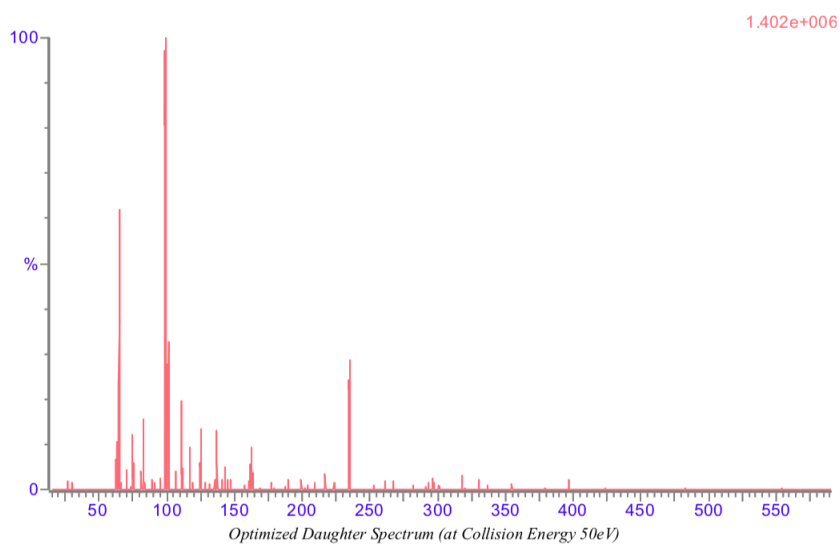


Figure 4.46: Optimized daughter spectrum for V6 at collision energy 50eV.

Compound	Formula/Mass		Parent m/z	Cone Voltage	Daughters	Collision Energy	Ion Mode
2020_V6	C13H24Cl6O8P2	1	581.00	4	358.99	18	ES+
		2	581.00	4	234.96	34	ES+
		3	581.00	4	297.01	28	ES+
		4	581.00	4	98.99	50	ES+

Table 4.24: SRM transitions for V6.

For V6 three spectra are needed to see clear peaks for all daughter fragments. It is evident by examining the spectra that increase in collision energy facilitates fragmentation and the detection of smaller fragments and rearrangement. The molecular ion is only visible in the spectrum with collision energy 18eV, while the daughter ion at m/z 99 not is visible in the same spectrum but evident first at a collision energy of 50eV. The suggested structures of m/z 359, m/z 235 and m/z 297 is presented in Figure 4.47. The m/z 99 fragment is suggested to be the protonated phosphoric acid like the m/z 99 in TEP, TnPP, TnBP, TiBP, TBOEP, TEHP, TCEP, TCIPP and TDCIPP. No structures for fragmentation of V6 was found in literature, and the mechanism from Figure 2.7 did not match the detected m/z . Fragmentation was therefore done to match the m/z from the SRM.

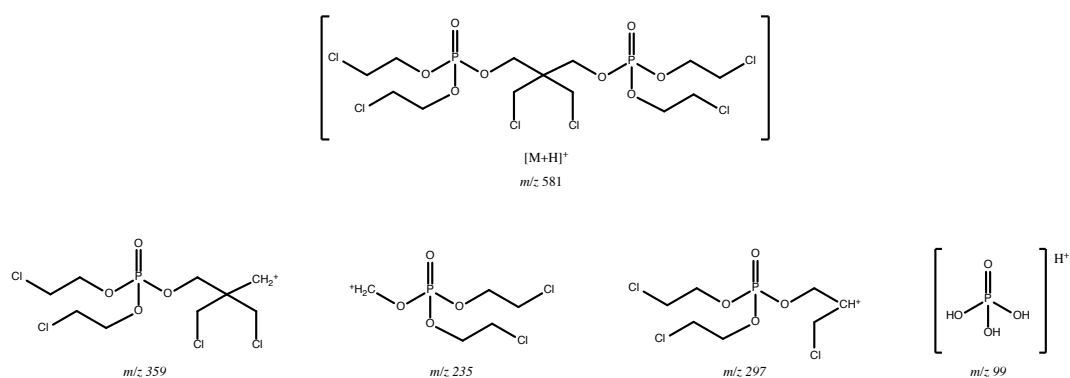


Figure 4.47: Suggested V6 daughter fragments.

4.6.21 BPA-BDPP

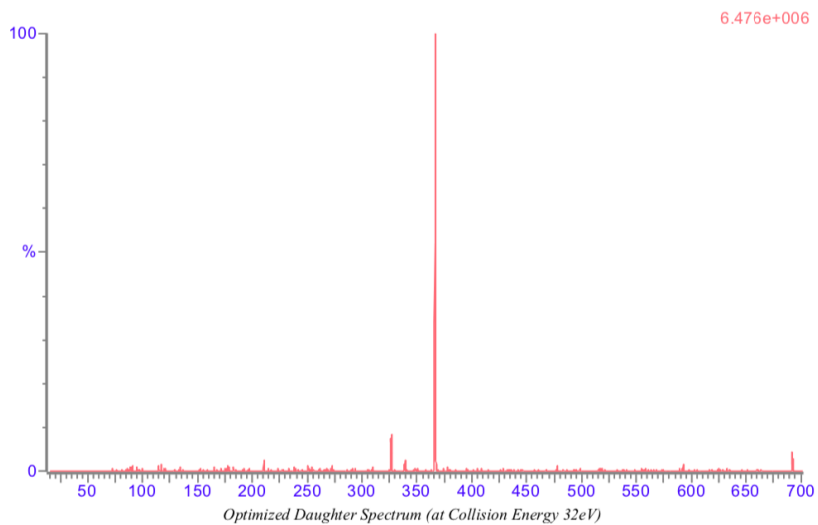


Figure 4.48: Optimized daughter spectrum for BPA-BDPP at collision energy 32eV.

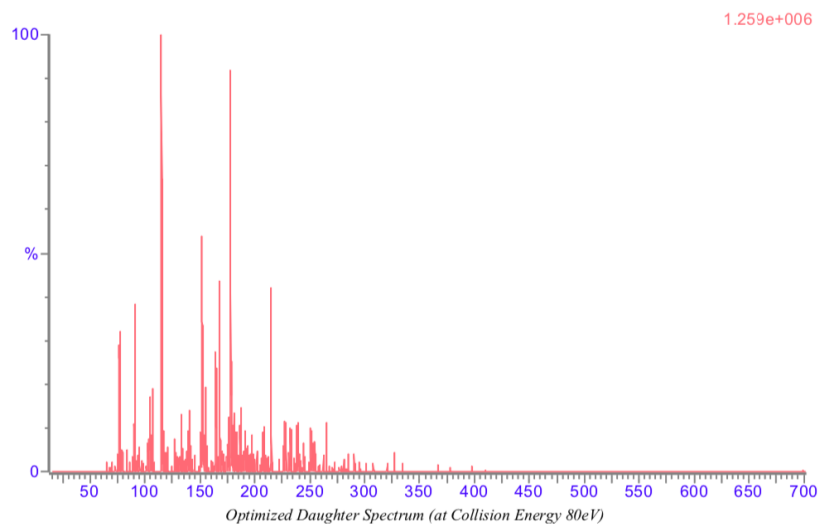


Figure 4.49: Optimized daughter spectrum for BPA-BDPP at collision energy 80eV.

Compound	Formula/Mass		Parent m/z	Cone Voltage	Daughters	Collision Energy	Ion Mode
BPA-BDPP	C39H34O8P2	1	692.50	84	366.72	32	ES+
		2	692.50	84	177.95	58	ES+
		3	692.50	84	114.92	80	ES+
		4	692.50	84	214.79	64	ES+

Table 4.25: SRM transitions for BPA-BDPP.

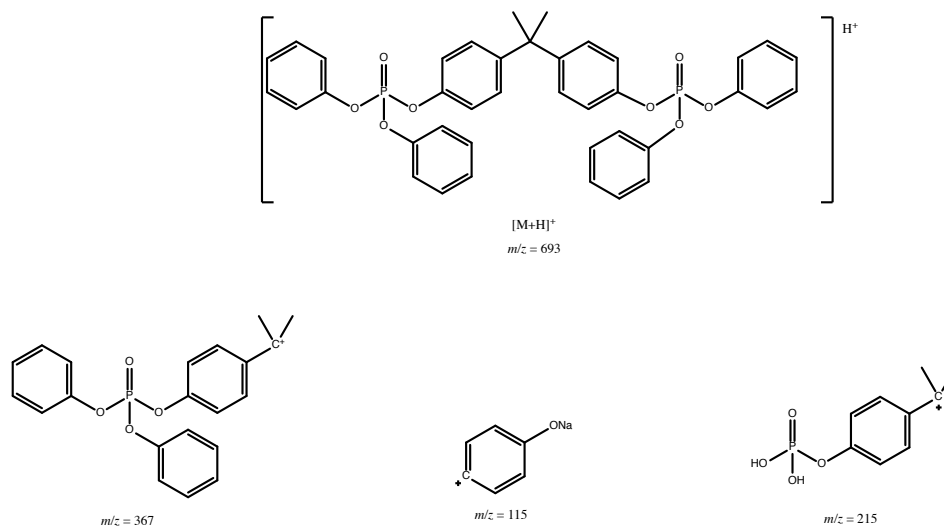


Figure 4.50: Suggested BPA-BDPP daughter fragments.

For BPA-BDPP the molecular ion is only visible as a small peak in the spectrum at the lowest suggested collision energy for daughter detection. The peak at m/z 367 in the spectrum at collision energy 32eV is clear and with abundance close to 100%. The suggested ion at m/z 367 is a splitting of the symmetrical BPA-BDPP molecule at the central carbon. The ion at m/z 367 is also the most documented one from fragmentation of BPA-BDPP, and is often the only fragment presented in literature (see Table 4.32). The peaks at m/z 178, m/z 115 and m/z 215 were first detected when collision energy was risen to 80eV. This may lead to more rearrangement and unstable smaller ions, which also can make it more challenging to predict the structure of the cations when the fragmentation does not follow any clear pattern. For the ion detected at m/z 115 an adduct with sodium is suggested. Here the suggested ion could also have had a -OH group instead of the -ONa and had the sodium added in the para position from the C-ONa. At m/z 215 a cation where the two phenyl groups is fragmented off m/z 367, leaving the m/z 215 ion, is presented in Figure 4.50. No structure was suggested for the m/z 178 as no ion with matching mass could be predicted with base in the molecular ion at m/z 693.

4.6.22 BBOEHEP

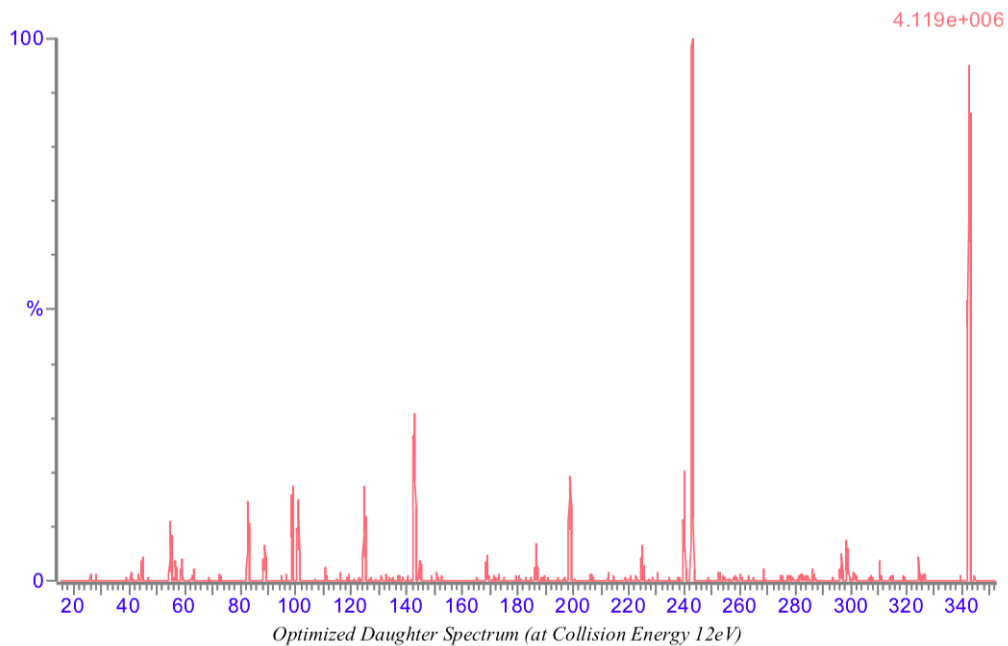


Figure 4.51: Optimized daughter spectrum for BBOEHEP at collision energy 12eV.

Compound	Formula/Mass		Parent m/z	Cone Voltage	Daughters	Collision Energy	Ion Mode
BBOEHEP	C ₁₄ H ₃₁ O ₇ P	1	342.83	8	242.84	10	ES+
		2	342.83	8	142.82	12	ES+
		3	342.83	8	98.76	26	ES+
		4	342.83	8	198.84	12	ES+

Table 4.26: SRM transitions for BBOEHEP.

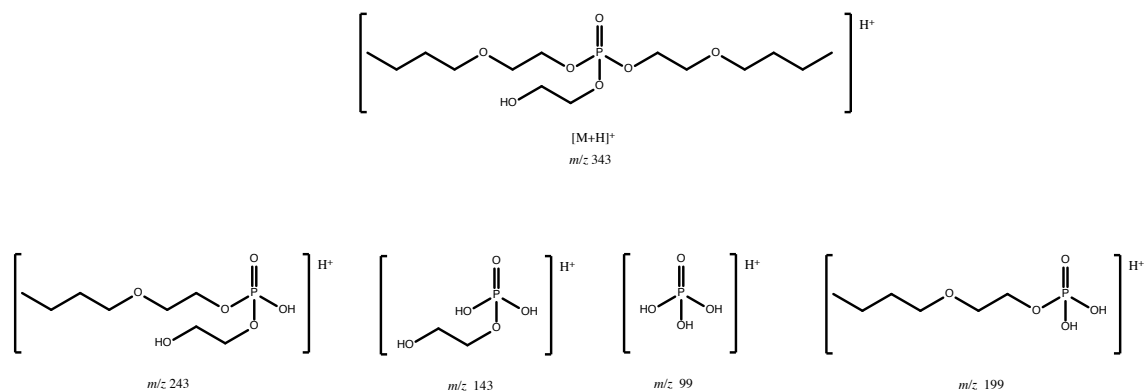


Figure 4.52: Suggested BBOEHEP daughter fragments.

For BBOEHEP all fragments were able to be suggested according to the step wise fragmentation suggested in Figure 2.7. The recognizable m/z 99 is also present as the smallest detected daughter, together with cations induced by cleavage of one or two of the O-C bonds at the phosphate. All fragments are visible in the presented spectrum obtained with collision energy at 12eV. Other unstable fragments are also probable to exist when observing the multiple small peaks in the spectrum.

4.6.23 3OH-BOEP

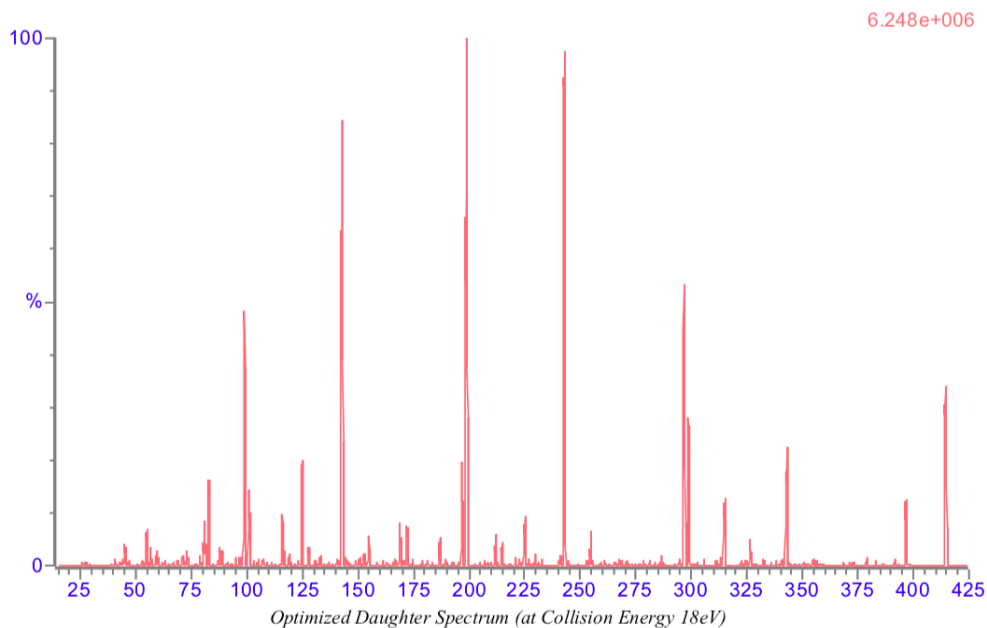


Figure 4.53: Optimized daughter spectrum for 3OH-BOEP at collision energy 18eV.

Compound	Formula/Mass		Parent m/z	Cone Voltage	Daughters	Collision Energy	Ion Mode
3OH-TBOEP	C ₁₈ H ₃₉ O ₈ P	1	414.82	28	242.87	14	ES+
		2	414.82	28	299.16	14	ES+
		3	414.82	28	198.82	14	ES+
		4	414.82	28	142.81	18	ES+

Table 4.27: SRM transitions for 3OH-BOEP.

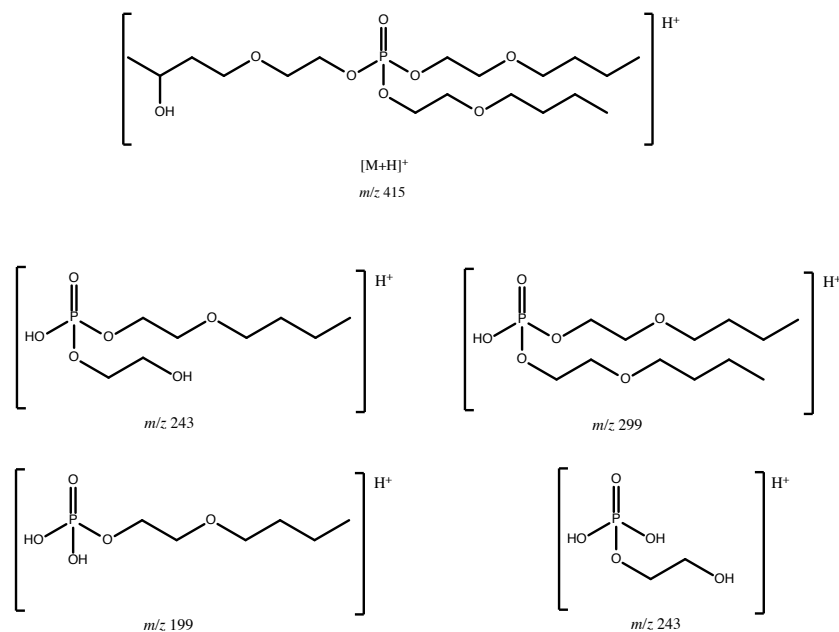


Figure 4.54: Suggested 3OH-BOEP daughter fragments.

Fragmentation of 3OH-BOEP partly follows the general fragmentation. Nevertheless all suggested daughters are results of a C-O bond breaking. The peaks for the daughters at m/z 243, m/z 299, m/z 199 and m/z 243 are all visible as main peaks in the spectrum presented in Figure 4.53. Also smaller peaks can be observed in the spectrum which can indicate that other fragment also may be present, just not detected as one of the four daughters. In example there is a clearly visible peak at around m/z 99 which most probably is the protonated phosphoric acid detected in several other OPFRs like BCIPP, BCEP, DnBP, V6, TCIPP, TCEP, TEHP, TBOEP amongst others.

4.6.24 DnBP

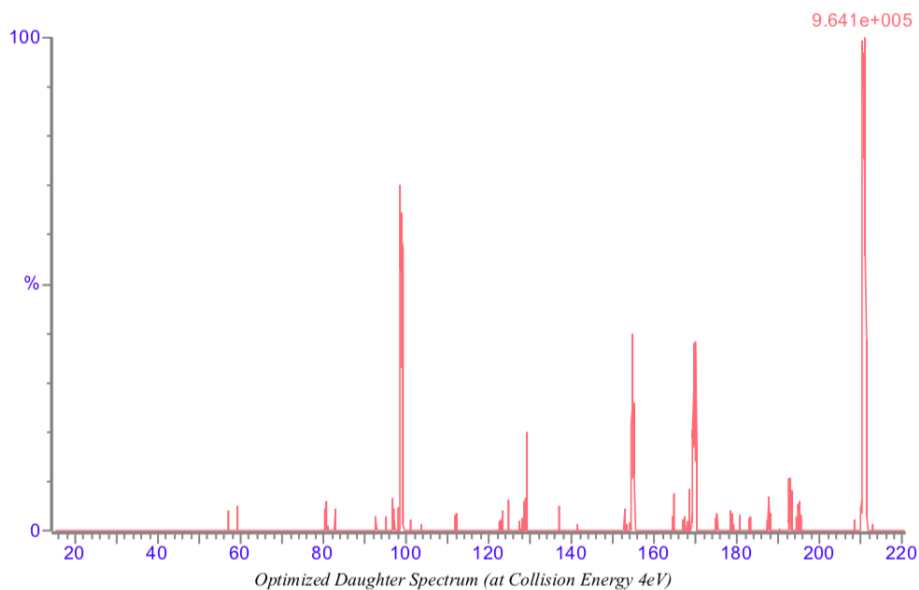


Figure 4.55: Optimized daughter spectrum for DnBP at collision energy 4eV.

Compound	Formula/Mass		Parent m/z	Cone Voltage	Daughters	Collision Energy	Ion Mode
DnBP	C8H19O4P	1	210.88	12	98.78	12	ES+
		2	210.88	12	154.86	4	ES+
		3	210.88	12	169.75	4	ES+
		4	210.88	12	128.80	10	ES+

Table 4.28: SRM transitions for DnBP.

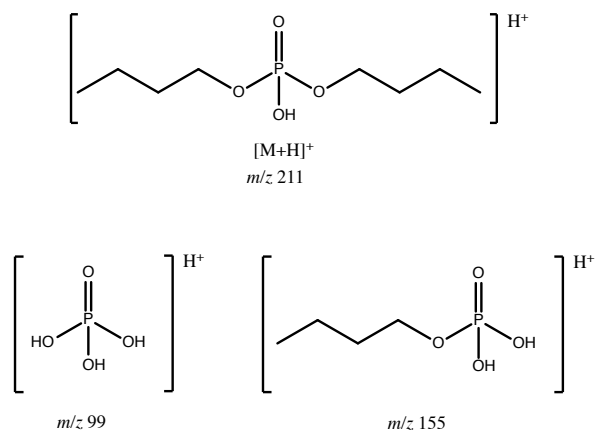


Figure 4.56: Suggested DnBP daughter fragments.

In the obtained spectrum at collision energy 4eV the molecular ion at m/z 211 is clearly visible together with the four daughter ions at m/z 99, m/z 155, m/z 170 and m/z 129. The ions at respectively m/z 99 and m/z 155 are predicted by following the suggested fragmentation pathway from Figure 2.7 where the C-O bond is broken, leaving an OH-group at the end. The first fragmentation from the molecular ion creates the m/z 155, while the second and consecutive loss of the butyl-group leads to the protonated phosphoric acid at m/z 99 which is a repeating fragment from the OPFRs. For the detected daughter fragments at m/z 170 and m/z 129 structures were not able to be predicted by following suggested mechanisms from Section 2.4.8 or by breaking bonds in the molecule.

4.6.25 BCEP

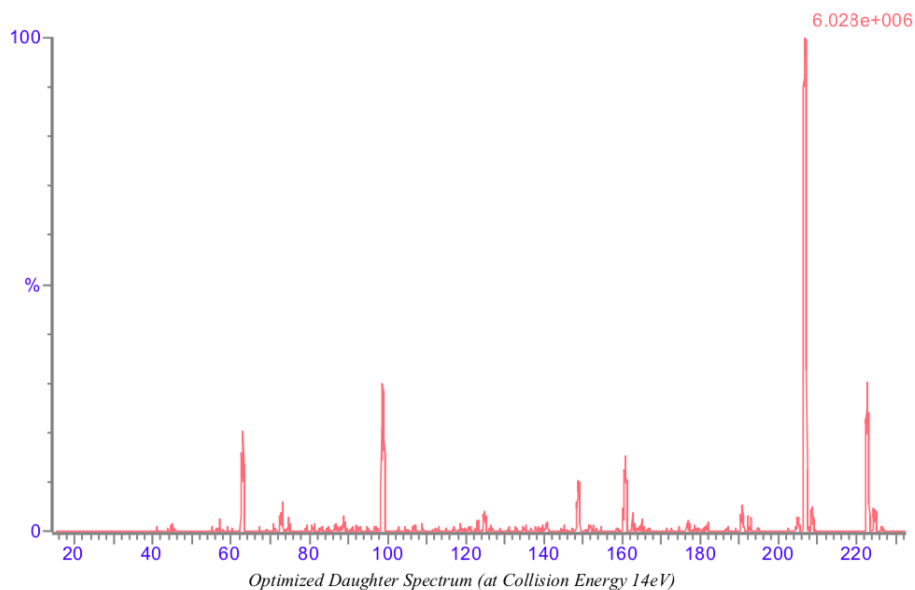


Figure 4.57: Optimized daughter spectrum for BCEP at collision energy 14eV.

Compound	Formula/Mass		Parent m/z	Cone Voltage	Daughters	Collision Energy	Ion Mode
BCEP	C ₄ H ₉ Cl ₂ O ₄ P	1	222.87	76	190.78	28	ES+
		2	222.87	76	98.76	14	ES+
		3	222.87	76	160.75	10	ES+
		4	222.87	76	62.89	16	ES+

Table 4.29: SRM transitions for BCEP.

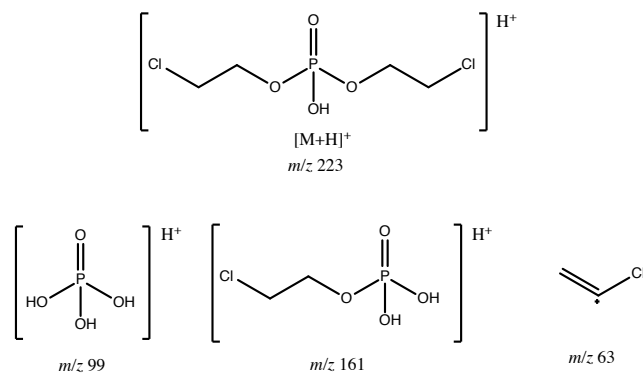


Figure 4.58: Suggested BCEP daughter fragments.

For BCEP three of the predicted daughters ions can be formed by following the suggested order of fragmentation from Figure 2.7. The first fragmentation creates the suggested daughter ion at m/z 161, while the second leads to the ion with m/z 99. The fragment at m/z 63 is suggested as the same ion at m/z 63 that is proposed in Figure 4.21. The fragment detected with abundance at almost 100% at m/z 191 is strangely not any fragment that follows the suggested fragmentation mechanism. It was also not possible to obtain a fragment with m/z 191 by breaking any of the bonds in the molecular ion, and the structure is therefore not predicted.

4.6.26 BCIPP

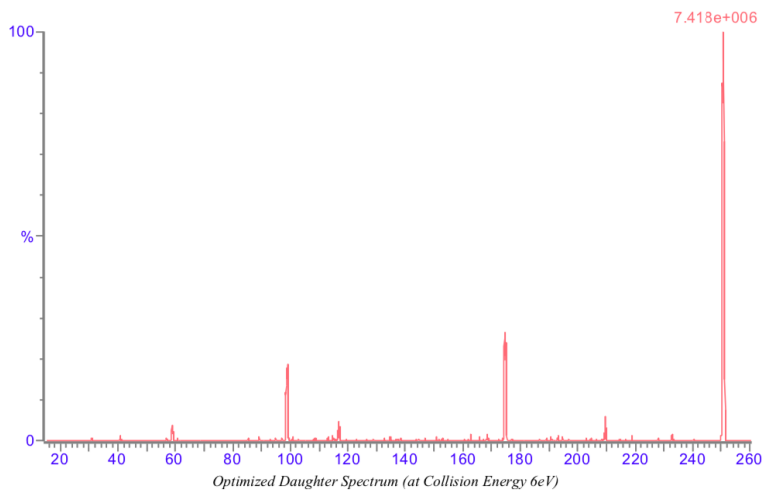


Figure 4.59: Optimized daughter spectrum for BCIPP at collision energy 6eV.

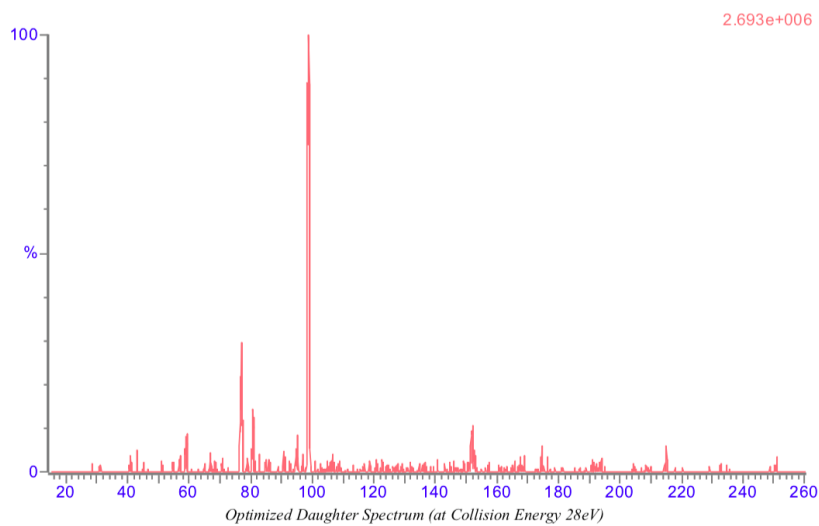


Figure 4.60: Optimized daughter spectrum for BCIPP at collision energy 28eV.

Compound	Formula/Mass		Parent m/z	Cone Voltage	Daughters	Collision Energy	Ion Mode
BCIPP	C ₆ H ₁₃ Cl ₂ O ₄ P	1	250.77	16	98.83	16	ES+
		2	250.77	16	174.79	6	ES+
		3	250.77	16	58.99	10	ES+
		4	250.77	16	76.93	28	ES+

Table 4.30: SRM transitions for BCIPP.

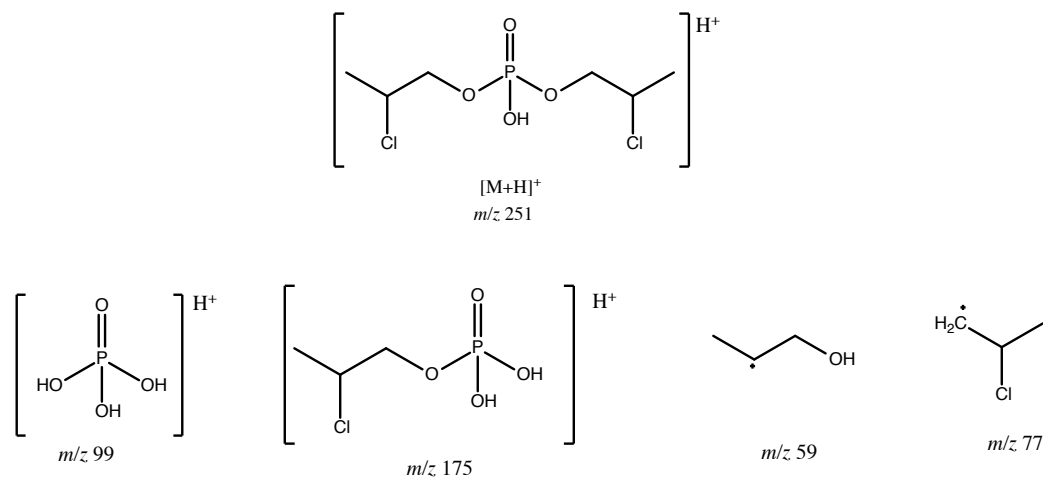


Figure 4.61: Suggested BCIPP daughter fragments.

Two spectra are required to observe peaks for all suggested daughter ions for BCIPP. The fragments visible at m/z 175 and m/z 99 follows the most evident fragmentation pattern by breaking the C-O bond and ending up with the protonated phosphoric acid at m/z 99. The fragments at m/z 59 and m/z 77 were clearly visible in the spectrum with collision energy set to 28eV. This facilitates more unstable fragments, and the suggested fragment m/z 77 is the part cleaved off from the molecular ion at m/z 251 to form m/z 175. The suggested cation at m/z 59 is a further divided part of a fragment possibly cleaved at the O-P bond.

4.6.27 BBOEP

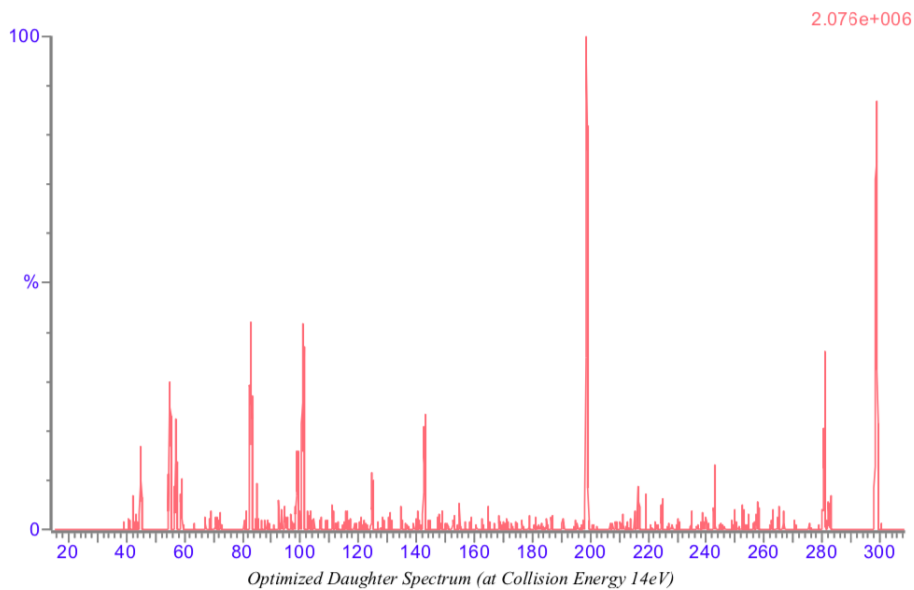


Figure 4.62: Optimized daughter spectrum for BBOEP at collision energy 14eV.

Compound	Formula/Mass		Parent m/z	Cone Voltage	Daughters	Collision Energy	Ion Mode
BBOEP	C ₁₂ H ₂₇ O ₆ P	1	298.87	16	198.83	10	ES+
		2	298.87	16	82.90	14	ES+
		3	298.87	16	100.96	14	ES+
		4	298.87	16	54.96	14	ES+

Table 4.31: SRM transitions for BBOEP.

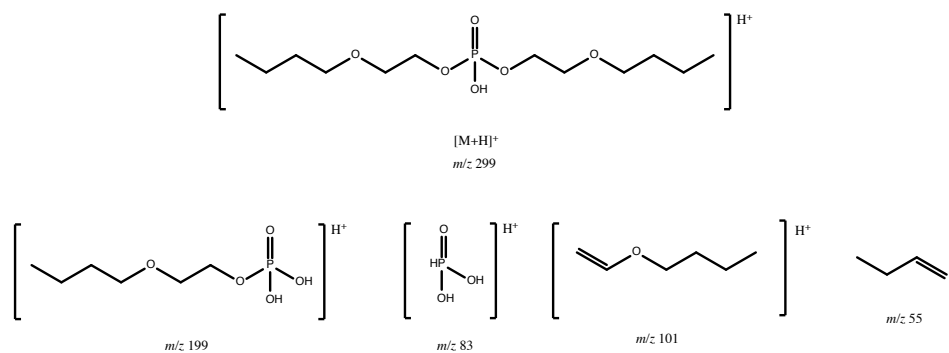


Figure 4.63: Suggested BBOEP daughter fragments.

All suggested daughters, and the molecular ion at m/z 299, are visible in the spectrum obtained at collision energy 14eV. The fragment at m/z 199 occurs according to the fragmentation pattern suggested in Figure 2.7. The fragment at m/z 101 is suggested to be the ion cleaved off the molecular ion to create the fragment at m/z 199. If the C-O bond at butyl group breaks, an ion at m/z 55 may be generated and is suggested, together with the daughters ions at m/z 83, m/z 101 and m/z 199, in Figure 4.63.

4.7 Summary of OPFR fragmentation

For the majority of the organophosphate flame retardants, three chains of carbons or variation of phenyls are bonded to three of the oxygen atoms in the phosphate. When the OPFRs undergo ionization, carbon chains or phenyls are broken off, resulting in the detected daughter fragments. The detected daughter fragments from this project (presented in Table 4.33) does for most of the compounds correspond to what is found in literature and presented in Table 4.32.

Three consecutive McLafferty rearrangements dominate the fragmentation of the trialkyl phosphate esters and the trichloroalkyl phosphate esters (Rodil et al., 2005). This is also suggested as the mechanism of fragmentation in Rodil et al. (2005) and in Bell et al. (1997). The alkyl groups are fragmented as neutral alkenes, and after three losses or rearrangements of the OPFRs the protonated phosphoric acid occurs as the final cation. Nevertheless, some of the OPFRs continue to fragment as a charge migration process follows the McLafferty rearrangements that leads to a positive charge on the fragmented alkyl or chloroalkyl groups making them detectable. For TCEP this can be seen as the m/z 63 which is visible in the spectrum, even though it was not detected as a daughter fragment in the SRM.

To predict a fragmentation pattern for each analyte is important to be able to further predict how they will break down in nature. Since ESI is a mild form of ionization the fragments can be similar to those detected in SRM and predicted in Section 4.6. The fragments proposed may not be the only possible fragments. Different m/z fragments are reported in literature and the peaks detected does not always replicate the suggested daughters from the SRM.

4.8 Fragment detection

Daughter fragments for each OPFR found in literature is presented in Table 4.32. The daughter fragments suggested by IntelliStart is presented in Table 4.33. In most studies only one or two daughter fragments are presented. As IntelliStart provides four daughters for each compound it is evident that all fragments may not be found in literature even though different studies report different daughters. For most of the compounds, the de-

tected ions, the quantification ion, and the confirmation ion are also reported as daughters in literature. Nevertheless, not all are found in literature, and not all detected fragments correspond to the data obtained from the chromatograms. This may come as a result of IntelliStart not always detecting what looks like the most evident daughter fragments when looking at the general mechanism presented in Section 4.6.1 and Figure 2.7, or even looking at the MS-spectra. Also, some daughters needed extensively increased collision energy to be detected which can indicate that the formation of those fragments are less likely to occur. Some of the spectra, in example Figure 4.43, are relatively messy which can indicate that several daughter fragments may be possible even though only some are detected. It is also important to remember that different instrumentation may lead to different fragments. Not only different instrumentation can facilitate this, but also the same instrument in different laboratories can give different fragments. This comes as a result of the ESI being highly dependent on the status of the instrument, and is linked to the status of the electrospray cone including in example the level of dirt, acid or salt residuals.

Table 4.32: Transitions for the OPFRs analyzed found in literature.

Compound	SRM1	SRM2	References
TMP	141>109/127	140>79/99	Fan et al. (2014)
			Wang et al. (2011)
			Bell et al. (1997)
TEP	183>155	182>127/138/99	Chu and Letcher (2015)
			Fan et al. (2014)
			Wang et al. (2011)
TnPP	225>99	225>183/141	Bell et al. (1997)
			Chen et al. (2012)
			Fan et al. (2014)
TnBP	267>99	267>155/210	Wang et al. (2011)
			Santín et al. (2016)
			Chu and Letcher (2015)
			Fan et al. (2014)
			Wang et al. (2011)
			Rodil et al. (2005)
			Cristale and Lacorte (2013)

Table 4.32 continued from previous page

Compound	SRM1	SRM2	References
TiBP	267>99	267>211/155	Fan et al. (2014) Rodil et al. (2005) Cristale and Lacorte (2013)
TBOEP	399>299	399>199	Chen et al. (2012) Santín et al. (2016) Chu and Letcher (2015) Fan et al. (2014) Rodil et al. (2005) Cristale and Lacorte (2013)
TEHP	435>99	435>80/133/113/71	Chen et al. (2012) Santín et al. (2016) Chu and Letcher (2015) Wang et al. (2011) Rodil et al. (2005) Cristale and Lacorte (2013)
TCEP	285>223	285>99/161/125/63	Chen et al. (2012) Santín et al. (2016) Chu and Letcher (2015) Wang et al. (2011) Rodil et al. (2005) Cristale and Lacorte (2013)
TCIPP	327>251/99	327>175/225/209	Matsukami et al. (2016) Santín et al. (2016) Chu and Letcher (2015) Fan et al. (2014) Wang et al. (2011) Rodil et al. (2005) Cristale and Lacorte (2013) Matsukami et al. (2016)

Table 4.32 continued from previous page

Compound	SRM1	SRM2	References
TDCIPP	431>319/99	431>320/209/211	Chen et al. (2012) Santín et al. (2016) Chu and Letcher (2015) Fan et al. (2014) Wang et al. (2011) Cristale and Lacorte (2013) Matsukami et al. (2016)
TPP	327>77	327>152/215/168	Chen et al. (2012) Santín et al. (2016) Chu and Letcher (2015) Wang et al. (2011) Rodil et al. (2005) Cristale and Lacorte (2013) Matsukami et al. (2016)
DCrP	341>152	341>99/228/91	Santín et al. (2016) Matsukami et al. (2016)
TMPP	369>165/91	369>99/178/243	Chen et al. (2012) Santín et al. (2016) Chu and Letcher (2015) Fan et al. (2014) Wang et al. (2011) Cristale and Lacorte (2013) Matsukami et al. (2016)
EHDP	363>251/247/51	363>233/151/77	Chen et al. (2012) Santín et al. (2016) Chu and Letcher (2015) Fan et al. (2014) Wang et al. (2011) Cristale and Lacorte (2013) Matsukami et al. (2016)
IDPP	391>251	391>151/77	Santín et al. (2016)
TTBPP	495>439	495>383	Guan et al. (2019)
RDP	575>481	575>419	Rodil et al. (2005) Matsukami et al. (2016)

Table 4.32 continued from previous page

Compound	SRM1	SRM2	References
V6	535>361	583>235	Santín et al. (2016) Chu and Letcher (2015)
BPA-BDPP	693>367	693>327	Matsukami et al. (2016)
<i>Metabolites</i>			
DnBP (ESI-)	209>153	209>79	Van den Eede et al. (2013) He et al. (2018)
BCEP (ESI-)	221>35	223>35	Van den Eede et al. (2013) He et al. (2018)
BCIPP (ESI-)	249>35	251>35	Van den Eede et al. (2013) He et al. (2018)
BBOEP (ESI-)	297>197/223	297>79	Van den Eede et al. (2013) He et al. (2018)
BBOEHEP	343>243		He et al. (2018)
3OH-BOEP	415>243		He et al. (2018)

Table 4.33: Daughter fragments detected in SRM for each analyte. (*) refers to the quantification ion, (**) refers to the confirmation ion and (***) refers to the ions where only one transition was detected with acceptable peaks.

Compound	Daughter 1	Daughter 2	Daughter 3	Daughter 4
TMP	141>109(*)	141>79(**)	141>47	141>95
TEP	183>99	183>142	183>127(*)	183>155(**)
TnPP	225>99(***)	225>141	225>85	225>81
TnBP	267>99	267>155(*)	267>211(**)	267>81
TiBP	267>99	267>211(*)	267>155(**)	267>81
TBOEP	399>299(*)	399>199(**)	399>99	399>143
TEHP	435>99(*)	435>323	435>71(**)	435>211
TCEP	285>99(**)	285>223(**)	285>161	285>125
TCIPP	327>99(***)	327>175	327>251	327>81
TDCIPP	429>99(***)	429>209	429>319	429>75
TPP	327>152(**)	327>77	327>215(*)	327>251
DCrP	363>102	363>77	363>123	363>84
TMPP	369>165(**)	369>91(*)	369>243	
EHDP	385>273(***)	385>281	385>344	
IDPP	–	–	–	–

Table 4.33 continued from previous page

Compound	Daughter 1	Daughter 2	Daughter 3	Daughter 4
TTBPP	495>327	495>439	495>383	495>152
RDP	597>441	597>23	597>77	–
V6	581>359(***)	581>235	581>297	581>99
BPA-BDPP	693>367(*)	693>178	693>115	693>215
BPDP	Not detected	Not detected	Not detected	Not detected
<i>Metabolites</i>				
DnBP	211>99	211>155	211>170	211>129
BCEP	223>191	223>99	223>161	223>63
BClPP	251>99	251>175	251>59	251>77
BBOEP	299>199	299>83	299>101	299>55
BBOEHEP	343>243(**)	343>143	343>99(*)	343>199
3OH-BOEP	415>243(*)	415>299	415>199(**)	415>143

4.9 Further work and suggestions

For determination and analysis of OPFRs in foodstuffs development of an effective and good extraction protocol is important. This step has proven to be one of the greatest challenges when analyzing OPFRs in complex matrices like foodstuffs. Since almost all previous studies have used SPE as a clean up step, testing this might be a pathway for further work. Also being extra careful when it comes to contamination of the samples during sample preparation is suggested. In example could the weighing of the samples be carried out in a fume hood to avoid contamination from dust in the laboratory. Another possibility is to analyze the used PP tubes to ensure and establish the content of OPFRs in the tubes. As they are made of plastic it is not impossible that they contain OPFRs. To use more target specific internal standards could also be a suggestion to obtain better recoveries.

As soon as a good extraction protocol is established, and the laboratories open again, it is recommended that the first planned lab-work, to analyze the 49 anticipated babyfoods, is carried out. This is important knowledge as children are more prone to the possible toxic effects of OPFRs.

More research on OPFRs in foodstuffs should be carried out to get a better understanding of the exposure of OPFRs through food. It is definitely an important part of the road to get a full understanding of all pathways for human exposure of OPFRs.

5 Conclusion

Two different extraction protocols for extraction of OPFRs from foodstuffs was tested. Extraction with ethyl acetate showed far better recoveries than the extraction where DCM:Hex(1:1) was used as the main solvents. Concentrations were consequently calculated from results obtained from the extraction with ethyl acetate. The LOD ranged from 0,02-3,97 ng/g for the 21 analyzed OPFRs. Concentration of nine compounds were under the limit of detection (TiBP, TCEP, DPMP, TMPP, TBOEP, 3OH-TBOEP, TTBPP, V6 and BPA-BDPP), while four showed concentrations under the limit of quantification (TnPP, BBOEP, IDPP and RDP). Five OPFRs (TMP, TEP, TnBP, TCIPP and TPP) was able to be quantified with concentrations varying from 0,25 ng/g dw to 23,5 ng/g dw, while quantitative calculations was unable to be performed for three TEHP, TDCIPP and EHDP due to very high blank values.

Satisfactory recoveries were obtained for the majority of the OPFRs when following the extraction protocol with ethyl acetate, while the majority of the recoveries from the extraction with DCM:Hex showed poor recoveries.

Structures for detected daughter fragments for 26 OPFRs were suggested based on optimized MS spectra and results provided from the SRM. A general pattern for the fragmentation was also suggested for the OPFRs. It should be noted that not all compounds followed the mechanism.

To develop an optimized extraction technique for all OPFRs should be a priority. Previous studies on OPFRs in foodstuffs have screened the samples for six to fifteen OPFRs, and no studies have analyzed foodstuffs for TTBPP, V6, BPA-BDPP and RDP as fist planned in this study.

More research is needed on OPFRs in foodstuffs to get a complete picture of the human exposure. This is important to be able to evaluate the overall toxicological effects of the OPFRs.

References

- Asimakopoulos, A. G., Wang, L., Thomaidis, N. S., and Kannan, K. (2014). A multi-class bioanalytical methodology for the determination of bisphenol A diglycidyl ethers, p-hydroxybenzoic acid esters, benzophenone-type ultraviolet filters, triclosan, and triclocarban in human urine by liquid chromatography–tandem mass spectrometry. *Journal of Chromatography A*, 1324:141–148.
- Asimakopoulos, A. G., Xue, J., De Carvalho, B. P., Iyer, A., Abualnaja, K. O., Yaghmoor, S. S., Kumosani, T. A., and Kannan, K. (2016). Urinary biomarkers of exposure to 57 xenobiotics and its association with oxidative stress in a population in Jeddah, Saudi Arabia. *Environmental Research*, 150:573–581.
- Ballesteros-Gómez, A., Erratico, C. A., Eede, N. V. d., Ionas, A. C., Leonards, P. E. G., and Covaci, A. (2015a). In vitro metabolism of 2-ethylhexyldiphenyl phosphate (EHD-PHP) by human liver microsomes. *Toxicology Letters*, 232(1):203–212.
- Ballesteros-Gómez, A., Van den Eede, N., and Covaci, A. (2015b). In Vitro Human Metabolism of the Flame Retardant Resorcinol Bis(diphenylphosphate) (RDP). *Environmental Science & Technology*, 49(6):3897–3904.
- Barceló, D. and Petrovic, M. (2007). Challenges and achievements of LC-MS in environmental analysis: 25 years on. *TrAC Trends in Analytical Chemistry*, 26(1):2–11.
- Bell, A. J., Despeyroux, D., Murrell, J., and Watts, P. (1997). Fragmentation and reactions of organophosphate ions produced by electrospray ionization. *International Journal of Mass Spectrometry and Ion Processes*, 165-166:533–550.
- Berdasco, N. A. M. and McCready, D. (2011). Risk Assessment and Class-Based Evaluation of Three Phosphate Esters. *Human and Ecological Risk Assessment: An International Journal*, 17(2):367–380.
- Berk, Z. (2018). Extraction. In *Food process engineering and technology*, chapter 11, pages 289–310. Academic Press, third edition.
- Blum, A., Behl, M., Birnbaum, L. S., Diamond, M. L., Phillips, A., Singla, V., Sipes, N. S., Stapleton, H. M., and Venier, M. (2019). Organophosphate Ester Flame Re-

- tardants: Are They a Regrettable Substitution for Polybrominated Diphenyl Ethers? *Environmental Science & Technology Letters*, 6(11):638–649.
- Boer, J. D. (2012). Persistent Organic Pollutants – Are Our Methods Sensitive and Selective Enough? *Analytical Letters*, 45(5-6):485–494.
- Brandsma, S. H., de Boer, J., Leonards, P. E. G., Cofino, W. P., Covaci, A., and Leonards, P. E. G. (2013a). Organophosphorus flame-retardant and plasticizer analysis, including recommendations from the first worldwide interlaboratory study. *TrAC Trends in Analytical Chemistry*, 43:217–228.
- Brandsma, S. H., Sellstroöm, U., de Wit, C. A., de Boer, J., and Leonards, P. E. G. (2013b). Dust measurement of two organophosphorus flame retardants, resorcinol bis (diphenylphosphate)(RBDPP) and bisphenol A bis (diphenylphosphate)(BPA-BDPP), used as alternatives for BDE-209. *Environmental science & technology*, 47(24):14434–14441.
- Brooke, D. (2009). *Environmental Risk Evaluation Report: Cresyl Diphenyl Phosphate (CAS No. 26444-49-5)*. Environment Agency.
- Bruchajzer, E., Frydrych, B., and Szymańska, J. A. (2015). Organophosphorus flame retardants – Toxicity and influence on human health. *Medycyna Pracy*, 66(2):235–264.
- Caban, M., Migowska, N., Stepnowski, P., Kwiatkowski, M., and Kumirska, J. (2012). Matrix effects and recovery calculations in analyses of pharmaceuticals based on the determination of β -blockers and β -agonists in environmental samples. *Journal of Chromatography A*, 1258:117–127.
- Castorina, R., Bradman, A., Stapleton, H. M., Butt, C., Avery, D., Harley, K. G., Gunier, R. B., Holland, N., and Eskenazi, B. (2017). Current-use flame retardants: Maternal exposure and neurodevelopment in children of the CHAMACOS cohort. *Chemosphere*.
- Castro-Jiménez, J., González-Gaya, B., Pizarro, M., Casal, P., Pizarro-Álvarez, C., and Dachs, J. (2016). Organophosphate Ester Flame Retardants and Plasticizers in the Global Oceanic Atmosphere. *Environmental Science & Technology*, 50(23):12831–12839.

-
- Cech, N. B. and Enke, C. G. (2001). Practical implications of some recent studies in electrospray ionization fundamentals. *Mass spectrometry reviews*, 20(6):362–387.
- Chen, D., Letcher, R. J., and Chu, S. (2012). Determination of non-halogenated, chlorinated and brominated organophosphate flame retardants in herring gull eggs based on liquid chromatography–tandem quadrupole mass spectrometry. *Journal of Chromatography A*, 1220:169–174.
- Chu, S. and Letcher, R. J. (2015). Determination of organophosphate flame retardants and plasticizers in lipid-rich matrices using dispersive solid-phase extraction as a sample cleanup step and ultra-high performance liquid chromatography with atmospheric pressure chemical ionization mass . *Analytica Chimica Acta*, 885:183–190.
- Cooper, E. M., Covaci, A., Van Nuijs, A. L. N., Webster, T. F., and Stapleton, H. M. (2011). Analysis of the flame retardant metabolites bis (1, 3-dichloro-2-propyl) phosphate (BDCPP) and diphenyl phosphate (DPP) in urine using liquid chromatography–tandem mass spectrometry. *Analytical and bioanalytical chemistry*, 401(7):2123.
- Cristale, J. and Lacorte, S. (2013). Development and validation of a multiresidue method for the analysis of polybrominated diphenyl ethers, new brominated and organophosphorus flame retardants in sediment, sludge and dust. *Journal of Chromatography A*, 1305:267–275.
- Cristale, J., Ramos, D. D., Dantas, R. F., Machulek Junior, A., Lacorte, S., Sans, C., and Esplugas, S. (2016). Can activated sludge treatments and advanced oxidation processes remove organophosphorus flame retardants? *Environmental Research*, 144:11–18.
- Dass, C. (2007a). Quantitative Analysis. In *Fundamentals of contemporary mass spectrometry*, chapter 14, pages 485–498. John Wiley & Sons.
- Dass, C. (2007b). Tandem mass spectrometry. In *Fundamentals of contemporary mass spectrometry*, volume 16, chapter 4, pages 119–143. John Wiley & Sons.
- de Hoffmann, E. (1996). Tandem mass spectrometry: a primer. *Journal of mass spectrometry*, 31(2):129–137.
- de Hoffmann, E. and Stroobant, V. (2007). Mass Analyzers - Quadrupole Analysers. In
-

- Mass spectrometry - Principles and Applications*, chapter 2.1, pages 85–98. John Wiley & Sons, Ltd, West Sussex, England, 3rd editio edition.
- Ding, J., Deng, T., Xu, M., Wang, S., and Yang, F. (2018). Residuals of organophosphate esters in foodstuffs and implication for human exposure. *Environmental Pollution*, 233:986–991.
- Dishaw, L. V., Powers, C. M., Ryde, I. T., Roberts, S. C., Seidler, F. J., Slotkin, T. A., and Stapleton, H. M. (2011). Is the PentaBDE replacement, tris (1,3-dichloro-2-propyl) phosphate (TDCPP), a developmental neurotoxicant? Studies in PC12 cells. *Toxicology and Applied Pharmacology*, 256(3):281–289.
- Doherty, B. T., Hammel, S. C., Daniels, J. L., Stapleton, H. M., and Hoffman, K. (2019). Organophosphate Esters: Are These Flame Retardants and Plasticizers Affecting Children’s Health? *Current Environmental Health Reports*, 6(4):201–213.
- Douglas, D. J. (1998). Applications of Collision Dynamics in Quadrupole Mass Spectrometry. *Journal of the American Society for Mass Spectrometry*, 9(2):101–113.
- Du, J., Li, H., Xu, S., Zhou, Q., Jin, M., and Tang, J. (2019). A review of organophosphorus flame retardants (OPFRs): occurrence, bioaccumulation, toxicity, and organism exposure. *Environmental Science and Pollution Research*, 26(22):22126–22136.
- Du, Z., Wang, G., Gao, S., and Wang, Z. (2015). Aryl organophosphate flame retardants induced cardiotoxicity during zebrafish embryogenesis: By disturbing expression of the transcriptional regulators. *Aquatic Toxicology*, 161:25–32.
- European Chemical Agency (2020a). Substance Infocard - Diphenyl tolyl phosphate.
- European Chemical Agency (2020b). Substance Infocard - Tributyl Phosphate.
- European Chemical Agency (2020c). Substance Infocard - Triethyl phosphate.
- European Chemical Agency (2020d). Substance Infocard - Triisobutyl phosphate.
- European Chemical Agency (2020e). Substance Infocard - Trimethyl phosphate.
- European Chemical Agency (2020f). Substance Infocard - Tripropyl phosphate.

-
- European Chemical Agency (2020g). Substance Infocard - Tris(2-chloro-1-methylethyl) phosphate.
- European Chemical Agency (2020h). Substance Inforcard - Tris(2-chloroethyl) phosphate.
- Fan, X., Kubwabo, C., Rasmussen, P. E., and Wu, F. (2014). Simultaneous determination of thirteen organophosphate esters in settled indoor house dust and a comparison between two sampling techniques. *Science of The Total Environment*, 491-492:80–86.
- Fu, S., Song, P., and Liu, X. (2017). Thermal and flame retardancy properties of thermoplastics/natural fiber biocomposites. *Advanced High Strength Natural Fibre Composites in Construction*, pages 479–508.
- Gao, Z., Deng, Y., Yuan, W., He, H., Yang, S., and Sun, C. (2014). Determination of organophosphorus flame retardants in fish by pressurized liquid extraction using aqueous solutions and solid-phase microextraction coupled with gas chromatography-flame photometric detector. *Journal of Chromatography A*, 1366:31–37.
- Gibson, E. A., Stapleton, H. M., Calero, L., Holmes, D., Burke, K., Martinez, R., Cortes, B., Nematollahi, A., Evans, D., and Herbstman, J. B. (2019). Flame retardant exposure assessment: findings from a behavioral intervention study. *Journal of Exposure Science & Environmental Epidemiology*, 29(1):33–48.
- Giri, D. (2020). High Performance Liquid Chromatography (HPLC) : Principle, Types, Instrumentation and Applications.
- Guan, Q., Tan, H., Yang, L., Liu, X., Fiedler, H., Li, X., and Chen, D. (2019). Isopropylated and tert-butylated triarylphosphate isomers in house dust from South China and Midwestern United States. *Science of The Total Environment*, 686:1113–1119.
- Gumbmann, M. R., Gagné, W. E., and Williams, S. N. (1968). Short-term toxicity studies of rats fed triethyl phosphate in the diet. *Toxicology and Applied Pharmacology*, 12(3):360–371.
- Guo, X., Mu, T., Xian, Y., Luo, D., and Wang, C. (2016). Ultra-performance liquid chromatography tandem mass spectrometry for the rapid simultaneous analysis of nine organophosphate esters in milk powder. *Food Chemistry*, 196:673–681.
-

- Hartwig, A. and Commission, M. A. K. (2016). Diphenyl cresyl phosphate [MAK Value Documentations, 2003].
- He, C., Toms, L.-M. L., Thai, P., Van den Eede, N., Wang, X., Li, Y., Baduel, C., Harden, F. A., Heffernan, A. L., Hobson, P., Covaci, A., and Mueller, J. F. (2018). Urinary metabolites of organophosphate esters: Concentrations and age trends in Australian children. *Environment International*, 111:124–130.
- Hou, R., Xu, Y., and Wang, Z. (2016). Review of OPFRs in animals and humans: Absorption, bioaccumulation, metabolism, and internal exposure research. *Chemosphere*, 153:78–90.
- Humbert, L., Hoizey, G., and Lhermitte, M. (2014). Chapter 7 - Drugs Involved in Drug-Facilitated Crimes (DFC): Analytical Aspects: 1—Blood and Urine. In Kintz, P. B. T. T. A. o. D.-F. C., editor, *Toxicological Aspects of Drug-Facilitated Crimes*, pages 159–180. Academic Press, Oxford.
- Kademoglou, K., Xu, F., Padilla-Sanchez, J. A., Haug, L. S., Covaci, A., and Collins, C. D. (2017). Legacy and alternative flame retardants in Norwegian and UK indoor environment: Implications of human exposure via dust ingestion. *Environment International*, 102:48–56.
- Kimura, Y. (2019). *Determination of profiles of occurrence of parabens, triclocarban and elements in select snack foodstuffs from Norway and other countries*. PhD thesis, Norwegian University of Science and Technology.
- Kruve, A. and Kaupmees, K. (2017). Adduct Formation in ESI/MS by Mobile Phase Additives. *Journal of the American Society for Mass Spectrometry*, 28(5):887–894.
- Li, J., Zhao, L., Letcher, R. J., Zhang, Y., Jian, K., Zhang, J., and Su, G. (2019). A review on organophosphate Ester (OPE) flame retardants and plasticizers in foodstuffs: Levels, distribution, human dietary exposure, and future directions. *Environment International*, 127:35–51.
- Liu, X., Ji, K., and Choi, K. (2012). Endocrine disruption potentials of organophosphate flame retardants and related mechanisms in H295R and MVLN cell lines and in zebrafish. *Aquatic Toxicology*, 114-115:173–181.

-
- Lorenzo, M., Campo, J., and Picó, Y. (2016). Ultra-high-pressure liquid chromatography tandem mass spectrometry method for the determination of 9 organophosphate flame retardants in water samples. *MethodsX*, 3:343–349.
- Lores, M., Cabaleiro, O., and Cela, R. (1999). Post-column photochemical derivatization in high-performance liquid chromatography. *TrAC Trends in Analytical Chemistry*, 18(6):392–400.
- Lundanes, E. (2014). Chromatography : basic principles, sample preparations and related methods.
- Malarvannan, G., Belpaire, C., Geeraerts, C., Eulaers, I., Neels, H., and Covaci, A. (2015). Organophosphorus flame retardants in the European eel in Flanders, Belgium: Occurrence, fate and human health risk. *Environmental Research*, 140:604–610.
- Marklund, A., Andersson, B., and Haglund, P. (2003). Screening of organophosphorus compounds and their distribution in various indoor environments. *Chemosphere*, 53(9):1137–1146.
- Marklund, A., Andersson, B., and Haglund, P. (2005). Traffic as a source of organophosphorus flame retardants and plasticizers in snow. *Environmental science & technology*, 39(10):3555–3562.
- Matsukami, H., Suzuki, G., Tue, N. M., Tuyen, L. H., Viet, P. H., Takahashi, S., Tanabe, S., and Takigami, H. (2016). Analysis of monomeric and oligomeric organophosphorus flame retardants in fish muscle tissues using liquid chromatography–electrospray ionization tandem mass spectrometry: Application to Nile tilapia (*Oreochromis niloticus*) from an e-waste processing area. *Emerging Contaminants*, 2(2):89–97.
- Matthews, H., Eustis, S., and Haseman, J. (1993). Toxicity and Carcinogenicity of Chronic Exposure to Tris(2-chloroethyl)phosphate. *Fundamental and Applied Toxicology*, 20(4):477–485.
- McMaster, M. C. (2005). *LC/MS: a practical user's guide*. John Wiley & Sons.
- McMaster, M. C. (2007). *HPLC: a practical user's guide*. John Wiley & Sons.
-

- McWilliams, A. (2018). Flame Retardant Chemicals: Technologies and Global Markets. Technical report, BCC Publishing.
- Meyer, J. and Bester, K. (2004). Organophosphate flame retardants and plasticisers in wastewater treatment plants. *Journal of Environmental Monitoring*, 6(7):599–605.
- Muir, D. (1984). *Phosphate Esters*, volume 3. Springer Verlag.
- Neta, P., Simon-Manso, Y., Yang, X., and Stein, S. E. (2009). Collisional Energy Dependence of Peptide Ion Fragmentation. *Journal of the American Society for Mass Spectrometry*, 20(3):469–476.
- Niessen, W. M. A. (2006). *Liquid chromatography-mass spectrometry*. CRC press.
- Patisaul, H. B., Roberts, S. C., Mabrey, N., McCaffrey, K. A., Gear, R. B., Braun, J., Belcher, S. M., and Stapleton, H. M. (2013). Accumulation and Endocrine Disrupting Effects of the Flame Retardant Mixture Firemaster® 550 in Rats: An Exploratory Assessment. *Journal of Biochemical and Molecular Toxicology*, 27(2):124–136.
- Pavlović, D. M., Babić, S., Horvat, A. J. M., and Kaštelan-Macan, M. (2007). Sample preparation in analysis of pharmaceuticals. *TrAC Trends in Analytical Chemistry*, 26(11):1062–1075.
- Poma, G., Glynn, A., Malarvannan, G., Covaci, A., and Darnerud, P. O. (2017). Dietary intake of phosphorus flame retardants (PFRs) using Swedish food market basket estimations. *Food and Chemical Toxicology*, 100:1–7.
- Poma, G., Sales, C., Bruyland, B., Christia, C., Gosciny, S., Van Loco, J., and Covaci, A. (2018). Occurrence of Organophosphorus Flame Retardants and Plasticizers (PFRs) in Belgian Foodstuffs and Estimation of the Dietary Exposure of the Adult Population. *Environmental Science & Technology*, 52(4):2331–2338.
- Reemtsma, T., Quintana, J. B., Rodil, R., García-López, M., and Rodríguez, I. (2008). Organophosphorus flame retardants and plasticizers in water and air I. Occurrence and fate. *TrAC Trends in Analytical Chemistry*, 27(9):727–737.
- Rodil, R., Quintana, J. B., and Reemtsma, T. (2005). Liquid Chromatography-Tandem

-
- Mass Spectrometry Determination of Nonionic Organophosphorus Flame Retardants and Plasticizers in Wastewater Samples. *Analytical Chemistry*, 77(10):3083–3089.
- Saillenfait, A.-M., Ndaw, S., Robert, A., and Sabaté, J.-P. (2018). Recent biomonitoring reports on phosphate ester flame retardants: a short review. *Archives of Toxicology*, 92(9):2749–2778.
- Santín, G., Eljarrat, E., and Barceló, D. (2016). Simultaneous determination of 16 organophosphorus flame retardants and plasticizers in fish by liquid chromatography-tandem mass spectrometry. *Journal of Chromatography A*, 1441:34–43.
- Schang, G., Robaire, B., and Hales, B. F. (2016). Organophosphate flame retardants act as endocrine-disrupting chemicals in MA-10 mouse tumor leydig cells. *Toxicological Sciences*, 150(2):499–509.
- Schwarzenberg, A., Ichou, F., Cole, R. B., Machuron-Mandard, X., Junot, C., Lesage, D., and Tabet, J. (2013). Identification tree based on fragmentation rules for structure elucidation of organophosphorus esters by electrospray mass spectrometry. *Journal of Mass Spectrometry*, 48(5):576–586.
- Sheftel, V. O. (2000). *Indirect food additives and polymers: migration and toxicology*. CRC Press.
- Skoog, D. A., West, D. M., Holler, F. J., and Crouch, S. R. (2003). *Fundamentals of Analytical Chemistry with Infotrac*.
- Sleno, L. and Volmer, D. A. (2004). Ion activation methods for tandem mass spectrometry. *Journal of mass spectrometry*, 39(10):1091–1112.
- Snyder, L. R. and Dolan, J. W. (2017). Milestones in the development of liquid chromatography. In *Liquid Chromatography*, chapter 1, pages 1–15. Elsevier, 2 edition.
- Speight, J. G. and Speight, J. G. (2017). Sources and Types of Organic Pollutants. In *Environmental Organic Chemistry for Engineers*, chapter 4, pages 153–201. Butterworth-Heinemann.
- Tan, A., Boudreau, N., and Lévesque, A. (2012). Internal Standards for Quantitative
-

- LC-MS Bioanalysis BT - LC-MS in Drug Bioanalysis. In Xu, Q. A. and Madden, T. L., editors, *LC-MS in Drug Bioanalysis*, pages 1–32. Springer US, Boston, MA.
- The Freedonia Group (2011). Global demand for flame retardants to rise 6.1% per year through 2014. *Additives for Polymers*, 2011(3):9–10.
- Van De Steene, J. C. and Lambert, W. E. (2008). Comparison of matrix effects in HPLC-MS/MS and UPLC-MS/MS analysis of nine basic pharmaceuticals in surface waters. *Journal of the American Society for Mass Spectrometry*, 19(5):713–718.
- Van den Eede, N., Neels, H., Jorens, P. G., and Covaci, A. (2013). Analysis of organophosphate flame retardant diester metabolites in human urine by liquid chromatography electrospray ionisation tandem mass spectrometry. *Journal of Chromatography A*, 1303:48–53.
- van der Veen, I. and de Boer, J. (2012). Phosphorus flame retardants: Properties, production, environmental occurrence, toxicity and analysis. *Chemosphere*, 88(10):1119–1153.
- Wang, S., Cyronak, M., and Yang, E. (2007). Does a stable isotopically labeled internal standard always correct analyte response?: A matrix effect study on a LC/MS/MS method for the determination of carvedilol enantiomers in human plasma. *Journal of Pharmaceutical and Biomedical Analysis*, 43(2):701–707.
- Wang, X.-w., Liu, J.-f., and Yin, Y.-g. (2011). Development of an ultra-high-performance liquid chromatography–tandem mass spectrometry method for high throughput determination of organophosphorus flame retardants in environmental water. *Journal of Chromatography A*, 1218(38):6705–6711.
- Wang, Y. and Kannan, K. (2018). Concentrations and Dietary Exposure to Organophosphate Esters in Foodstuffs from Albany, New York, United States. *Journal of Agricultural and Food Chemistry*, 66(51):13525–13532.
- Watson, J. T. and Sparkman, O. D. (2007). *Introduction to mass spectrometry: instrumentation, applications, and strategies for data interpretation*. John Wiley & Sons.
- Wei, G.-L., Li, D.-Q., Zhuo, M.-N., Liao, Y.-S., Xie, Z.-Y., Guo, T.-L., Li, J.-J., Zhang,

-
- S.-Y., and Liang, Z.-Q. (2015). Organophosphorus flame retardants and plasticizers: Sources, occurrence, toxicity and human exposure. *Environmental Pollution*, 196:29–46.
- Weil, E. and Levchik, S. (2017). Flame Retardants, Phosphorus. In *Kirk-Othmer Encyclopedia of Chemical Technology*. Journal of Fire Sciences.
- Wieling, J. (2002). LC-MS-MS experiences with internal standards. *Chromatographia*, 55(1):S107–S113.
- Wolschke, H., Sühling, R., Xie, Z., and Ebinghaus, R. (2015). Organophosphorus flame retardants and plasticizers in the aquatic environment: A case study of the Elbe River, Germany. *Environmental Pollution*, 206:488–493.
- Xu, F., García-Bermejo, A., Malarvannan, G., Gómara, B. B., Neels, H., and Covaci, A. (2015). Multi-contaminant analysis of organophosphate and halogenated flame retardants in food matrices using ultrasonication and vacuum assisted extraction, multi-stage cleanup and gas chromatography–mass spectrometry. *Journal of Chromatography A*, 1401:33–41.
- Yadav, I. C., Devi, N. L., Zhong, G., Li, J., Zhang, G., and Covaci, A. (2017). Occurrence and fate of organophosphate ester flame retardants and plasticizers in indoor air and dust of Nepal: implication for human exposure. *Environmental Pollution*, 229:668–678.
- Yang, J., Zhao, Y., Li, M., Du, M., Li, X., and Li, Y. (2019). A Review of a Class of Emerging Contaminants: The Classification, Distribution, Intensity of Consumption, Synthesis Routes, Environmental Effects and Expectation of Pollution Abatement to Organophosphate Flame Retardants (OPFRs). *International journal of molecular sciences*, 20(12):2874.
- Zhang, X., Zou, W., Mu, L., Chen, Y., Ren, C., Hu, X., and Zhou, Q. (2016). Rice ingestion is a major pathway for human exposure to organophosphate flame retardants (OPFRs) in China. *Journal of Hazardous Materials*, 318:686–693.
- Zhao, L., Jian, K., Su, H., Zhang, Y., Li, J., Letcher, R. J., and Su, G. (2019). Organophosphate esters (OPEs) in Chinese foodstuffs: Dietary intake estimation via a market basket method, and suspect screening using high-resolution mass spectrometry. *Environment International*, 128:343–352.
-

A Appendix

A.1 Protocol for extraction of OPFRs from foodstuffs - Ethyl Acetate

The following LLE extraction method has followed the protocol from Kimura (2019), with minor adjustments.

Samples were freeze dried and homogenized. Approximately 1g for each sample was transferred into a 15 mL PP tube. 2 mL of 1 M ammonium acetate solution was added to each PP tube. Addition of IS and TA follows Table A.1.

10 μL of a 1 ppm IS-mix solution was spiked to the samples, vortexed and allowed to equilibrate. 6 mL of ethyl acetate was added to each tube and shaken by hand to mix before 10 minutes of UV-sonication. Tubes were then transferred to a mechanical shaker (KS501 digital, IKA) for 45 minutes. Centrifuging at 3500 rpm for 10 min was carried out before the supernatant was transferred into another 15 mL PP tube. This extraction process was repeated two more times with 6 mL of ethyl acetate, hand and mechanical shaking, centrifuging and supernatant transferring.

To remove the salts, 1mL of Milli-Q water was added to PP tube and shaken for approximately 2 minutes, before centrifuging for 5 minutes and water removal.

PP tubes were kept in the refrigerator at 4 °C over night. Samples were evaporated to near dryness (150-250 μL) under a gentle stream of nitrogen at 25 °C in the TurboVap Classic LV (Biotage). Further, it was reconstituted with 1 mL of 50:50 milli-Q water and acetonitrile (MQ:ACN), and transferred into vials for UHPLC analysis. After a night in the refrigerator a thin lipid layer were gently pipetted out.

For each test-extraction ten PP-tubes were prepared. One reagent blank (RB), three samples(S1-S3), four spiked samples (SP1-SP4) and two matrix match samples (MM1-MM2).

A.2 Protocol for extraction of OPFRs from foodstuffs - Hexane:DCM

The following LLE extraction method has followed the protocol from Kimura (2019), with minor adjustments and change of the solvents from ethyl acetate to dichloro-methane (DCM) and hexane (HEX).

Samples were freeze dried and homogenized. Approximately 1g for each sample was transferred into a 15 mL PP tube. 2 mL of 1 M ammonium acetate solution was added to each PP tube. Addition of IS and TA follows Table A.1.

10 μ L of a 1 ppm IS-mix solution was spiked to the samples, vortexed and allowed to equilibrate. 6 mL of was added to each tube and shaken by hand to mix before 10 minutes of UV-sonication. Tubes were then transferred to a mechanical shaker (KS501 digital, IKA) for 45 minutes. Centrifuging at 3500 rpm for 10 min was carried out before the supernatant was transferred into another 15 mL PP tube. This extraction process was repeated two more times with 6 mL of ethyl acetate, hand and mechanical shaking, centrifuging and supernatant transferring.

To remove the salts, 1mL of Milli-Q water was added to PP tube and shaken for approximately 2 minutes, before centrifuging for 5 minutes and water removal.

PP tubes were kept in the refrigerator at 4 °C over night. Samples were evaporated to near dryness (150-250 μ L) under a gentle stream of nitrogen at 25 °C in the TurboVap® Classic LV (Biotage). Further, it was reconstituted with 1 mL of 50:50 milli-Q water and acetonitrile (MQ:ACN), and transferred into vials for UHPLC analysis. After a night in the refrigerator a thin lipid layer was gently pipetted out.

For each test-extraction ten PP-tubes were prepared. One reagent blank (RB), three samples (S1-S3), four spiked samples (SP1-SP4) and two matrix match samples (MM1-MM2).

Table A.1: Overview of internal standard (IS) and target analyte (TA) addition.

ID	TA pre-ext.	IS pre-ext.	TA post-ext.	IS post-ext.
Sample		X		
RB		X		
S_SP	X	X		
MM			X	X

